

1 **Optimizing sampling strategies in high-resolution paleoclimate records**

2

3 Niels J. de Winter^{1,2} *, Tobias Agterhuis¹, Martin Ziegler¹

4

5 ¹Department of Earth Sciences, Utrecht University, Princetonlaan 8a, 3584 CB Utrecht, the Netherlands

6 ²AMGC research group, Vrije Universiteit Brussel, Pleinlaan 2, 1050 Brussels, Belgium

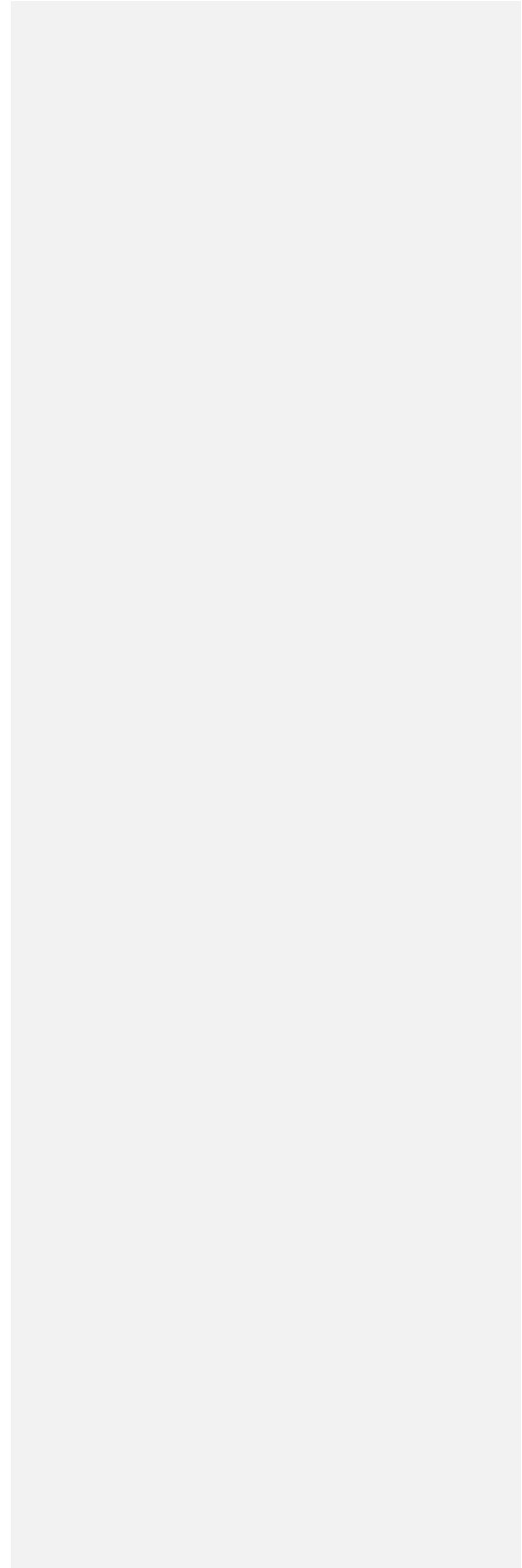
7

8 Correspondence to: Niels J. de Winter (n.j.dewinter@uu.nl)

9

10 Abstract

11 The aim of paleoclimate studies to resolve climate variability from noisy proxy records can in essence be
12 reduced to a statistical problem. The challenge is to ~~isolate~~ extract meaningful information ~~on~~ about climate
13 ~~events~~ variability from these records by reducing measurement uncertainty through a combination of proxy
14 data while retaining the temporal resolution needed to assess the timing and duration of ~~the event~~ variations
15 in climate parameters. In this study, we explore the limits of this compromise by testing different methods
16 for combining proxy data (smoothing, binning and sample size optimization) on a particularly challenging
17 paleoclimate problem: resolving seasonal variability in stable isotope records. We test and evaluate the
18 effects of changes in the seasonal temperature and ~~the hydrology~~ hydrological cycle as well as changes in
19 accretion rate of the archive and parameters such as sampling resolution and age model uncertainty on the
20 reliability of seasonality reconstructions based on clumped and oxygen isotope analyses in 33 real and
21 virtual datasets. Our results show that strategic combinations of clumped isotope analyses can significantly
22 improve the accuracy of seasonality reconstructions ~~if compared~~ with ~~to~~ conventional stable oxygen isotope
23 analyses, especially in settings where the isotopic composition of the water is poorly constrained.
24 Smoothing data using a moving average often leads to ~~an~~ apparent dampening of the seasonal cycle,
25 significantly reducing the accuracy of reconstructions. A statistical sample size optimization protocol yields
26 more precise results than smoothing. However, the most accurate results are obtained through monthly
27 binning of proxy data, especially in cases where growth rate or water composition cycles ~~dampen~~ obscure
28 the seasonal temperature cycle. Our analysis of a wide range of natural situations reveals that the effect of
29 temperature seasonality on oxygen isotope records almost invariably exceeds that of changes in water
30 composition. Thus, in most cases, oxygen isotope records allow reliable identification of growth seasonality
31 as a basis for age modelling ~~and seasonality reconstructions~~ in absence of independent chronological
32 markers in the record. These specific findings allow us to formulate general recommendations for sampling
33 and combining data in paleoclimate research and have implications beyond the reconstruction of
34 seasonality. We briefly discuss the implications of our results for solving common problems in
35 paleoclimatology and stratigraphy, ~~including cyclostratigraphy, strontium isotope dating and event~~
36 ~~stratigraphy.~~



38 1. Introduction

39 Improving the resolution of climate reconstructions is a key objective in paleoclimate studies because it
40 allows climate variability to be studied on different timescales and sheds light on the continuum of climate
41 variability (Huybers and Curry, 2006). However, the temporal resolution of climate records is limited by the
42 accretion rate (growth or sedimentation rate) of the archive and the spatial resolution of sampling for climate
43 reconstructions, which is a function of the ~~size of sample~~ sizes required for a given climate proxy. This
44 tradeoff between sample size and sampling resolution is especially prevalent when using state-of-the-art
45 climate proxies which require large sample sizes, such as the carbonate clumped isotope
46 paleothermometer (Δ_{47} ; see applications in Rodríguez-Sanz et al., 2017; Briard et al., 2020; [Caldarescu et](#)
47 [al., 2021](#)) or stable isotope ratios in specific compounds or of rare isotopes (e.g. phosphate-oxygen isotopes
48 in tooth apatite, triple oxygen isotopes in speleothems or carbon isotopes of CO₂ in ice cores; Jones et al.,
49 1999; Schmitt et al., 2012; Sha et al., 2020). The challenge of sampling resolution persists on a wide range
50 of timescales: from attempts to resolve geologically short-lived (kyr-scale) climate events from deep sea
51 cores with low sedimentation rates (e.g. Stap et al., 2010; Rodríguez-Sanz et al., 2017) to efforts to
52 characterize tidal or daily variability in accretionary carbonate archives (e.g. Warter and Müller, 2017; de
53 Winter et al., 2020a). What constitutes “high-resolution” is therefore largely dependent on the specifics of
54 the climate archive.

55 Sample size limitations are especially important in paleoseasonality reconstructions. Reliable archives for
56 seasonality (e.g. corals, mollusks and speleothem records) are in high demand in the paleoclimate
57 community, because the seasonal cycle is one of the most important cycles in Earth's climate and
58 seasonality reconstructions complement more common long-term (kyr to -Myr) records of past climate
59 variability (e.g. Morgan and van Ommen, 1997; Tudhope et al., 2001; Steuber et al., 2005; Steffensen et
60 al., 2008; Denton et al., 2005; Huyghe et al., 2015; Vansteenberge et al., 2019). A more detailed
61 understanding of climate dynamics at the human timescale is increasingly relevant for improving climate
62 projections (IPCC, 2013). Unfortunately, the growth and mineralization rates of archives that capture high-
63 resolution variability (rarely exceeding 10 mm/yr) limit the number and size of samples that can be obtained
64 at high temporal resolutions (e.g. Mosley-Thompson et al., 1993; Passey and Cerling, 2002; Treble et al.,

65 2003; Goodwin et al., 2003). This problem is exacerbated by the fact that accurate methods for climate
66 reconstructions often require comparatively large sample sizes while methods relying on smaller sample
67 sizes rely on uncertain assumptions. A case in point is the popular carbonate stable oxygen isotope
68 temperature proxy ($\delta^{18}\text{O}_c$) which relies on assumptions of the water composition ($\delta^{18}\text{O}_w$) which that become
69 progressively more uncertain further back in geological history (e.g. Veizer and Prokoph, 2015). Contrarily,
70 the clumped isotope proxy (Δ_{47}) does not rely on this assumption but requires larger amounts of sample
71 (e.g. Müller et al., 2017)

72 A promising technique for circumventing sample size limitations is to analyze larger numbers of small
73 aliquots from the same sample or from similar parts of the climate archive. These smaller aliquots typically
74 have a poorer precision, but precision but averaging multiple aliquots into one estimate while propagating
75 the measurement uncertainty leads to a more reliable estimate of the climate variable (Dattalo, 2008;
76 Meckler et al., 2014; Müller et al., 2017; Fernandez et al., 2017). This approach yields improved sampling
77 flexibility since aliquots can be combined in various ways after measurement. It also allows outlier detection
78 at the level of individual aliquots, thereby spreading the risk of instrumental failure and providing improved
79 control on changes in measurement conditions that may bias results.

80 Previous studies have applied several different methods for combining data from paleoclimate records to
81 reduce analytical noise or higher order variability, and extract variability with a specific frequency (e.g. a
82 specific orbital cycle or seasonality; e.g. Lisiecki and Raymo, 2004; Cramer et al., 2009). These data
83 reduction approaches can in general be categorized into: **smoothing** techniques, in which a sliding window
84 or range of neighboring datapoints is used to smooth high resolution records (see e.g. Cramer et al., 2009)
85 or **binning** techniques, in which the record is divided into equal bins ~~along its length axis~~ in sampling
86 direction (e.g. time, depth or length in growth direction; e.g. Lisiecki and Raymo, 2004; Rodríguez-Sanz et
87 al., 2017). In addition, a third approach is proposed here based on **optimization** of sample size for dynamic
88 binning of data along the climate cycle using a moving window in the domain of the climate variable (as
89 opposed to the depth sampling domain) combined with a T-test routine (see ~~section~~ 3.42.1). All three
90 approaches have advantages and caveats.

91

Formatted: Font: (Default) Arial

Formatted: Font: (Default) Arial

92 **2. Aim**

93 In this study, we explore the (dis)advantages of these three data reduction approaches by testing their
94 reliability in resolving seasonal variability in sea surface temperature (SST) and seawater stable oxygen
95 isotope composition ($\delta^{18}\text{O}_w\delta^{18}\text{O}_{sw}$), both highly sought-after variables in paleoclimate research. We
96 compare reconstructions of SST and $\delta^{18}\text{O}_w\delta^{18}\text{O}_{sw}$ in real and virtual datasets from accretionary carbonate
97 archives (e.g. shells, corals and speleothems) using the clumped isotope thermometer (Δ_{47}) combined with
98 stable oxygen isotope ratios of the carbonate ($\delta^{18}\text{O}_c$).

Formatted: Font: (Default) Arial, 10 pt

Formatted: Font: (Default) Arial, 10 pt

99

100 **2. Methods**

101 **2.1 Reconstruction methods approaches**

Formatted: Font: Bold

102 -Throughout the remainder of this work, the three ~~methods approaches~~ for combining data for
103 reconstructions are ~~abbreviated defined~~ as follows (see also **Fig. 1 and 3.4**):

104 **Smoothing**: ~~refers to the R~~reconstructions of SST and $\delta^{18}\text{O}_w\delta^{18}\text{O}_{sw}$ based on **moving averages** of Δ_{47}
105 ~~and $\delta^{18}\text{O}_c$ records~~ (Fig. 1B). For every ~~case study~~ dataset, the full possible range of moving window sizes
106 ~~(from 1 sample to the full length of the record) were tested~~ for SST and $\delta^{18}\text{O}_w$ reconstructions was explored.
107 ~~The window size that resulted in the most significant difference between maximum and minimum Δ_{47} values~~
108 ~~(based on a student's T-test) was applied to reconstruct SST and $\delta^{18}\text{O}_w$ from Δ_{47} and $\delta^{18}\text{O}_c$ records. SST~~
109 ~~and $\delta^{18}\text{O}_w$ were calculated for all case studies using thea combination of empirical temperature~~
110 ~~relationships by Kim and O'Neil (1997; $\delta^{18}\text{O}_c$ - $\delta^{18}\text{O}_w$ -temperature relationship) and Bernasconi et al. (2018;~~
111 ~~Δ_{47} -temperature relationship). Here and in ~~all~~ other approaches, a typical analytical uncertainty on~~
112 ~~measurements of Δ_{47} (one standard deviation of 0.04‰) and $\delta^{18}\text{O}_c$ (one standard deviation of 0.05‰) was~~
113 ~~used to include uncertainty due to measurement precision. These analytical uncertainties were chosen~~
114 ~~based on typical uncertainties reported for these measurements in the literature (e.g. Schöne et al., 2005;~~
115 ~~Huyghe et al., 2015; Vansteenberge et al., 2016) and long-term precision uncertainties obtained by~~
116 ~~measuring in-house standards using the MAT253+ with Kiel IV setup in the clumped isotope laboratory at~~
117 ~~Utrecht University (e.g. Kocken et al., 2019). The measurement uncertainty was propagated through all~~

Formatted: Font: (Default) Arial, 10 pt

118 calculations using a Monte Carlo simulation (N = 1000) in which Δ_{47} and $\delta^{18}\text{O}_c$ records were randomly
119 sampled from a normal distribution with the virtual Δ_{47} and $\delta^{18}\text{O}_c$ values as means and analytical
120 uncertainties as standard deviations.

121
122 **Binning** refers to R_rreconstructions of SST and $\delta^{18}\text{O}_w$ / $\delta^{18}\text{O}_{sw}$ based on binning of Δ_{47} and $\delta^{18}\text{O}_c$ records
123 into monthly time bins (Fig. 1C). The Δ_{47} and $\delta^{18}\text{O}_c$ data from each case study were grouped into monthly
124 time bins and converted to SST and $\delta^{18}\text{O}_w$ using the Kim and O'Neil (1997) and Bernasconi et al. (2018)
125 formulae. Here too, Monte Carlo simulation was applied to propagate measurement uncertainties onto
126 monthly SST and $\delta^{18}\text{O}_w$ reconstructions. Note that the prerequisite for this method is that the data is aligned
127 using a (floating) age model accurate enough to allow samples to be placed in the right bin. The age of
128 virtual samples in this study is known so this prerequisite poses no problems in this case. However, in the
129 fossil record this alignment might be less certain in absence of accurate chronologies within the archive
130 (e.g. through daily growth increments in mollusk shells; e.g. Schöne et al., 2008; Huyghe et al., 2019; see
131 4.1.3).

132
133 **Optimization** refers to R_rreconstructions of SST and $\delta^{18}\text{O}_w$ / $\delta^{18}\text{O}_{sw}$ based on sample size optimization in Δ_{47}
134 records (Fig. 1D). In this approach aliquots of each virtual dataset are ordered from warm (low $\delta^{18}\text{O}_c$) to
135 cold (high $\delta^{18}\text{O}_c$) data samples, regardless of their position relative to the seasonal cycle. From this ordered
136 dataset, increasingly large samples of multiple aliquots (from 2 aliquots to half the length of the record) are
137 taken from both the warm ("summer") and the cold ("winter") side of the distribution. Summer and winter
138 samples were kept equal (symmetrical grouping) to reduce the number of possible sample size
139 combinations and allow for more efficient computation. However, asymmetrical grouping with differing
140 sample sizes on the summer and winter ends of the $\delta^{18}\text{O}_c$ -spectrum are possible (see 4.1.3 and 4.2.2).
141 Sample sizes with significant difference in Δ_{47} value between summer and winter groups ($p \leq 0.05$ based
142 on a student's T-test) were selected as optimal sample sizes. The moving window T-test in the proxy domain
143 ensures that an optimal compromise is reached between high precision and resolving differences between
144 seasonal extremes. For each successful sample size, SST and $\delta^{18}\text{O}_w$ values were calculated from Δ_{47} and

Formatted: Font: (Default) Arial, 10 pt

Formatted: Font: Not Bold

Formatted: Font: (Default) Arial, 10 pt

Formatted: Font: Not Bold

145 $\delta^{18}\text{O}_c$ data according to Kim and O'Neil (1997) and Bernasconi et al. (2018) formulae. The relationship
146 between SST and $\delta^{18}\text{O}_w$ obtained from these reconstructions was used to convert all Δ_{47} and $\delta^{18}\text{O}_c$ data to
147 SST and $\delta^{18}\text{O}_w$, which are then grouped into monthly SST and $\delta^{18}\text{O}_w$ reconstructions. Measurement
148 uncertainties were propagated through the entire approach by Monte Carlo simulation ($N = 1000$).

149 For comparison, we also include reconstructions based ~~pur~~solely on individual $\delta^{18}\text{O}_c$ measurements with
150 an (often inaccurate) assumption of a constant $\delta^{18}\text{O}_w$ (equal to the modern ocean value of 0‰ VSMOW),
151 which form the most common method for carbonate-based temperature reconstructions in paleoclimate
152 research (see e.g. Schöne et al., 2005; Westerhold et al., 2020; **Fig. 1A**, hereafter: **$\delta^{18}\text{O}$**). For these
153 reconstructions, $\delta^{18}\text{O}_c$ records were grouped into monthly time bins with analytical uncertainties propagated
154 using the Monte Carlo approach ($N = 1000$) and were directly converted to SST using the Kim and O'Neil
155 (1997) temperature relationship.

Formatted: Font: Not Bold

156 For each case study, sampling interval and reconstruction method, SST and $\delta^{18}\text{O}_w$ results were aggregated
157 into monthly averages, medians, standard deviations, and standard errors. Step by step documentation of
158 calculations made for the three Δ_{47} -based reconstruction approaches and the $\delta^{18}\text{O}_c$ reconstructions are
159 given in **S7** and in the complementary R package (de Winter, 2021 a).

160 **2.2 Benchmarks for accuracy and precision**

Formatted: Font: Bold

161 Accuracy and precision of reconstructions of the following four parameters were evaluated against official
162 USGS definitions of climate parameters (O'Donnell et al., 2012):

- 163 1. mean annual SST (MAT), defined as the average of all 12 monthly temperature reconstructions.
- 164 2. seasonal range in SST, (defined as the temperature difference between warmest and coldest
165 month.)
- 166 3. mean annual $\delta^{18}\text{O}_w$, defined as the average of all 12 monthly $\delta^{18}\text{O}_w$ reconstructions.
- 167 4. seasonal range in $\delta^{18}\text{O}_w$, defined as the $\delta^{18}\text{O}_w$ difference between most enriched (highest $\delta^{18}\text{O}_w$)
168 and most depleted (lowest $\delta^{18}\text{O}_w$) monthly reconstruction.

169 Accuracy was defined as the absolute offset of the mean value of the reconstructed climate parameter
170 from the actual "true" data value. Precision was defined as the (relative) standard deviation of the

171 reconstruction, as calculated from the variability within monthly time bins resulting from error propagation
172 through the reconstruction methods Monte Carlo error propagation (see 2.1). An overview of monthly SST
173 and $\delta^{18}\text{O}_w$ reconstructions using the four approaches in all cases is given in S4. Raw data results and
174 figures of reconstructions of all cases using all sampling resolutions are compiled in S8.

175 For comparison, we also include reconstructions based purely on individual $\delta^{18}\text{O}_w$ measurements with an
176 (often inaccurate) assumption of constant $\delta^{18}\text{O}_{sw}$, which form the most common method for carbonate-
177 based temperature reconstructions in paleoclimate research. These reconstructions were not subject to
178 any of the data combination methods outlined above and mostly serve as a benchmark to compare with
179 the performance of the Δ_{47} methods. SST reconstructions assuming constant $\delta^{18}\text{O}_{sw}$ are hereafter referred
180 to as " $\delta^{18}\text{O}$ " reconstructions.

181 We evaluate the reliability of all four approaches through measures of accuracy (offset of reconstruction
182 from the true value) and precision (variability between reconstructions due to random errors in the data) of
183 reconstructions and highlight biases inherent to specific approaches and in specific situations. In the end,
184 we provide guidelines for choosing the right sampling approach for studies on seasonality reconstructions
185 from accretionary carbonate archives. In addition, we discuss implications of our findings for other sampling
186 problems in the geosciences.

187

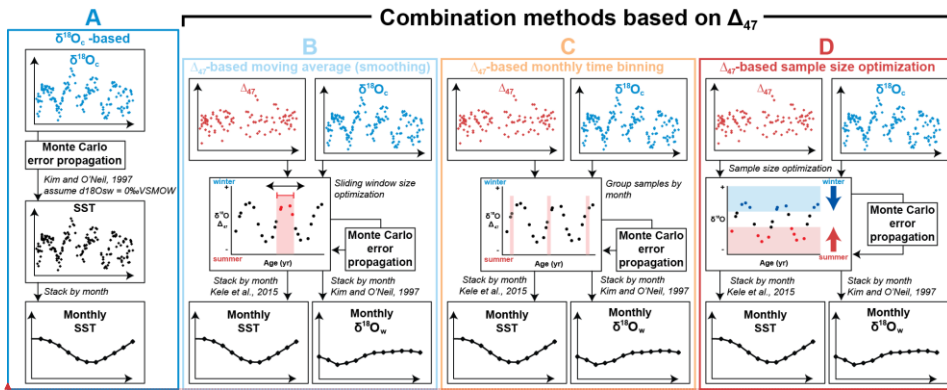


Figure 1: Schematic overview of the four approaches for seasonality reconstructions: (A) $\delta^{18}\text{O}_c$ -based reconstructions, assuming constant $\delta^{18}\text{O}_{sw}$ and $\delta^{48}\text{O}_{sw}$. (B) Reconstructions based on smoothing $\delta^{18}\text{O}_c$ and Δ_{47} data using a moving average. (C) Reconstructions based on binning $\delta^{18}\text{O}_c$ and Δ_{47} data in monthly time bins. (D) Reconstructions based on optimization of the sample size for combining $\delta^{18}\text{O}_c$ and Δ_{47} data (see description in 3.42.1). Colored curves represent virtual $\delta^{18}\text{O}_c$ (blue) and Δ_{47} (red) depth-series in sampling domain. Black curves represent reconstructed monthly SST and $\delta^{18}\text{O}_{sw}$ / $\delta^{48}\text{O}_{sw}$ averages.

Formatted: Font: (Default) Arial, 10 pt

Formatted: Line spacing: Multiple 1.08 li

Formatted: Font: (Default) Arial, 10 pt

Formatted: Font: (Default) Arial, 10 pt

3. Methods

3.42.3 SST and $\delta^{18}\text{O}_{sw}$ / $\delta^{48}\text{O}_{sw}$ datasets

The reliability (accuracy and precision) of the three reconstruction approaches was were illustrated and tested and compared in-based on three waystypes of data: Firstly, by-evaluating data from a real specimen of a Pacific oyster (*Crassostrea gigas*, syn. *Magallana gigas*) reported in Ullmann et al. (2010). Secondly, by-application-on data based on actual measurements of natural variability in SST and sea surface salinity (SSS; case 30-33) converted to virtual Δ_{47} and $\delta^{18}\text{O}_c$ records. Thirdly, by-applying-the-approaches-on-a set of virtual-datasets based on completely-fully-virtual-artificial SST and $\delta^{18}\text{O}_{sw}$ / $\delta^{48}\text{O}_{sw}$ data (case 1-29; see Fig. 2) converted to virtual Δ_{47} and $\delta^{18}\text{O}_c$ records. For virtual-datasets, records of SST and $\delta^{18}\text{O}_{sw}$ were converted to the depth domain (along the length of the record) by defining a virtual growth rate in the sampling direction. Adding this growth rate as a variable allowed us to test the sensitivity of approaches to changes in the extension rate of the archive, including hiatuses (growth rate = 0). This is important, because fluctuations in linear extension rate and periods in which no mineralization occurs (hiatuses or growth

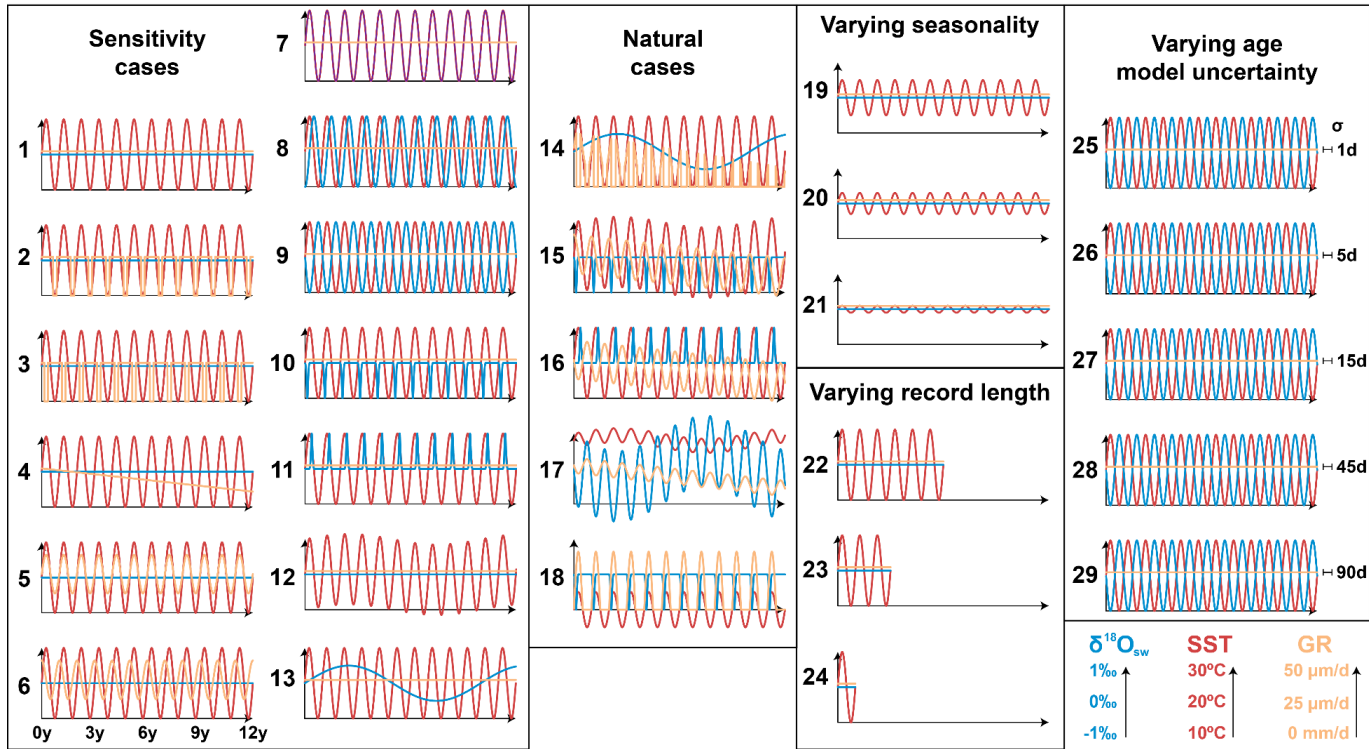
Formatted: Font: (Default) Arial, 10 pt

Formatted: Font: (Default) Arial, 10 pt

210 cessations) are common in all climate archives (e.g. Treble et al., 2003; Ivany, 2012). An overview of the
211 virtual SST and $\delta^{18}\text{O}_{\text{sw}}$ time series in all test cases is shown in **Fig. 2** and a description of all cases is given
212 in **S1**.

Virtual cases

Formatted: Font: (Default) Arial, 10 pt



213

214 **Figure 2:** Overview of time series of all virtual test cases. Colored curves represent time series of SST (red), $\delta^{18}\text{O}_{\text{sw}}$ (blue) and growth rate
 215 (~~green~~orange, abbreviated as “GR”). Horizontal axes in all plots are 12 years long (see legend below case 6). Vertical axis of all plots has the same
 216 scale (SST: 10 to 30°C; $\delta^{18}\text{O}_{\text{sw}}$: -1 to +1‰ VSMOW; Growth rate: 0–50 $\mu\text{m}/\text{day}$; see legend in bottom right corner). Horizontal error bars and
 217 labels on the right side of cases 25–29 represent standard errors introduced on the age model (bars not to scale). The $\delta^{18}\text{O}_{\text{c}}$ and Δ_{47} records resulting
 218 from these virtual datasets are provided in **S8–S6** (see also Fig. 3 for natural examples).

Formatted: Font: (Default) Arial, 10 pt, Italic

Formatted: Font: (Default) Arial, 10 pt, Italic

Formatted: Font: (Default) Arial

230
$$f = \frac{SSS_{sample} - SSS_{ocean}}{SSS_{freshwater} - SSS_{ocean}} \quad (2)$$

231 Here, we assume salinity (SSS_{sample}) results from a mixture of a fraction (f) isotopically light and low-salinity
232 ($\delta^{18}O_{w,freshwater} = -8.5\text{‰}$; $SSS_{freshwater} = 0$) freshwater and a fraction ($1-f$) ocean water ($\delta^{18}O_{w,ocean} = 0\text{‰}$;
233 $SSS_{ocean} = 35$), with negative amounts of freshwater contribution ($f < 0$) representing net evaporation
234 ($SSS_{sample} > SSS_{ocean}$). The value for $\delta^{18}O_{w,freshwater}$ was based on the discharge weighted average $\delta^{18}O_w$ of
235 water in the nearby Elbe and Weser rivers (see Ullmann et al., 2010). All references to $\delta^{18}O_w$ values
236 throughout the text are with reference to the VSMOW scale. Contrary to the virtual datasets (cases 1-33;
237 see 2.3.2 and 2.3.3), the Ullmann et al. (2010) data was already available in the sampling domain, hence
238 no subsampling was required.

Formatted: Font: Bold

Formatted: Font: Bold

239 2.3.2 Cases based on real climate data

240 ~~Natural environmental time series were~~ Four test cases were based on time series of real SST and SSS
241 data from four different locations, selected to capture a variety of environments with different SST and SSS
242 variability (see Fig. 3):

- 243 1. Tidal flats of the Wadden Sea near Texel, the Netherlands (case 30)
- 244 2. Great Barrier Reef in Australia (case 31)
- 245 3. Gulf of Aqaba between Egypt and Saudi Arabia (case 32)
- 246 4. Northern Atlantic Ocean east of Iceland (case 33).

247 Daily measurements of SST and SSS for case 31-33 were obtained from worldwide open-access datasets
248 of the National Oceanic and Atmospheric Administration (NOAA, 2020) and European Space Agency (ESA,
249 2020) respectively. Hourly SST and SSS measured *in situ* in the Wadden Sea (case 30) were obtained
250 from the Dutch Institute for Sea Research (NIOZ, Texel, the Netherlands). Since direct, *in situ*
251 measurements of $\delta^{18}O_w$ variability at a high temporal resolution are scarce, $\delta^{18}O_w$ was estimated from (more
252 widely available) SSS data using the same mass balance described in 2.3.1. The value for $\delta^{18}O_{w,freshwater}$
253 was based on the $\delta^{18}O_w$ of rain in the Netherlands (-8‰; Mook, 1970; Bowen, 2020). and Applying this
254 mass balance on the SSS record of the Wadden Sea tidal flats (case 30) results in $\delta^{18}O_w$ values and a

255 SSS- $\delta^{18}\text{O}_w$ relationship in agreement with measurements in this region (Harwood et al., 2008). SST and
256 $\delta^{18}\text{O}_w$ time series for all cases are given in **S4** and natural cases are plotted in **Fig. 3**.

257 For all virtual datasets (cases 1-33), records of SST and $\delta^{18}\text{O}_w$ were converted to the sampling domain
258 (along the length of the record) by defining a virtual growth rate in the sampling direction. Adding this growth
259 rate as a variable allowed us to test the sensitivity of approaches to changes in the extension rate of the
260 archive, including hiatuses (growth rate = 0). This is important, because fluctuations in linear extension rate
261 and periods in which no mineralization occurs (hiatuses or growth cessations) are common in all climate
262 archives (e.g. Treble et al., 2003; Ivany, 2012). *2.1.1 Modern oyster data*

263 After conversion to the sampling domain, virtual aliquots were subsampled at equal distance from the SST
264 and $\delta^{18}\text{O}_w$ series of all cases using six sampling intervals: 0.1 mm, 0.2 mm, 0.45 mm, 0.75 mm, 1.55 mm
265 and 3.25 mm. The four largest sampling intervals were chosen such that the standard growth rate (10
266 mm/yr) was not an integer multiple of the sampling interval (e.g. 0.45 mm instead of 0.5 mm, and 3.25 mm
267 instead of 3 mm). This decision prevents sampling the same parts of the seasonal cycle (e.g. same months)
268 every year, which biases both the mean value and the precision of monthly SST and $\delta^{18}\text{O}_w$ reconstructions.
269 This bias towards certain parts of the seasonal cycle is much stronger at low sample sizes (large sampling
270 intervals) and is illustrated in the **Supplementary Information**.

271 Environmental SST and $\delta^{18}\text{O}_{sw}$ data from the List Basin in Denmark (54°59.25N, 8°23.51E) where the
272 modern oyster specimen originated were obtained from local *in situ* measurements of SST and SSS
273 described in Ullmann et al. (2010). Since direct, *in situ* measurements of $\delta^{18}\text{O}_{sw}$ variability at a high temporal
274 resolution were not available, $\delta^{18}\text{O}_{sw}$ was estimated from (more widely available) SSS data using a mass
275 balance (equation 1 and 2; following e.g. Ullmann et al., 2010):

$$276 \delta^{18}\text{O}_{sw} = \delta^{18}\text{O}_{sw, \text{freshwater}} * f + \delta^{18}\text{O}_{sw, \text{freshwater}} * (1 - f) \quad (1)$$

$$277 f = \frac{\text{SSS}_{\text{sample}} - \text{SSS}_{\text{ocean}}}{\text{SSS}_{\text{freshwater}} - \text{SSS}_{\text{ocean}}} \quad (2)$$

278 Here, we assume salinity ($\text{SSS}_{\text{sample}}$) results from a mixture of a fraction (f) isotopically light and low-salinity
279 ($\delta^{18}\text{O}_{sw, \text{freshwater}} = -8.5\text{‰ VSMOW}$; $\text{SSS}_{\text{freshwater}} = 0$) freshwater and a fraction ($1-f$) ocean water ($\delta^{18}\text{O}_{sw, \text{ocean}}$
280 $= 0\text{‰ VSMOW}$; $\text{SSS}_{\text{ocean}} = 35$), with negative amounts of freshwater contribution ($f < 0$) representing net

281 evaporation ($SSS_{sample} - SSS_{ocean}$). The value for $\delta^{18}O_{sw, freshwater}$ was based on the discharge-weighted
282 average $\delta^{18}O_{sw}$ of water in the nearby Elbe and Weser rivers (-8.5‰VSMOW; see Ullmann et al., 2010).

283 3.1.2 Cases based on real climate data

284 Natural environmental time-series were based on SST and SSS data from four different locations, selected
285 to capture a variety of environments with different SST and SSS variability:

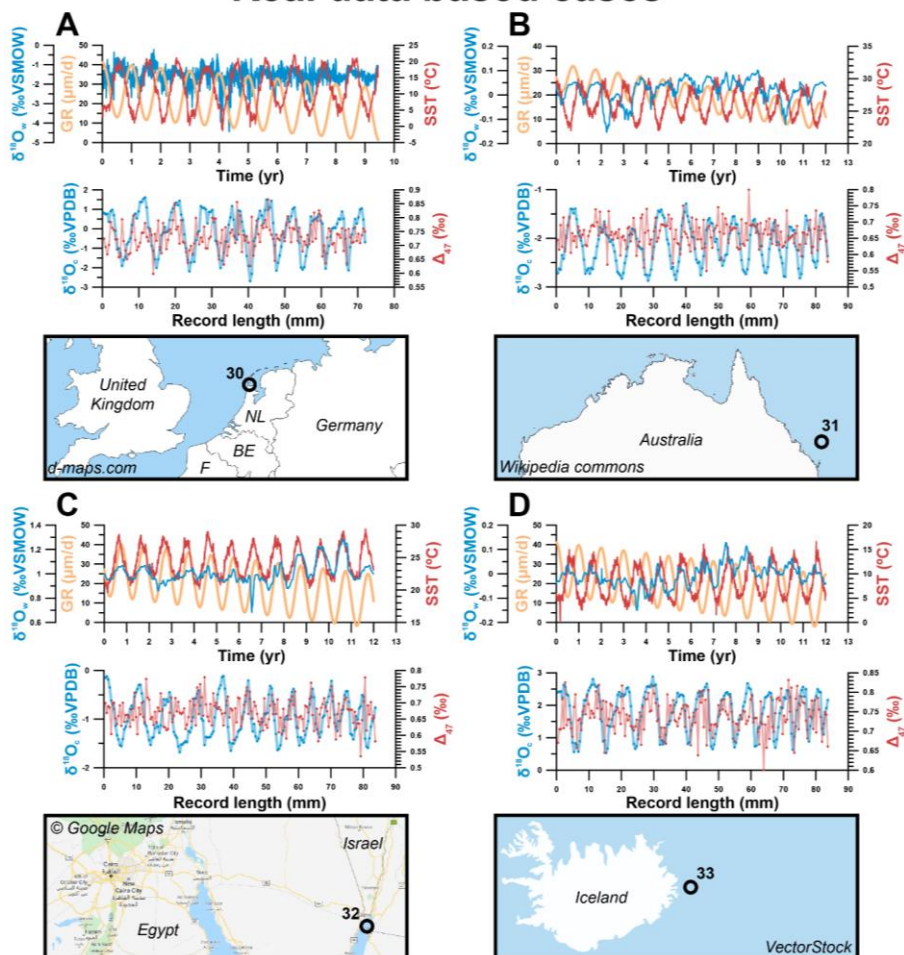
- 286 1. Tidal flats of the Wadden Sea near Texel, the Netherlands (case 30)
- 287 2. Great Barrier Reef in Australia (case 31)
- 288 3. Gulf of Aqaba between Egypt and Saudi Arabia (case 32)
- 289 4. Northern Atlantic Ocean east of Iceland (case 33).

290 Daily measurements of SST and SSS for case 31-33 were obtained from worldwide open-access datasets
291 of the National Oceanic and Atmospheric Administration (NOAA, 2020) and European Space Agency (ESA,
292 2020) respectively. Hourly SST and SSS measured *in situ* in the Wadden Sea (case 30) were obtained
293 from the Dutch Institute for Sea Research (NIOZ, Texel, the Netherlands). Since direct, *in situ*
294 measurements of $\delta^{18}O_{sw}$ variability at a high temporal resolution is scarce, $\delta^{18}O_{sw}$ was estimated from (more
295 widely available) SSS data using the same mass balance described in 3.1.1. The value for $\delta^{18}O_{sw, freshwater}$
296 was based on the $\delta^{18}O_{sw}$ of rain in the Netherlands (-8‰VSMOW; Mook, 1970; Bowen, 2020), and applying
297 this mass balance on the SSS record of the Wadden Sea tidal flats (case 30) results in $\delta^{18}O_{sw}$ values and
298 a SSS- $\delta^{18}O_{sw}$ relationship in agreement with measurements in this region (Harwood et al., 2008). SST and
299 $\delta^{18}O_{sw}$ time series for all cases are given in **S5** and natural cases are plotted in **Fig. 3**.

300

Commented [WNd(1): Numbering!]

Real data based cases



301

302 **Figure 3:** Overview of the four cases of virtual data based on natural SST and SSS measurements explored
 303 in this study. (A) Case 30: Tidal flats on the Wadden Sea, Texel, the Netherlands. (B) Case 31 Great Barrier
 304 Reef, Australia. (C) Case 32: Gulf of Aqaba between Egypt and Saudi Arabia. (D) Case 33: Atlantic Ocean
 305 east of Iceland. For all cases, graphs on top show environmental data, with SST plotted in red, $\delta^{18}\text{O}_w$ and $\delta^{18}\text{O}_{sw}$
 306 in blue and growth rate (abbreviated as "GR") in green-orange (as in Fig. 2). The graph below shows virtual
 307 $\delta^{18}\text{O}_c$ (blue) and Δ_{47} (red) records created from these data series using a sampling interval of 0.45 mm and
 308 including analytical noise (see 3.3). Note that the scale of vertical axes varies between plots.

309

310 2.4.3.3 Virtual cases

Formatted: Font: (Default) Arial, 10 pt

Formatted: Font: (Default) Arial, 10 pt, Italic

Formatted: Font: Bold

311 Virtual SST and $\delta^{18}\text{O}_w\delta^{18}\text{O}_{sw}$ time series were artificially constructed to test the effect of various SST and
312 $\delta^{18}\text{O}_w\delta^{18}\text{O}_{sw}$ scenarios on the effectivity of the reconstruction methods. The default test case (case 1)
313 contained an ideal, 12-year sinusoidal SST curve with a period of 1 year (seasonality), a mean value of
314 20°C and a seasonal amplitude of 10°C, a constant $\delta^{18}\text{O}_w\delta^{18}\text{O}_{sw}$ value of 0‰ VSMOW and a constant
315 growth rate of 10 mm/yr. Other cases contain various deviations from this ideal case (see also Fig. 2, Table
316 1 and S1):

- 317 • Linear and/or seasonal changes in growth rate, including growth stops (cases 2-6, 14-18)
- 318 • Seasonal and/or multi-annual changes in $\delta^{18}\text{O}_w\delta^{18}\text{O}_{sw}$ (cases 7-11, 13-18)
- 319 • Multi-annual trends in SST superimposed on the seasonality (cases 12, 15 and 17)
- 320 • Variations in the seasonal SST amplitude (cases 19-21)
- 321 • Change in the total length of the time series (cases 22-24).
- 322 • Variation in uncertainty on the age of each virtual datapoint (cases 25-29)

323 Comparison of the virtual time series (case 1-29; **Fig. 2**) with the natural variability (case 30-33; **Fig. 3**)
324 shows that the virtual cases are not realistic approximations of natural variability in SST and $\delta^{18}\text{O}_w\delta^{18}\text{O}_{sw}$.
325 Natural SST and $\delta^{18}\text{O}_w\delta^{18}\text{O}_{sw}$ variability are not limited to the seasonal or multi-annual scale but contain
326 a fair amount of higher order (daily to weekly scale) variability. In order to simulate this natural variability,
327 we extracted the seasonal component of SST and $\delta^{18}\text{O}_w\delta^{18}\text{O}_{sw}$ variability from our highest resolution record
328 of measured natural SST and SSS data (case 30: data from Texel, the Netherlands, see 3.1.22.3.2 and
329 **Fig. 3**). The standard deviation of residual variability of this data after subtraction of the seasonal cycle was
330 used to add random high-frequency noise to the SST and $\delta^{18}\text{O}_w\delta^{18}\text{O}_{sw}$ variability in virtual cases. Note that
331 while sub-annual environmental variability can be approximated by Gaussian noise (Wilkinson and Ivany,
332 2002), this representation is an oversimplification of reality. In the case of our Texel data, the SST and SSS
333 residuals are not exactly normally distributed (Kolmogorov-Smirnov test: $D = 0.010$; $p = 7.2 \cdot 10^{-14}$ and $D =$
334 0.039 ; $p < 2.2 \cdot 10^{-16}$ for SST and SSS residuals respectively; see **S2-4**). SST and $\delta^{18}\text{O}_w$ data from cases 1-
335 29 was converted to the sampling domain and subsampled at a range of sampling resolutions following the
336 same procedure applied to cases 30-33 (see 2.3.2).

Formatted: Font: (Default) Arial, 10 pt

Formatted: Font: Bold

3.2. Subsampling

Virtual aliquots were subsampled at equal distance from the SST and $\delta^{18}\text{O}_{\text{sw}}$ depth series of all cases using six sampling intervals: 0.1 mm, 0.2 mm, 0.45 mm, 0.75 mm, 1.55 mm and 3.25 mm. The four largest sampling intervals were chosen such that the standard growth rate (10 mm/yr) was not an integer multiple of the sampling interval (e.g. 0.45 mm instead of 0.5 mm, and 3.25 mm instead of 3 mm). This decision prevents sampling the same parts of the seasonal cycle (e.g. same months) every year, which biases both the mean value and the precision of monthly SST and $\delta^{18}\text{O}_{\text{sw}}$ reconstructions. This bias towards certain parts of the seasonal cycle is much stronger at low sample sizes (large sampling intervals) and is illustrated in S6.

3.32.4 Conversion to $\delta^{18}\text{O}_c$ and Δ_{47} data

After subsampling, SST and $\delta^{18}\text{O}_w$ series were converted to $\delta^{18}\text{O}_c$ and Δ_{47} using a carbonate model based on empirical relationships between Δ_{47} and $\delta^{18}\text{O}_c$ with and SST and $\delta^{18}\text{O}_w$ (equation 3 and 4; Kim and O'Neil, 1997; Kele et al., 2015; Bernasconi et al., 2018) and the conversion of $\delta^{18}\text{O}$ values from VSMOW to VPDB scale (equation 5; Brand et al., 2014):

$$\Delta_{47} = \frac{0.0449 \cdot 10^6}{(SST + 273.15)^2} + 0.167 \quad (3)$$

$$1000 \cdot \ln \frac{\left(\frac{^{18}\text{O}}{^{16}\text{O}}\right)_{\text{CaCO}_3}}{\left(\frac{^{18}\text{O}}{^{16}\text{O}}\right)_{\text{H}_2\text{O}}} = 18.03 \cdot \left(\frac{10^3}{(SST + 273.15)}\right) - 32.42 \quad (4)$$

$$\delta^{18}\text{O}_{\text{VPDB}} = 0.97002 \cdot \delta^{18}\text{O}_{\text{VSMOW}} - 29.98 \quad (5)$$

For the real oyster data (Ullmann et al., 2010; see 2.3.1), only the Δ_{47} data needed to be created because $\delta^{18}\text{O}_c$ was directly measured. As a result, each case study yielded "sampled" depth-records of Δ_{47} and $\delta^{18}\text{O}_c$ in the sampling domain and their associated corresponding "true" SST and $\delta^{18}\text{O}_w$ records in the time domain. These allowed us to test assessment of reconstruction approaches in different scenarios. (Figure 4) gives a schematic step-by-step schematic overview of all steps taken to create of virtual data how virtual Δ_{47} and $\delta^{18}\text{O}_c$ data was created, used in to test reconstruction approaches, and finally compared to the original "true" seasonality

Formatted: Font: (Default) Arial, 10 pt

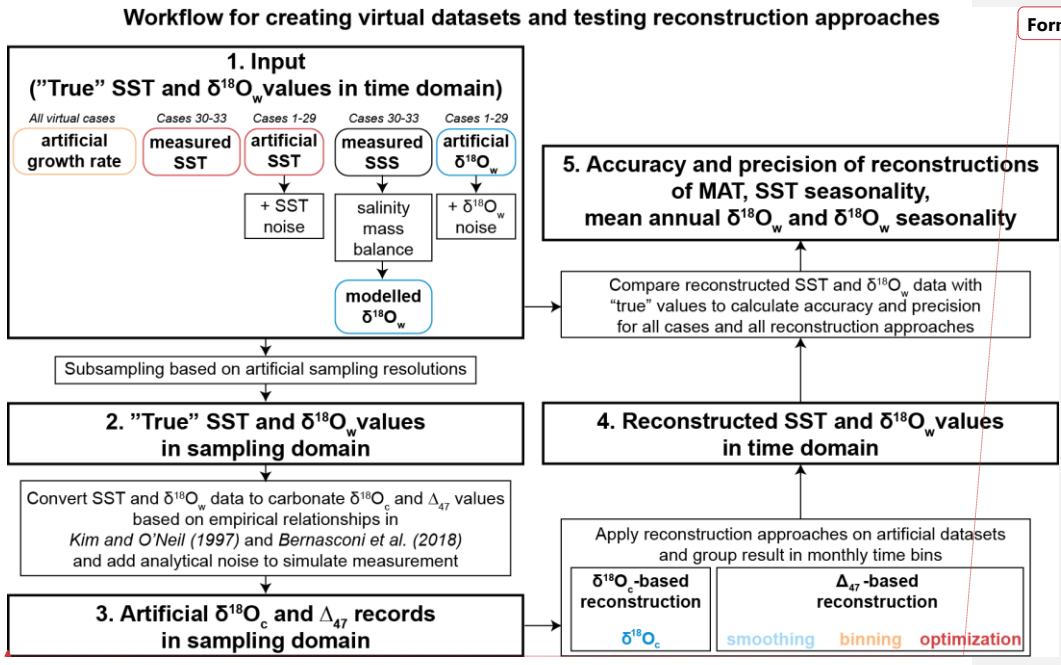
Formatted: Font: (Default) Arial, 10 pt

Formatted: Font: (Default) Arial, 10 pt

362 ~~in SST and $\delta^{18}\text{O}_w$. The result of applying these steps is illustrated on and test the four reconstruction~~
363 ~~approaches as well as an example of case 310 (Great Barrier reef data, see also Fig. 25) is provided in~~
364 ~~Fig. 4.~~ All calculations for creating Δ_{47} and $\delta^{18}\text{O}_c$ ~~depth-series in sampling domain~~ were carried out using
365 the open-source computational software R (R core team, 2013), and scripts for these calculations are given
366 in ~~S7~~ and compiled in the documented R package- "seasonalclumped" (de Winter, 2021a). All Δ_{47} and $\delta^{18}\text{O}_c$
367 datasets are provided in ~~S8~~ S6.

368

369 -In the case of the real oyster data, $\delta^{18}\text{O}_c$ data from Ullmann et al. (2010) was used and Δ_{47} -data was
 370 created from the seasonal-SST record provided in the same study with added natural residual variability
 371 (as explained in 3.1.3).

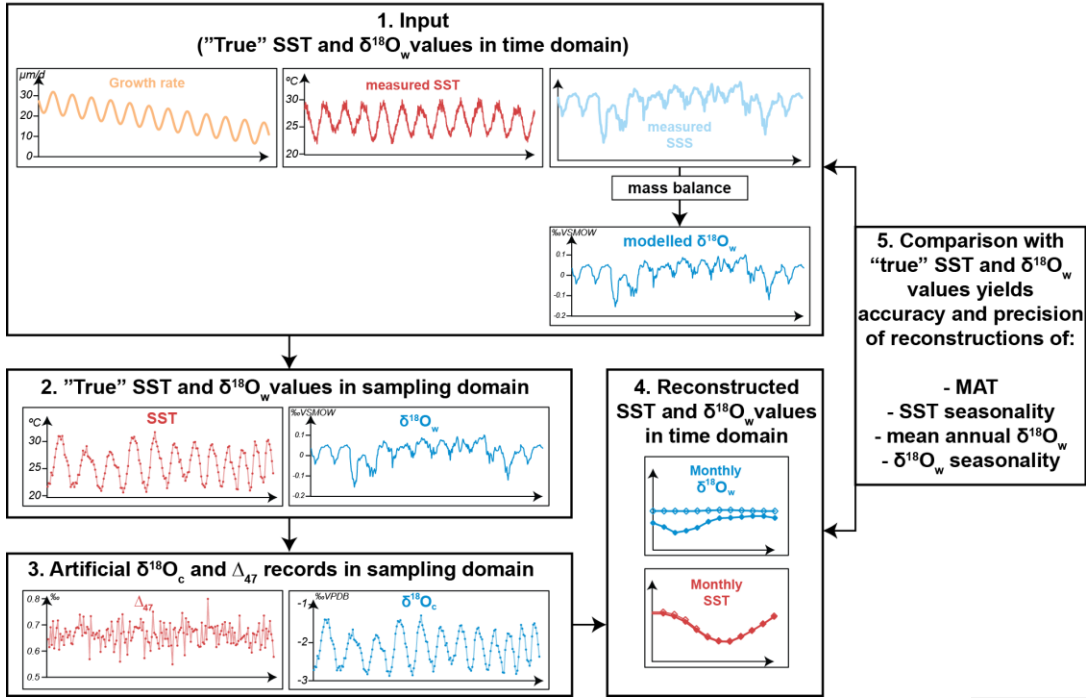


Formatted: Font: (Default) Arial, 10 pt

372
 373 **Figure 4: A)** Flow diagram showing the steps taken to create virtual data (Δ_{47} and $\delta^{18}\text{O}_c$; cases 1-33) and
 374 compare results of SST and $\delta^{18}\text{O}_w$ reconstructions with the actual SST and $\delta^{18}\text{O}_w$ data the
 375 record was based on (counterclockwise direction). Steps 1-3 outline the procedure for
 376 creating virtual Δ_{47} and $\delta^{18}\text{O}_c$ datasets (see sections 2.3 and 2.4), step 4 shows the application of the
 377 different reconstruction methods on this virtual data (see Fig. 2 for details) and step 5 illustrates how the
 378 reconstructions are compared with the original ("true") SST and $\delta^{18}\text{O}_w$ data to calculate accuracy and
 379 precision of the reconstruction approaches. Note that step 1 is different for cases 1-29 (based on fully
 380 artificial SST and $\delta^{18}\text{O}_w$ records; 2.3.3) than for cases 30-33 (SST and $\delta^{18}\text{O}_w$ records based on real SST
 381 and SSS data; see 2.3.2).

- Formatted: Not Superscript/ Subscript
- Formatted: Font: (Default) Arial, 10 pt, Italic
- Formatted: Font: (Default) Arial, 10 pt, Italic
- Formatted: Font: Bold
- Formatted: Font: Bold
- Formatted: Font: Italic
- Formatted: Font: Italic
- Formatted: Font: Italic

Workflow for creating virtual datasets and testing reconstruction approaches:
 Example for case 31 (Great Barrier Reef satellite data)



382
 383 **-B)Figure 5X:** An example of the steps highlighted in **A)Fig. 4** using case 31 (Great Barrier Reef data)
 384 **meant** to illustrate the data processing steps. Virtual data plots include normally distributed measurement
 385 uncertainty on Δ_{47} and $\delta^{18}\text{O}_c$.

Formatted: Font: (Default) Arial, 10 pt

3.4 SST and $\delta^{18}\text{O}_e$ -reconstructions

SST and $\delta^{18}\text{O}_{\text{sw}}$ seasonality were reconstructed from the Δ_{47} and $\delta^{18}\text{O}_e$ records to test the reliability of the sample reduction approaches (see Fig. 1). In all approaches, a typical analytical uncertainty on measurements of Δ_{47} (one standard deviation of 0.04‰) and $\delta^{18}\text{O}_e$ (one standard deviation of 0.05‰) was used to include measurement precision. These analytical uncertainties were chosen based on typical uncertainties reported for these measurements in the literature (e.g. Schöne et al., 2005; Huyghe et al., 2015; Vansteenberghe et al., 2016) and long-term precision uncertainties obtained by measuring in-house standards using the MAT253+ with Kiel IV setup in the clumped isotope laboratory at Utrecht University (e.g. Kocken et al., 2019). Virtual measurement uncertainty was propagated through all reconstruction approaches using a Monte Carlo simulation ($N = 1000$) in which Δ_{47} and $\delta^{18}\text{O}_e$ records were randomly sampled from a normal distribution with the virtual Δ_{47} and $\delta^{18}\text{O}_e$ values as means and analytical uncertainties as standard deviations. For each case study, sampling interval and reconstruction method, SST and $\delta^{18}\text{O}_{\text{sw}}$ results were aggregated into monthly averages, medians, standard deviations, and standard errors. Step by step documentation of calculations made for the three Δ_{47} -based reconstruction approaches and the $\delta^{18}\text{O}_e$ reconstructions are given in S9 and are detailed below.

For $\delta^{18}\text{O}$ reconstructions (Fig. 1A), only the $\delta^{18}\text{O}_e$ records were used. Seawater $\delta^{18}\text{O}_{\text{sw}}$ values were assumed to remain 0‰VSMOW throughout the year. The simulated $\delta^{18}\text{O}_e$ records with analytical uncertainties added were directly converted to SST using the Kim and O'Neil (1997) temperature relationship (see equation 4).

Smoothing reconstructions (Fig. 1B) were carried out by defining a range of moving window sizes (from $N=1$ to the complete record). For every simulated Δ_{47} and $\delta^{18}\text{O}_e$ record, all moving windows were tested. The window size that resulted in the most significant difference between maximum and minimum Δ_{47} values using a student's T-test was applied on both Δ_{47} and $\delta^{18}\text{O}_e$ records. This process was repeated for all virtual records to propagate simulated analytical uncertainty through the protocol. SST and $\delta^{18}\text{O}_{\text{sw}}$ were calculated for each set of Δ_{47} and $\delta^{18}\text{O}_e$ records using the combination of empirical temperature relationships by Kim and O'Neil (1997) and Bernasconi et al. (2018; equation 3)

414 In **binning** reconstructions (**Fig. 1C**), virtual Δ_{47} and $\delta^{18}\text{O}_e$ data were grouped into monthly time bins and
415 converted to SST and $\delta^{18}\text{O}_{sw}$ using the Kim and O'Neil (1997) and Bernasconi et al. (2018) formulae. The
416 prerequisite for this method is that the data is aligned using a (floating) age model accurate enough to allow
417 samples to be placed in the right bin. The age of virtual samples in this study is known so this prerequisite
418 poses no problems in this case, but the same may not be true in the fossil record.

419 Finally, the **optimization** reconstruction approach (**Fig. 1D**) was carried out by ordering the aliquots of each
420 virtual dataset from warm (low $\delta^{18}\text{O}_e$) to cold (high $\delta^{18}\text{O}_e$) data samples, regardless of their position relative
421 to the seasonal cycle. From this ordered dataset, increasingly large samples of multiple aliquots (from $N=1$
422 to the complete record) are taken from both the warm ("summer") and the cold ("winter") side of the
423 distribution. Sample sizes with significant difference in Δ_{47} value between summer and winter groups ($p \leq$
424 0.05 based on a student's T-test) were selected as optimal sample sizes. For each successful sample size,
425 SST and $\delta^{18}\text{O}_{sw}$ values were calculated from Δ_{47} and $\delta^{18}\text{O}_e$ data according to Kim and O'Neil (1997) and
426 Bernasconi et al. (2018) formulae. The relationship between SST and $\delta^{18}\text{O}_{sw}$ obtained from these
427 reconstructions was used to convert all data to SST and $\delta^{18}\text{O}_{sw}$.

428 Accuracy and precision of reconstructions of the following four parameters were evaluated:

- 429 1. mean annual SST (MAT)
- 430 2. seasonal range in SST (temperature difference between warmest and coldest month)
- 431 3. mean annual $\delta^{18}\text{O}_{sw}$
- 432 4. seasonal range in $\delta^{18}\text{O}_{sw}$ ($\delta^{18}\text{O}_{sw}$ difference between warmest and coldest month).

433 Accuracy was defined as the absolute offset of the reconstruction from the actual data. Precision was
434 defined as the (relative) standard deviation of the reconstruction, as calculated from the variability within
435 monthly time bins resulting from error propagation through the reconstruction methods. An overview of
436 monthly SST and $\delta^{18}\text{O}_{sw}$ reconstructions using the four approaches in all cases is given in **S5**. Raw data
437 results and figures of reconstructions of all cases using all sampling resolutions are compiled in **S10**.

438

439

440 **43. Results**

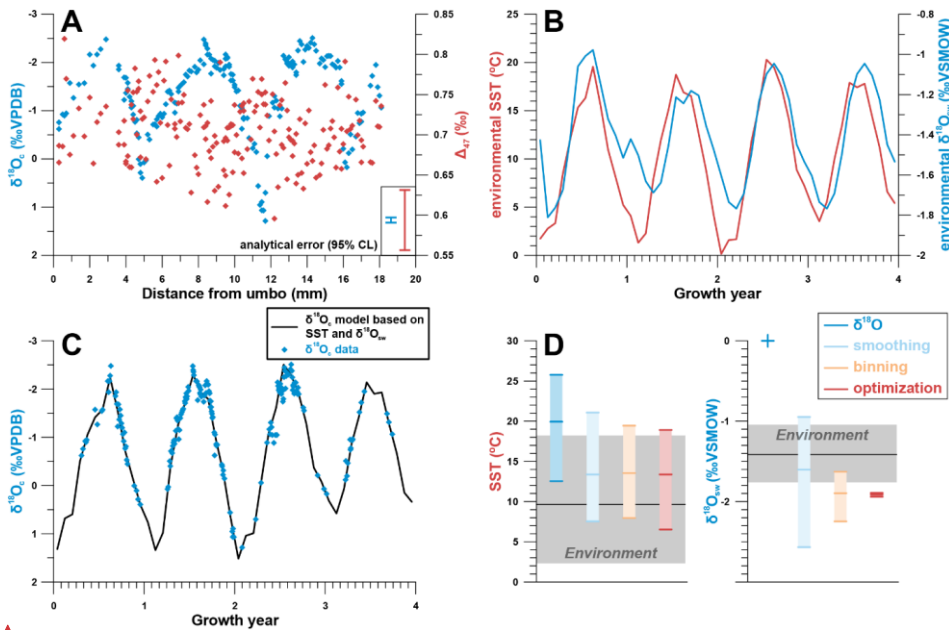
441 **43.1 Real example**

442 Measured ($\delta^{18}\text{O}_c$) and simulated (Δ_{47}) data from the Pacific oyster from the Danish List Basin yielded ~~various~~
443 estimates ~~for of~~ SST and $\delta^{18}\text{O}_w\delta^{18}\text{O}_{sw}$ seasonality ~~depending on which~~ using all reconstruction approaches
444 ~~is taken~~ (Fig. 5B). While a model of shell $\delta^{18}\text{O}_c$ based on SST and SSS data closely approximates the
445 measured $\delta^{18}\text{O}_c$ record (Fig. 5C), basing SST reconstructions solely on $\delta^{18}\text{O}_c$ data without any *a priori*
446 knowledge of $\delta^{18}\text{O}_w\delta^{18}\text{O}_{sw}$ variability (assuming constant $\delta^{18}\text{O}_w\delta^{18}\text{O}_{sw}$ equal to the global marine value)
447 leads to high inaccuracy in SST seasonality and mean annual SST (Fig. 5D). The in-phase relationship
448 between SST and SSS (Fig. 5B) dampens the seasonal $\delta^{18}\text{O}_c$ cycle, causing underestimation of
449 temperature seasonality, while a negative mean annual $\delta^{18}\text{O}_w\delta^{18}\text{O}_{sw}$ value in the List Basin biases SST
450 reconstructions towards higher temperatures. In terms of SST reconstructions, the **smoothing**, **binning**
451 and **optimization** approaches based on Δ_{47} and $\delta^{18}\text{O}_c$ data yield more accurate reconstructions, albeit with
452 a reduced seasonality and a bias towards the summer season. The latter is a result of severely reduced
453 growth rates in the winter season, which was therefore undersampled (see Fig. 5A-6A and 5C).
454 Approaches including Δ_{47} data also yield far more accurate $\delta^{18}\text{O}_w\delta^{18}\text{O}_{sw}$ estimates than the $\delta^{18}\text{O}$ approach.
455 However, the accuracy of ~~for both~~ $\delta^{18}\text{O}_w$ seasonality and mean annual $\delta^{18}\text{O}_w\delta^{18}\text{O}_{sw}$ estimates is ~~high-low~~ in
456 these approaches too, largely because of the limited sampling resolution, especially in winter. The
457 **optimization** approach suffers ~~especially~~ from the strong in-phase relationship between SST and SSS,
458 which obscures the difference between the $\delta^{18}\text{O}_w\delta^{18}\text{O}_{sw}$ effect and the temperature effect on shell
459 carbonate. Yet, disentangling SST from $\delta^{18}\text{O}_w\delta^{18}\text{O}_{sw}$ seasonality is central to the success of the approach
460 (see 3.4). Fig. 5D-6D does not show the reproducibility error on SST and $\delta^{18}\text{O}_w\delta^{18}\text{O}_{sw}$ estimates, which is
461 much larger for the **smoothing** approach than for the **binning** and **optimization** approaches due to the
462 limited data in the winter seasons (see S5).

463 These results ~~highlight-show~~ that several properties of carbonate archives, such as growth rate variability,
464 phase relationships between SST and $\delta^{18}\text{O}_w\delta^{18}\text{O}_{sw}$ seasonality and sampling resolution, can ~~negatively~~
465 impact the reliability of paleoseasonality reconstructions. The virtual and real data cases in this study were
466 tailored to test the effects of these archive properties more thoroughly.

Formatted: Line spacing: Multiple 1.08 li

Formatted: Font: (Default) Arial, 10 pt



467

468 **Figure 56:** (A) Plot of $\delta^{18}\text{O}_c$ and (virtual) Δ_{47} data from a modern Pacific oyster (*Crassostrea gigas*; see
 469 Ullmann et al., 2010). (B) shows SST and $\delta^{18}\text{O}_{sw}$ data from the List Basin (Denmark) in which the
 470 oyster grew. (C) shows the fit between $\delta^{18}\text{O}_c$ data and modelled $\delta^{18}\text{O}_c$ calculated from SST and $\delta^{18}\text{O}_{sw}$
 471 on which the shell age model was based. (D) Shows a summary of the results of different approaches for
 472 reconstructing SST and $\delta^{18}\text{O}_{sw}$ from the $\delta^{18}\text{O}_c$ and Δ_{47} data. The vertical colored bars show the
 473 reconstructed seasonal variability using all methods with ticks indicating warmest month, coldest month,
 474 and annual mean. The grey horizontal bars show the actual seasonal variability in the environment.
 475 Precision errors on monthly reconstructions are not shown but are given in [S5S4](#).

476

477 3.2-2 Case-specific results

478 A case-by-case breakdown of the precision (Fig. 67) and accuracy (Fig. 78) of reconstructions using the
 479 four approaches shows that reliability of reconstructions varies significantly between approaches and is
 480 highly case-specific. In general, precision is highest in $\delta^{18}\text{O}$ reconstructions, followed by optimization and
 481 binning with smoothing generally yielding the worst precision. Average precision standard deviations of
 482 the underperforming methods (binning and smoothing) are up to 2-3 times larger than those of $\delta^{18}\text{O}$ (e.g.
 483 respectively 3.9°C and 3.5°C vs. 1.3°C for $\delta^{18}\text{O}$ MAT reconstructions; see also [Supplementary](#)
 484 [Information](#)). It is worth noting that precision on $\delta^{18}\text{O}$ -based estimates is mainly driven by measurement

Formatted: Font: (Default) Arial, 10 pt

Formatted: Font: (Default) Arial

Formatted: Font: (Default) Arial, 10 pt

Formatted: Font: (Default) Arial

Formatted: Font: (Default) Arial

Formatted: Font: (Default) Arial, 10 pt

Formatted: Font: (Default) Arial, 10 pt

Formatted: Font: (Default) Arial

485 precision (which is better for $\delta^{18}\text{O}_e$ than for Δ_{47} measurements, see section 45.1.1), while Δ_{47} -based
486 reconstructions lose precision due to the higher measurement error on Δ_{47} measurements and the method
487 used for combining measurements for seasonality reconstructions. On a case-by-case basis, the hierarchy
488 of approaches can differ, especially if strong variability in growth rate is introduced, such as in case 14,
489 where the size of hiatuses in the record increases progressively, or in case 18, in which half of the year is
490 missing due to growth hiatuses (see Table 1, S1 and S5S4). Between the Δ_{47} -based methods
491 (smoothing, binning and optimization), optimization is rarely outcompeted in terms of precision in both
492 SST and $\delta^{18}\text{O}_w\delta^{48}\text{O}_{sw}$ reconstructions.

Formatted: Font: (Default) Arial, 10 pt

493 The comparison based on precision alone is misleading, as the most precise approach which is most
494 precise ($\delta^{18}\text{O}$) runs the risk of being highly inaccurate (offsets exceeding 4°C on some MAT reconstructions;
495 see Fig. 7C), especially in cases based on natural SST and SSS (case 30-33). The smoothing approach
496 also often yields highly inaccurate results, especially in cases with substantial variability in $\delta^{18}\text{O}_w\delta^{48}\text{O}_{sw}$
497 (e.g. case 9-11). Accuracy of optimization and binning outcompete the other methods in most

Formatted: Font: (Default) Arial, 10 pt

498 circumstances. Binning outperforms optimization in reconstructions of $\delta^{18}\text{O}_w\delta^{48}\text{O}_{sw}$ seasonality, making
499 it overall the most accurate approach. Interestingly, optimization is less accurate specifically in cases with
500 sharp changes in growth rate in summer (e.g. cases 11, 14, 16 and 17), with while binning performing

Formatted: Font: (Default) Arial, 10 pt

501 performs better in these cases. Reconstructions of mean annual SST and $\delta^{18}\text{O}_w\delta^{48}\text{O}_{sw}$ of in case 18 are
502 especially inaccurate regardless of which method is applied. This extreme case with hiatuses lasting growth
503 only during one half of the year combined with seasonal fluctuations in both SST and $\delta^{18}\text{O}_w\delta^{48}\text{O}_{sw}$ presents

Formatted: Font: (Default) Arial, 10 pt

504 a worst-case scenario for seasonality reconstructions leading to strong biases in mean annual temperature
505 reconstructions. In situations like case 18, the optimization approach is most accurate in MAT and SST
506 seasonality reconstructions, but $\delta^{18}\text{O}_w\delta^{48}\text{O}_{sw}$ is more accurately reconstructed using the binning approach.

Formatted: Font: (Default) Arial, 10 pt

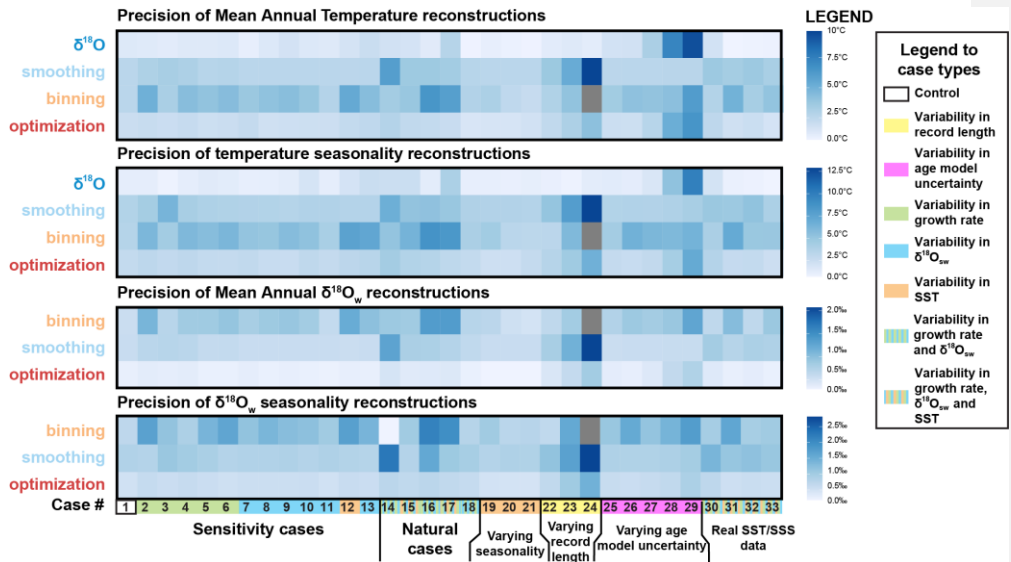
507 Finally, it is worth noting that in natural situations (Fig. 3), variability in SST almost invariably has a larger
508 influence on $\delta^{18}\text{O}_e$ and Δ_{47} records than $\delta^{18}\text{O}_w$, such that fluctuations in $\delta^{18}\text{O}_e$ records closely follow the
509 SST seasonality even in cases with relatively large $\delta^{18}\text{O}_w\delta^{48}\text{O}_{sw}$ variability (e.g. case 30). Chronologies

Formatted: Subscript

Formatted: Font: (Default) Arial, 10 pt

510 based on these $\delta^{18}\text{O}_e$ fluctuations are therefore generally accurate.

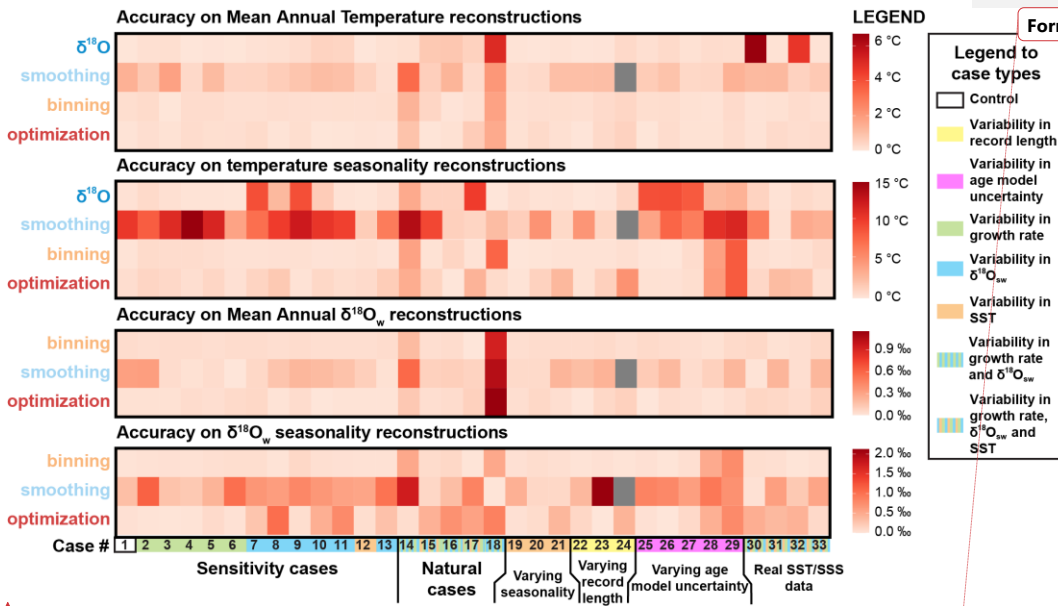
511



513

Formatted: Width: 8.5", Height: 11"

514 **Figure 67:** Overview of precision (propagated standard deviation of variability within reconstructions, see
 515 [2.2](#)) of reconstructions of mean annual temperature (A), seasonal temperature range (B), mean annual
 516 $\delta^{18}O_w$ (C) and seasonal range in $\delta^{18}O_w$ (D), with higher values (darker colors) indicating lower precision
 517 (more variability between reconstructions) based on average sampling resolution (sampling interval of 0.45
 518 mm). The different cases on the horizontal axis are color coded by their difference from the control case
 519 (case 1; see legend on the right-hand side). Grey boxes indicate cases for which reconstructions were not
 520 successful. All data on precision Overview of precision (one standard deviation) of reconstructions of mean
 521 annual $\delta^{18}O_{sw}$ (A), seasonal range in $\delta^{18}O_{sw}$ (B), mean annual SST (C) and seasonal range in SST (D),
 522 with higher values indicating lower precision (higher precision errors) based on average sampling resolution
 523 (sampling interval of 0.45 mm). The horizontal axis displays the different cases, color coded by their
 524 difference from the control case (case 1; see legend on the left-hand side). Colored lines indicate the
 525 different data treatment approaches. Box-whisker plots to the right show medians and distributions of
 526 precision on cases using different reconstruction approaches (outliers are identified as black dots based on
 527 2x interquartile distance). Color coding follows the scheme in Fig. 1. (standard deviation values) is provided
 528 in [Supplementary data4](#).

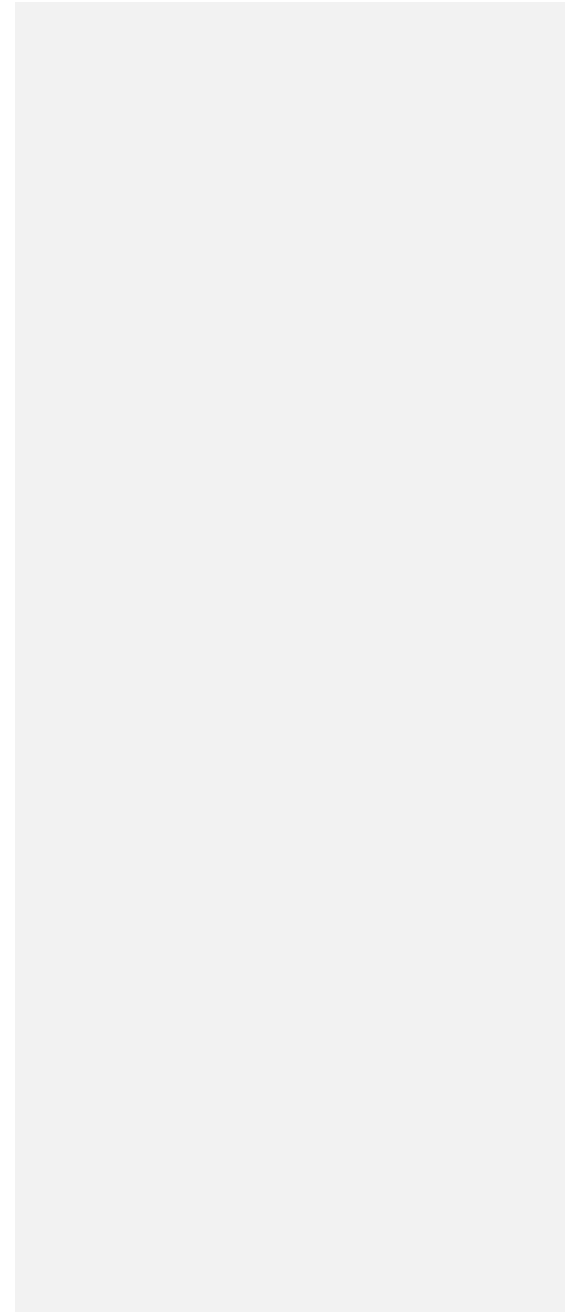


Formatted: Font: (Default) Arial, 10 pt

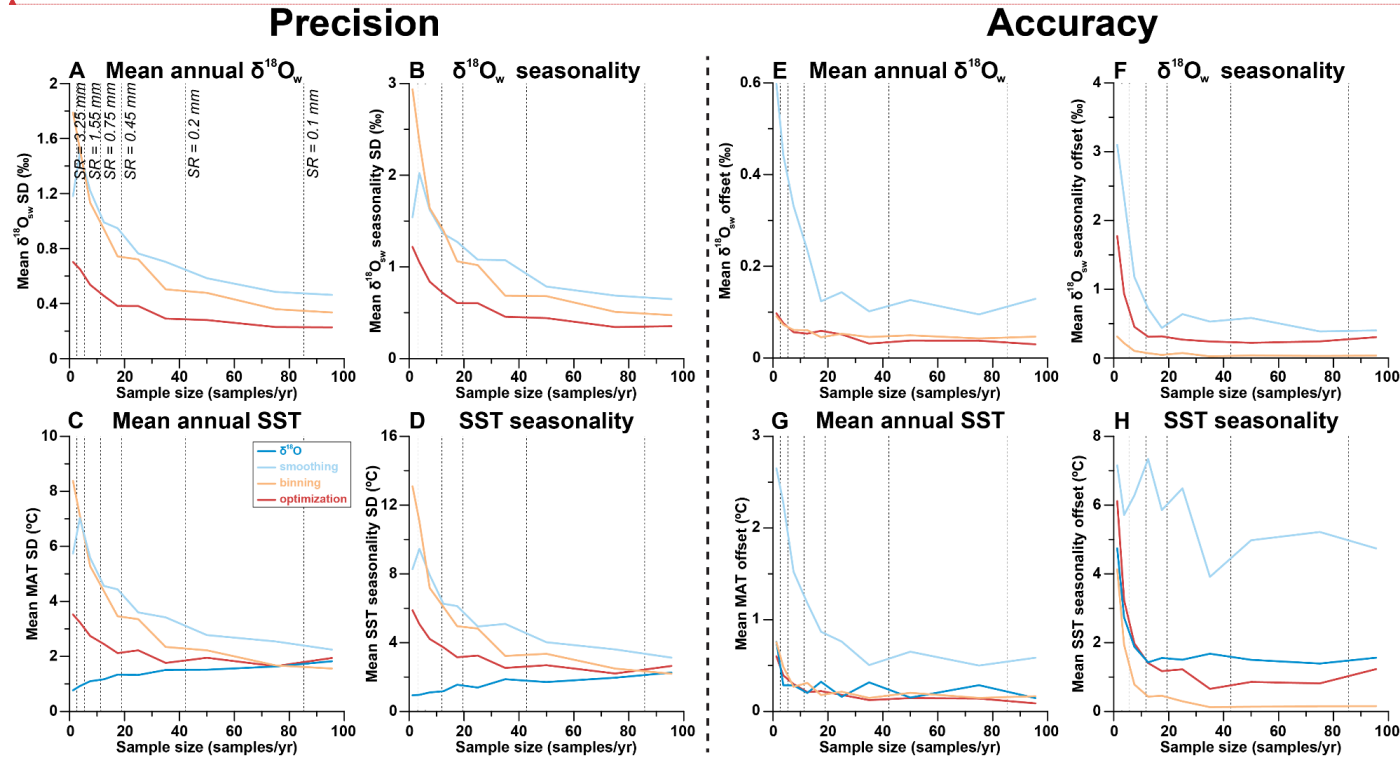
529

530 **Figure 78:** Overview of accuracy (absolute offset from actual "true" values) of reconstructions of mean
 531 annual $\delta^{18}O_w$, $\delta^{18}O_{sw}$, temperature (A), seasonal temperature range in $\delta^{18}O_w$, $\delta^{18}O_{sw}$ (B), mean annual
 532 $\delta^{18}O_w$, SST (C) and seasonal range in $\delta^{18}O_w$, SST (D), with higher values (darker colors) indicating lower
 533 accuracy (higher offsets) based on average sampling resolution (sampling interval of 0.45 mm). The
 534 horizontal axis displays the different cases on the horizontal axis, are color coded by their difference from
 535 the control case (case 1; see legend on the left/right-hand side). Box-whisker plots to the right show
 536 medians and distributions of accuracy on cases using different reconstruction approaches (outliers are
 537 identified as black dots based on 2x interquartile distance). Color coding follows the scheme in Fig. 1 and
 538 Fig. 6. Grey boxes indicate cases for which reconstructions were not successful. All data on accuracy
 539 (difference between reconstructed and "true" values) is provided in [Supplementary data4](#).

Formatted: Font: Italic



Formatted: Font: (Default) Arial, 10 pt



541

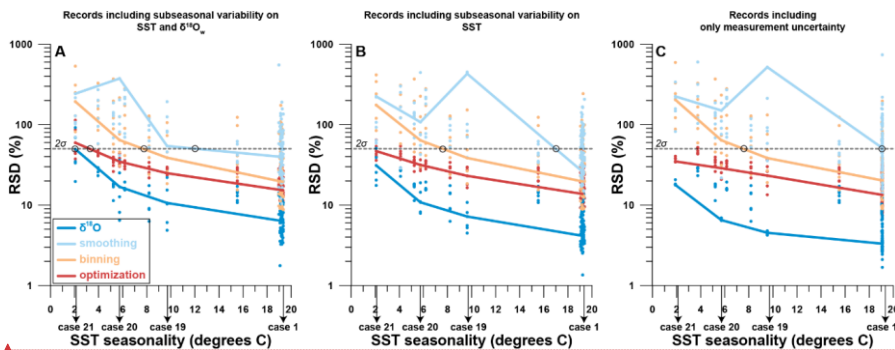
542 **Figure 89:** Effect of sampling resolution (in samples per year, see S5) on the precision (one standard deviation) of results of reconstructions of mean
543 annual $\delta^{18}\text{O}_w$ $\delta^{18}\text{O}_w$ (A), seasonal range in $\delta^{18}\text{O}_w$ $\delta^{18}\text{O}_w$ (B), mean annual SST (C) and seasonal range in SST (D). Effect on the accuracy (absolute
544 offset from actual value) of results of reconstructions of mean annual $\delta^{18}\text{O}_w$ $\delta^{18}\text{O}_w$ (E) and seasonal range in $\delta^{18}\text{O}_w$ $\delta^{18}\text{O}_w$ (F), mean annual SST (G)
545 and seasonal range in SST (H). Color coding follows the scheme in Fig. 1 and Fig. 4.

Formatted: Font: (Default) Arial, 10 pt, Italic

546 **4.3.3 Effect of sampling resolution**

547 As expected, increasing the temporal sampling resolution (i.e. number of samples per year) almost
548 invariably increases the precision and accuracy (Fig. 89) of reconstructions using all methods. An exception
549 to this rule is the precision of $\delta^{18}\text{O}$ reconstructions, which decreases with increasing sampling resolution.
550 Precision errors of all Δ_{47} -based approaches eventually converge with the initially much lower precision
551 error of $\delta^{18}\text{O}$ reconstructions when sampling resolution increases. However, the sampling resolution ~~that is~~
552 required for Δ_{47} -based reconstructions to rival or outcompete the $\delta^{18}\text{O}$ reconstructions differs, with
553 **optimization** requiring lower sampling resolutions than the other methods (e.g. 20-40 samples/year
554 compared to 40-80 ~~samples~~ samples/year for **smoothing** and **binning**; Fig. 8A9A-D). Accuracy also
555 ~~decreases~~ improves with sampling resolution (Fig. 8E9E-H). When grouping all cases together, it becomes
556 clear that $\delta^{18}\text{O}$ reconstructions can only approach the accuracy of Δ_{47} -based approaches for
557 reconstructions of MAT. Seasonality in both SST and $\delta^{18}\text{O}_{\text{w}}/\delta^{18}\text{O}_{\text{sw}}$ is most accurately reconstructed using
558 **binning**, and the **smoothing** approach once again performs worst.

Formatted: Font: (Default) Arial, 10 pt



Formatted: Font: (Default) Arial, 10 pt

560 **Figure 910:** Effect of SST seasonality range (difference between warmest and coldest month) in the record
561 on the relative precision of SST seasonality reconstructions (*"RSD" defined as one standard deviation*
562 *divided by the mean value*). Panel A shows precision results if random variability ("weather patterns") in
563 both SST and $\delta^{18}\text{O}_{\text{w}}/\delta^{18}\text{O}_{\text{sw}}$ as well as measurement uncertainty is added to the records (see 32.1.13.3 and
564 S1). Panel B shows precision of records with random variability in SST and measurement uncertainty only.
565 Panel C shows precision if only measurement uncertainty is considered. Color coding follows the scheme
566 in Fig. 1 and Fig. 4. Shaded dots represent results at various sampling resolutions, while bold lines are
567 averages for all reconstruction approaches. Black circles highlight the places where curves cross the
568 threshold of two standard deviations, which indicates the minimum SST seasonality that can be resolved
569 within 2 standard deviations (~95% confidence level) using the reconstruction approach.

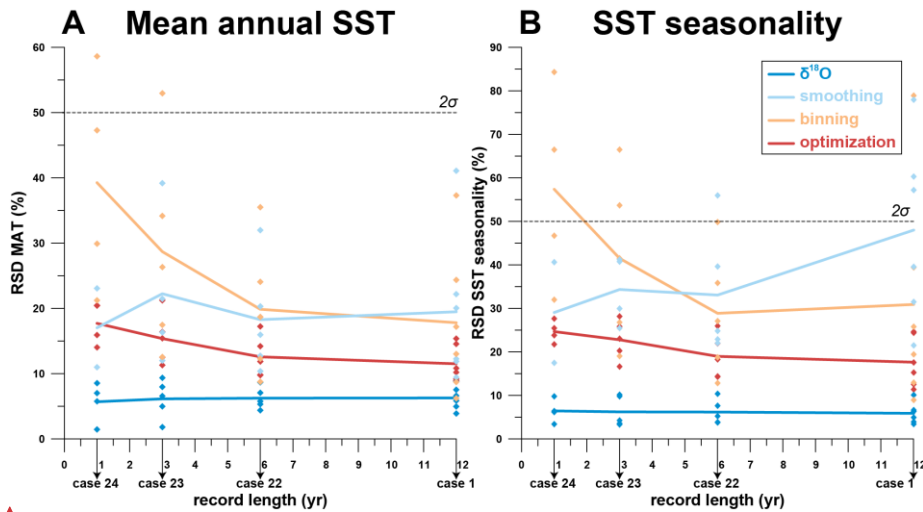
Formatted: Font: (Default) Arial, 10 pt, Italic

570

571 **4.3.4 Resolving SST seasonality**

572 Comparison of cases 19, 20 and 21 (SST seasonality of 9.7°C, 5.7°C and 2.1°C respectively) with control
573 case 1 (SST seasonality of 19.3°C) ~~allowed us to study~~shows how changes in the seasonal SST range
574 affect the precision of measurements (**Fig. 910**; see also **Table 1 and S1**). The data reconfirms that $\delta^{18}\text{O}$
575 reconstructions are most precise; a deceptive statistic given the risk of highly inaccurate results this
576 approach yields (see **Fig. 78**). Taking into consideration only analytical uncertainty, all approaches except
577 for **smoothing** can confidently resolve at least the highest SST seasonality within a significance level of
578 two standard deviations (~95%) using a moderate sampling resolution (mean of all resolutions shown in
579 **Fig. 10**). Increasing sampling resolution improves the precision of Δ_{47} -based reconstructions (see **Fig.**
580 **8D9D**), so high sampling resolutions (0.1 or 0.2 mm) allow smaller seasonal differences to be resolved.
581 When random sub-annual variability is added to the SST and $\delta^{18}\text{O}_w$ / $\delta^{18}\text{O}_{sw}$ records (see **3.1.32.3.3 and S4**),
582 the minimum seasonal SST extent that can be resolved decreases for all approaches (**Fig. 9B-10B** and
583 **9C10C**). Nevertheless, $\delta^{18}\text{O}$ and **optimization** reconstructions remain able to resolve a relatively small
584 SST seasonality of 2-4°C, ~~even with all noise added to the records.~~

Formatted: Font: (Default) Arial, 10 pt



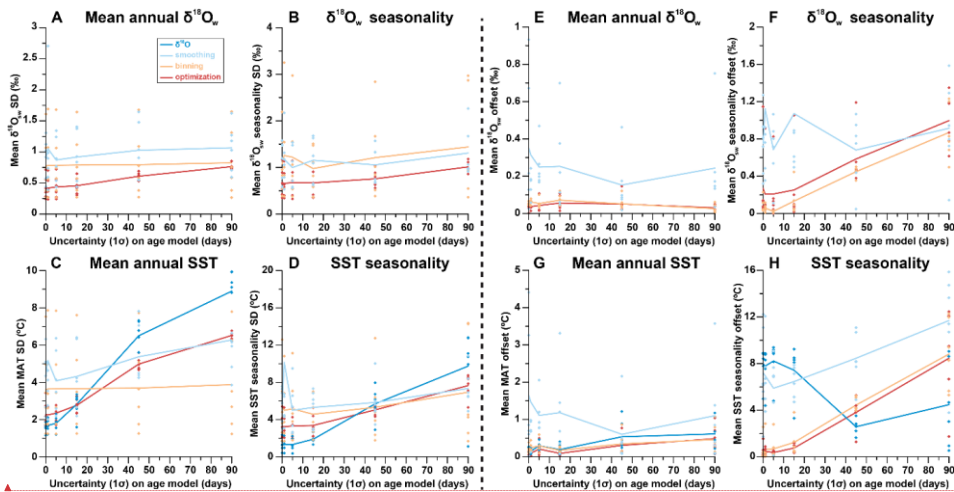
586 **Figure 10-11:** Effect of record length (in years) on the relative precision (one standard deviation as fraction
 587 of the mean value) of results of reconstructions of mean annual SST (**A**) and SST seasonality (**B**). Shaded
 588 dots represent results for the six different sampling resolutions. Solid lines connect averages for cases 1,
 589 22, 23 and 24 for each reconstruction approach. *Color-coding follows the scheme in Fig. 1 and Fig. 4.*
 590

591

592 43.5 Effect of record length

593 The effect of variation in the length of the record was investigated by comparing cases 22, 23 and 24 (record
 594 lengths of 6 years, 3 years and 1 year, respectively) with the control case (record length of 12 years; see
 595 Fig. 10-11 and S1Table 1). As expected, the precision of MAT and SST seasonality results
 596 reconstructions slightly increases in larger datasets (longer records) for optimization and
 597 binning. However, this pattern is not clear but not in for smoothing and $\delta^{18}\text{O}$ reconstructions. The
 598 differences between reconstruction approaches remains relatively constant regardless of the length of the
 599 record, with general precision hierarchy remaining intact ($\delta^{18}\text{O}$ > optimization > binning > smoothing).
 600 An exception occurs in the case of however, in very short records (1-2 years); where the smoothing gains
 601 an advantage over other Δ_{47} -based methods due to its lack of sensitivity to changes in the record length.
 602 For very short (<3 yr) records, and binning reconstructions are not precise enough to resolve MAT and
 603 SST seasonality within two standard deviations (~95% confidence level). Most of the variation in precision
 604 with record length is largely driven by very high precision errors of reconstructions based on records with

605 low sampling resolutions (sampling intervals of 1.55 mm or 3.25 mm; see also Fig. 8A9A-D). As a result,
 606 most of the reduction in precision in shorter records can be mitigated by denser sampling.



607 **Figure 14.12:** Effect of uncertainty in age model on the reproducibility (standard deviation on estimate) of
 608 results of reconstructions of mean annual $\delta^{18}\text{O}_{\text{sw}}$ (A) and seasonal range in $\delta^{18}\text{O}_{\text{sw}}$ (B), mean
 609 annual SST (C) and seasonal range in SST (D). Effect of uncertainty in age model on the accuracy (offset
 610 from true value) of results of reconstructions of mean annual $\delta^{18}\text{O}_{\text{sw}}$ (E) and seasonal range in
 611 $\delta^{18}\text{O}_{\text{sw}}$ (F), mean annual SST (G) and seasonal range in SST (H). Color coding follows the scheme
 612 in Fig. 1 and Fig. 4.

613
 614
 615 **43.6 Effect of age model uncertainty**
 616 Uncertainty on the age model has a significant effect on both the precision and the accuracy (Fig. 14.12) of
 617 reconstructions using all approaches. The $\delta^{18}\text{O}$ reconstructions are most strongly affected by uncertainties
 618 in the age model and suffer from a large decrease in precision with increasing age model uncertainty (Fig.
 619 14.12C-D). The high reproducibility of the $\delta^{18}\text{O}$ approach in comparison with the Δ_{47} approaches quickly
 620 disappears when age model uncertainty increases beyond 20-30 days. Interestingly, the accuracy of
 621 $\delta^{18}\text{O}$ -based SST seasonality reconstructions based on $\delta^{18}\text{O}$ initially improves with age model uncertainty
 622 (Fig. 14.12H). However, this observation is likely caused by the fact that age model uncertainty was
 623 compared based on conditions in case 9, which features a phase offset between SST and $\delta^{18}\text{O}_{\text{sw}}$
 624 seasonality causing the $\delta^{18}\text{O}$ method to be highly inaccurate even without age model uncertainty. The

Formatted: Font: (Default) Arial, 10 pt

Formatted: Font: (Default) Arial, 10 pt, Italic

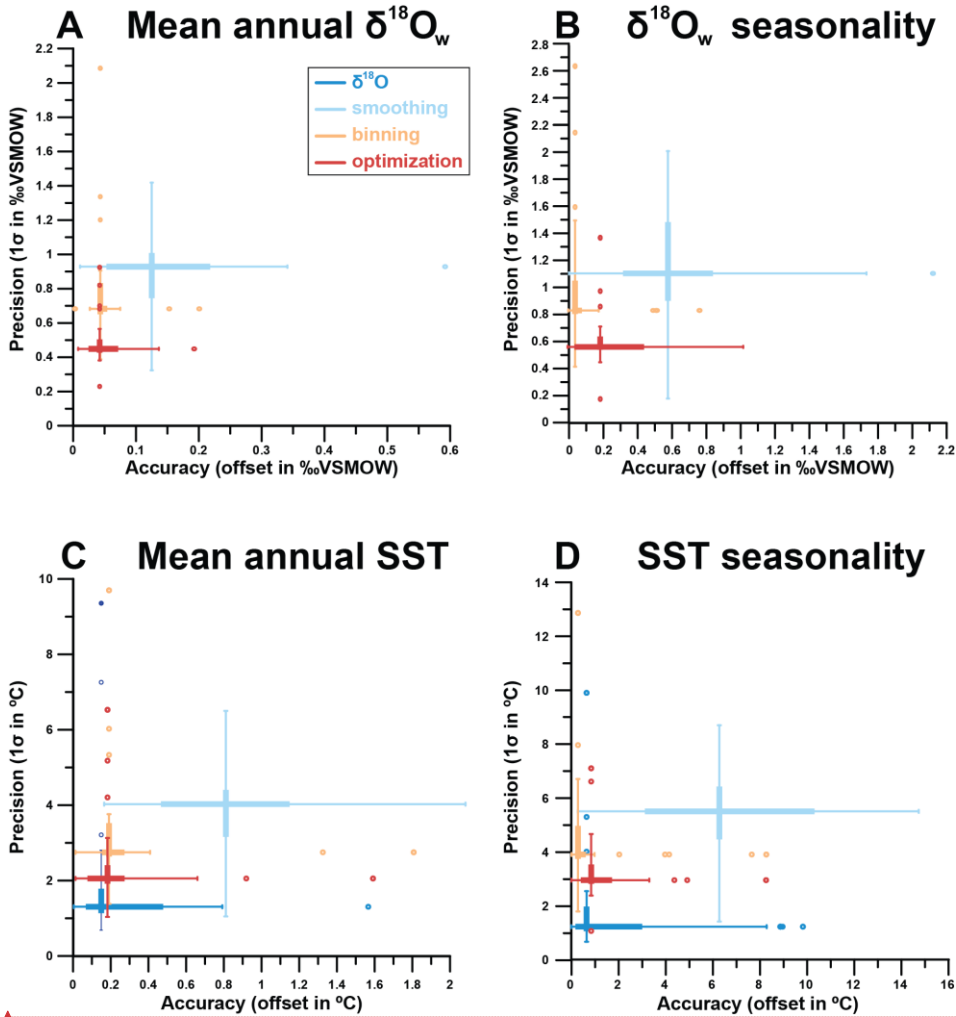
Formatted: Font: Not Bold

Formatted: Font: (Default) Arial, 10 pt

625 precision of **smoothing** and **optimization** approaches also decreases with increasing age model
626 uncertainty (Fig ~~41A12A-D~~), and the **optimization** approach loses its precision advantage over the
627 **binning** and **smoothing** approaches when age model uncertainty increases beyond 30 days. The monthly
628 **binning** approach ~~is is verymost robust, and its precision does not significantly decrease with resilient~~
629 ~~against~~ increasing age model uncertainty. Seasonality reconstructions through both the **binning** and
630 **optimization** approach quickly lose accuracy when age model uncertainty increases. ~~The but the~~ accuracy
631 of the **smoothing** approach remains the worst of all approaches in regardless of age model uncertainty
632 (Fig. ~~41E12E-H~~).

633

634



635

636 **Figure 4213:** Overview of averages and ranges of accuracy (absolute offset from real value) and precision
 637 (one standard deviation from the mean) on mean annual $\delta^{18}\text{O}_w$ (A) and seasonal range in
 638 $\delta^{18}\text{O}_w$ (B), mean annual SST (C) and seasonal range in SST (D) within all cases using the four
 639 different reconstruction approaches. Color coding follows the scheme in Fig. 1 and Fig. 4. Box-whisker
 640 plots for precision and accuracy cross at their median values and outliers (colored symbols) are identified
 641 based on 2x the interquartile difference (see Fig. 6 and 7).

642

Formatted: Font: (Default) Arial, 10 pt

Formatted: Font: (Default) Arial, 10 pt, Italic

Formatted: Font: (Default) Arial, 10 pt, Italic

643 **5.4. Discussion**

644 **5.4.1 Performance of reconstruction approaches**

645 **5.4.1.1 $\delta^{18}O_c$ vs Δ_{47} -based reconstructions**

646 A summary of the general reliability of the four approaches is shown in **Figure 12-13** summarizes the
647 general reliability of the four approaches. The $\delta^{18}O$ reconstructions are generally less accurate than Δ_{47} -
648 based reconstructions (especially **binning** and **optimization**; see **Fig 12** and see also **S40S9**). This is a
649 consequence of the assumption that $\delta^{18}O_w\delta^{18}O_{sw}$ remains constant year-round, and that we one knows its
650 true value. Both these assumptions are problematic in absence of independent evidence of the value of
651 $\delta^{18}O_w\delta^{18}O_{sw}$, especially in deep time settings (see e.g. Veizer and Prokoph, 2015; Henkes et al., 2018).
652 The risk of this assumption is made clear when comparing cases in which $\delta^{18}O_w\delta^{18}O_{sw}$ is indeed constant
653 year-round at the assumed value (0‰ **VSMOW**; e.g. cases 1-6 and 19-24) with cases in which shifts in
654 $\delta^{18}O_w\delta^{18}O_{sw}$ occur, especially when these shifts are out of phase with respect to the SST seasonality (e.g.
655 cases 9-11, 18 and 25-33; **Fig. 7C8C-D**). Cases mimicking or based on natural SST and SSS variability
656 (cases 14-18 and 30-33) as well as the modern oyster data (**Fig. 56**) yield stronger inaccuracies in MAT
657 and seasonality reconstructions, showing that even in many modern natural circumstances the assumption
658 of constant $\delta^{18}O_w\delta^{18}O_{sw}$ is problematic.

659 It is important to consider that the value of mean annual $\delta^{18}O_w\delta^{18}O_{sw}$ remained very close to the assumed
660 value of 0‰ **VSMOW** (within 0.15‰) in all cases except for natural data cases 30 (-1.55‰ **VSMOW**), 32
661 (1.01‰ **VSMOW**; see **S5**) and the real oyster data (-1.42‰ **VSMOW**; **Fig. 5**). The SST values of these cases
662 reconstructed using $\delta^{18}O_c$ data show large offsets from their actual values (+6.7°C, -4.7°C and +10.3°C for
663 case 30, case 32 and the real oyster data respectively; see **Fig. 5-6 and 78C** and **S5**). These offsets are
664 equivalent to the temperature offset one might expect from inaccurately estimating $\delta^{18}O_w\delta^{18}O_{sw}$ (-4.6
665 °C/‰ **VSMOW**; Kim and O'Neil, 1997) and are only rivaled by the offset in **MAT** reconstructions of case 18
666 (+5.0°C), which has growth hiatuses obscuring the coldest half of the seasonal cycle. The fact that such
667 differences in $\delta^{18}O_w\delta^{18}O_{sw}$ exist even in modern environments should not come as a surprise, given the
668 available data on variability of $\delta^{18}O_w\delta^{18}O_{sw}$ (at least -3‰ to +2‰ **VSMOW**; e.g. LeGrande and Schmidt,
669 2006) and SSS (30 to 40; ESA, 2020) in modern ocean basins. However, it should warrant caution in using

Formatted: Font: (Default) Arial, 10 pt

670 $\delta^{18}\text{O}_c$ data for SST reconstructions even in modern settings. Implications for deep time reconstructions are
671 even greater, given the uncertainty on and variability in global average (let alone local) $\delta^{18}\text{O}_w\delta^{18}\text{O}_{sw}$ values
672 (Jaffrés et al., 2007; Veizer and Prokoph, 2015). The complications of using $\delta^{18}\text{O}_c$ as a proxy for marine
673 temperatures in deep time are discussed in detail in O'Brien et al. (2017), and Tagliavento et al. (2019).
674 The analytical uncertainty of individual $\delta^{18}\text{O}_c$ aliquots (typically 1 S.D. of 0.05‰; e.g. de Winter et al., 2018)
675 represents only ~1.1% of the variability in $\delta^{18}\text{O}_c$ over the seasonal cycle (~4.3‰ for the default 20°C
676 seasonality in case 1, following Kim and O'Neil, 1997). This is much smaller than the analytical uncertainty
677 of Δ_{47} (typically 1 S.D. of 0.02-0.04‰; e.g. Fernandez et al., 2018; de Winter et al., 2020b), which equates
678 to 25-50% of the seasonal variability in Δ_{47} (~0.08‰ for 20°C seasonality, following Bernasconi et al., 2018;
679 see S8S7). This roughly 20-fold difference in relative precision causes $\delta^{18}\text{O}_c$ based SST reconstructions to
680 be much more precise (see Figs 67, 89-112) than those based on Δ_{47} , and forces the necessity for grouping
681 Δ_{47} data in reconstructions. However, as discussed above, the low-high precision of $\delta^{18}\text{O}$ reconstructions
682 is misleading and not a misleading useful-statistic if they are highly inaccurate.

683 Our results show that paleoseasonality reconstructions based on $\delta^{18}\text{O}_c$ can only be relied upon if there is
684 strong independent evidence of the value of $\delta^{18}\text{O}_w\delta^{18}\text{O}_{sw}$ and if significant sub-annual variability in
685 $\delta^{18}\text{O}_w\delta^{18}\text{O}_{sw}$ (>0.3‰, equivalent to a 2-3°C SST variability; see Fig. 8-99-10; Kim and O'Neil, 1997) can be
686 neglected-excluded with confidence. Examples of such cases include fully marine environments unaffected
687 by influxes of (isotopically light) freshwater or evaporation (increasing $\delta^{18}\text{O}_w\delta^{18}\text{O}_{sw}$; Rohling, 2013).
688 Carbonate records from suitable-environments includewith more stable $\delta^{18}\text{O}_w$ conditions include, for
689 example, the *A. islandica* bivalves from considerable depth (30-50m) in the open marine Northern Atlantic
690 (e.g. Schöne et al., 2005, on which case 33 is based). However, even here variability in $\delta^{18}\text{O}_{sw}$ due to, for
691 example, shifting influence of different bottom water masses cannot be fully excluded. Previous
692 reconstruction studies show that $\delta^{18}\text{O}_w\delta^{18}\text{O}_{sw}$ in smaller basins such as the Western Interior Seaway-are
693 heavily influenced by the processes affecting $\delta^{18}\text{O}_w\delta^{18}\text{O}_{sw}$ on smaller scales, such as local evaporation and
694 freshwater influx from nearby rivers (e.g. Surge et al., 2001; Petersen et al., 2016). Consequently, accurate
695 quantitative reconstructions of seasonal range in shallow marine environments with extreme seasonality

Formatted: Font: (Default) Arial, 10 pt

Formatted: Not Highlight

Formatted: Font: (Default) Arial, 10 pt

696 may not be feasible using the $\delta^{18}\text{O}$ approach, because these environments are invariably characterized by
697 significant fluctuations in $\delta^{18}\text{O}_w\delta^{18}\text{O}_{sw}$ and growth rate.

Formatted: Font: (Default) Arial, 10 pt

698 While variability in $\delta^{18}\text{O}_w\delta^{18}\text{O}_{sw}$ compromises accurate $\delta^{18}\text{O}$ -based seasonality reconstructions, the
699 compilation in **Fig. 3** shows that its influence on the $\delta^{18}\text{O}$ records is too small to affect the shape of the
700 record to such a degree that seasonality is fully obscured. While natural situations with $\delta^{18}\text{O}_w\delta^{18}\text{O}_{sw}$
701 fluctuations large enough to totally counterbalance the effect of temperature seasonality on $\delta^{18}\text{O}$ records
702 are imaginable, these cases are likely rare. This means that chronologies based on $\delta^{18}\text{O}$ seasonality, which
703 are a useful tool to anchor seasonal variability in absence of independent growth markers (e.g. Judd et al.,
704 2018; [de Winter, 2021b](#)), are reliable in most natural cases.

Formatted: Font: (Default) Arial, 10 pt

Formatted: Font: (Default) Arial, 10 pt

705 5.4.1.2 Seasonality reconstructions using moving averages (smoothing)

706 Of the three methods for combining Δ_{47} data, the **smoothing** approach clearly performs worst in all four
707 reconstructed parameters (MAT, SST seasonality, mean annual $\delta^{18}\text{O}_w\delta^{18}\text{O}_{sw}$ and $\delta^{18}\text{O}_w\delta^{18}\text{O}_{sw}$ seasonality),
708 both in terms of accuracy and precision (**Fig. 4213**). While applying a moving average may be a good
709 strategy for lowering the uncertainty of Δ_{47} -based temperature reconstructions in a long time series (e.g.
710 Rodríguez-Sanz et al., 2017), the method underperforms in cases where baseline and amplitude of a
711 periodic component, ~~spike or event~~ (e.g. MAT and SST seasonality) are extracted from a record. This is
712 likely due to the smoothing effect of the moving average, which reduces the seasonal cycle and causes
713 highly inaccurate seasonality reconstructions (offsets mounting to $>6^\circ\text{C}$; **Fig. 4213**). This bias is especially
714 detrimental in cases where the seasonal cycle is obscured by seasonal growth halts (e.g. case 18), multi-
715 annual trends in growth (e.g. case 4, 14 and 17) and multi-annual trends in SST (e.g. case 15 and 17; see
716 **Fig. 6-7, and Fig. and 78**). The ~~lack of poor~~ performance of the **smoothing** approach can be slightly
717 mitigated by increasing sampling resolution (**Fig 89**), but even at high sampling resolutions (every 0.1 or
718 0.2 mm) the method still fails to reliably resolve seasonal SST ranges below 5°C even in idealized cases
719 (case 19-21; **Fig. 910**). Increasing the number of samples by analyzing longer records does not improve
720 the result, because smoothing of the seasonal cycle by a moving average window introduces the same
721 dampening bias ~~as long as if~~ the temporal sampling resolution (number of samples per year) remains equal
722 (**Fig. 4011**).

Formatted: Font: (Default) Arial, 10 pt

Formatted: Font: (Default) Arial, 10 pt

Formatted: Font: Bold

Formatted: Font: Bold

723 More critically, employing the **smoothing** method may give the illusion that seasonality is more reduced,
724 and severely bias reconstructions. This bias highlights the importance of using the official meteorological
725 definition of seasonality as the difference between the averages of warmest and coldest month in
726 paleoseasonality work (O'Donnell et al., 2012). This definition is much more robust than the “annual range”
727 often cited based on maxima and minima in $\delta^{18}\text{O}_c$ records. This “annual range” strongly depends on
728 sampling resolution, which is typically $<12 \text{ samples/yr}^{-1}$ (Goodwin et al., 2003), equivalent to the third lowest
729 sampling interval (0.75 mm) simulated in this study. Therefore, we strongly recommend future studies to
730 adhere to the monthly definition of seasonality to foster comparison between studies. While inter-annual
731 variability is lost by combining data from multiple years into monthly estimates/averages of WMMT and
732 CMMT, this approach increases precision, accuracy and comparability of paleoseasonality results. Inter-
733 annual variability can still be discussed from plots of raw data against-plotted in age-or-depth/time or
734 sampling domain.

735 5.4.1.3 Monthly binning, sample size optimization and age model uncertainty

736 Overall, the most reliable paleoseasonality reconstructions can be obtained from either **binning** or
737 **optimization** (Fig. 4.2.13). In general, **optimization** is slightly more precise, while **binning** yields more
738 accurate estimates of seasonal range in SST and $\delta^{18}\text{O}_w\delta^{48}\text{O}_{sw}$ (Fig. 4.2B-13B and D). The more flexible
739 combination of aliquots in the **optimization** routine yields improved precision (especially on mean annual
740 averages) in cases where parts of the record are undersampled or affected by hiatuses and simultaneous
741 fluctuations in both SST and $\delta^{18}\text{O}_w\delta^{48}\text{O}_{sw}$ (e.g. case 3-6, 14-18, 30-33). The downside of this flexibility is
742 that in case of larger sample sizes, the seasonal variability may be dampened, like in the **smoothing**
743 approach (see 5.4.14.1.2). This apparent dampening effect may be reduced by allowing the sample size of
744 summer and winter samples to vary independently in the optimization routine, at the cost of higher
745 computational intensity due to the larger number of sample size combinations (see 2.1 and 4.2.2). The rigid
746 grouping of data in monthly bins in **binning** prevents this dampening and therefore yields slightly more
747 accurate estimates of seasonal ranges in SST and $\delta^{18}\text{O}_w\delta^{48}\text{O}_{sw}$. A caveat of **binning** is that it requires a
748 very reliable age model of the record, at least on a monthly scale. If the age model has a large uncertainty,
749 there is a risk that samples are grouped in the wrong month, which compromises the accuracy of **binning**

Formatted: Font: (Default) Arial, 10 pt

Formatted: Font: (Default) Arial, 10 pt

Formatted: Font: (Default) Arial, 10 pt

750 reconstructions, especially for reconstructions of seasonal range (Fig 4H12H). This problem is
751 exacerbated by potential phase shifts between seasonality in paleoclimate variables (SST and $\delta^{18}\text{O}_w$) and
752 calendar dates, which may occur in the presence of a reliable age model.

753 Previous authors attempted to circumvent the dating problem by analyzing high-resolution $\delta^{18}\text{O}_c$ transects
754 and subsequently sampling the seasonal extremes for clumped isotope analyses (Keating-Bitonti et al.,
755 2011; Briard et al., 2020). While this approach does not require sub-annual age models, it has several
756 disadvantages compared with the binning and optimization approaches: Firstly, it requires separate
757 sampling for $\delta^{18}\text{O}_c$ and Δ_{47} , which may not be possible in high-resolution carbonate archives due to sample
758 size limitations. Analyzing small aliquots for combined $\delta^{18}\text{O}_c$ and Δ_{47} analyses consumes less material.
759 Secondly, individual summer and winter temperature reconstructions require large (> 1.5 mg; e.g.
760 Fernandez et al., 2017) Δ_{47} samples from seasonal extremes, which causes more time-averaging than the
761 approaches combining small aliquots. Finally, the position of seasonal extremes estimated from the $\delta^{18}\text{O}_c$
762 record may not reflect the true seasonal extent if seasonal SST and $\delta^{18}\text{O}_w$ cycles are not in phase (as in
763 case 9), causing the seasonal Δ_{47} -based SST reconstructions to underestimate the temperature
764 seasonality. In such cases, $\delta^{18}\text{O}_c$ and Δ_{47} analyses on small aliquots allow the seasonality in SST and $\delta^{18}\text{O}_w$
765 to be disentangled, yielding more accurate seasonality reconstructions.

766 Techniques for establishing independent age models for climate archives range from counting of growth
767 layers or increments (Schöne et al., 2008; Huyghe et al., 2019), modelling and extracting of rhythmic
768 variability in climate proxies through statistical approaches (e.g. De Ridder et al., 2007; Goodwin et al.,
769 2009; Judd et al., 2018; de Winter, 2021b) and interpolation of uncertainty on absolute dates (e.g. Scholz
770 and Hoffman, 2011; Meyers, 2019; Sinnesael et al., 2019). While propagating uncertainty in the data on
771 which age models are based onto the age model is relatively straightforward, errors on underlying *a priori*
772 assumptions such as linear growth rate between dated intervals, (quasi-)sinusoidal forcing of climate cycles
773 and the uncertainty on human-generated data such as layer counting are very difficult to quantify (e.g.
774 Comboul et al., 2014). The uncertainty of such age models of climate records is thus difficult to assess and
775 may not be normally distributed. A simplified test of the effect of a normally distributed error on
776 the age value of each proxy data point (cases 25-29) shows that uncertainties in the age domain can

777 significantly compromise reconstructions (**Fig. 4.12**). Within the scope of this study, only the effect of
778 symmetrical, normally distributed uncertainties on an artificial case with phase decoupled SST and
779 $\delta^{18}\text{O}_w$ / $\delta^{18}\text{O}_{sw}$ seasonality (case 9) was tested. The effects of other types of uncertainties on ~~other cases the~~
780 ~~reconstructions~~ remains unknown, highlighting an unknown uncertainty in paleoseasonality and other high-
781 resolution paleoclimate studies that may introduce bias or lead to over-optimistic ~~errors-uncertainties~~ on
782 reconstructions. Future research could ~~aim to~~ quantify this unknown uncertainty by propagating estimates
783 of various types of uncertainty on depth values of samples and on the conversion ~~of from depth sampling~~
784 to time domain in age models.

785 **5.4.2 Conditions influencing success of reconstructions**

786 ~~Our results show that~~ The reliability (accuracy and precision) of SST and $\delta^{18}\text{O}_w$ / $\delta^{18}\text{O}_{sw}$ reconstructions
787 depends on case-specific conditions. The range of case studies tested in this study allowed us to evaluate
788 the effect of variability in SST, growth rate, $\delta^{18}\text{O}_w$ / $\delta^{18}\text{O}_{sw}$, sampling resolution and record length relative to
789 the control case (case 1; see **S1**). A summary of the effects of these changes is given in **Table 4.2**.

Formatted: Font: (Default) Arial, 10 pt

Formatted: Font: (Default) Arial, 10 pt

Formatted: Font: (Default) Arial, 10 pt

Variable	cases	Metric	Effect on reconstructions			
			$\delta^{18}\text{O}$	smoothing	binning	optimization
SST	12	Precision	0	+++	+	0
	15					
	17					
	19-21 30-33	Accuracy	+	+	0	+
Growth rate	2-6	Precision	+	++	++	+
	14-18					
	30-33	Accuracy	+	++	0	+
$\delta^{18}\text{O}_w$, $\delta^{18}\text{O}_{sw}$	7-11	Precision	+	++	0	0
	13-18					
	30-33	Accuracy	+++	+++	+	++
Sampling resolution	1-33	Precision	0	+++	++	++
		Accuracy	+	+	+++	+
Record length	22-24	Precision	0	0	+++	++
		Accuracy	+	0	++	++
Age model uncertainty?	25-29	Precision	+++	++	0	++
		Accuracy	+	+	++	++

Formatted: Font: (Default) Arial, Font color: Custom Color(RGB(44,123,182))

Formatted: Font color: Custom Color(RGB(44,123,182))

Formatted: Font color: Custom Color(RGB(171,217,233))

Formatted: Font color: Custom Color(RGB(253,174,97))

Formatted: Font color: Custom Color(RGB(215,25,28))

Formatted: Font: (Default) Arial, 10 pt, Bold

791 **Table 12:** Qualitative summary of the effects of changes in variables relative from the ideal case on
792 reconstructions using the four approaches. The “cases” column lists cases in which the changes in the
793 respective variable relative to the control case (case 1) were represented (see [Table 1 and S1](#)). “0” =
794 negligible effect, “+” = weak increase in uncertainty, “++” = moderate increase in uncertainty, “+++” = strong
795 increase in uncertainty. [Details on the precision and accuracy of all tests is given in S12S9.](#)

796

797 [5.4.2.1 SST variability](#)

798 Variability in water temperature most directly affects the proxies under study. By default (case 1), SST is
799 ~~taken to vary~~ varies sinusoidally around a MAT of 20°C with an amplitude of 10°C (see [3.4.12.3.3, Fig. 2](#)
800 and [S1](#)). ~~In the cases of exceptions,~~ in which multi-annual variability in SST is simulated (e.g. case 15 and
801 17), the accuracy of SST reconstructions using $\delta^{18}\text{O}$ and **optimization** are reduced, while the **binning**
802 approach is less strongly affected. Examples of such multi-annual cyclicity are El-Niño Southern Oscillation
803 (ENSO; Philander, 1983) or North Atlantic Oscillation (NOA; Hurrell, 1995). The effect is especially large in
804 case 17, which simulates a tropical environment with reduced SST seasonality and a strong multi-annual
805 cyclicity. This type of environment is analogous to the environment of tropical shallow water corals, which
806 are often used as archives for ENSO variability (e.g. Charles et al., 1997; Fairbanks et al., 1997). ~~As such,~~
807 ~~these virtual records and should be similar to analogous to~~ tropical cases from the Australian Great Barrier
808 Reef (case 31) and Red Sea (case 32; see [Fig. 6-73](#)). We therefore recommend ~~future researchers to use~~
809 [using](#) the **binning** approach on carbonate records where multi-annual cyclicity is prevalent and if a reliable

810 age model can be established for these records (as in e.g. Sato, 1999; Scourse et al., 2006; Miyaji et al.,
811 2010).

812 5.4.2.2 Growth rate variability and hiatuses

813 **Figures 76 and 78** show that variations in the growth rate of records, including the occurrence of hiatuses,
814 have a strong effect on reconstructions, especially using the **smoothing** approach. In general, hiatuses
815 and slower growth reduce precision of monthly SST and $\delta^{18}\text{O}_w$ / $\delta^{18}\text{O}_{sw}$ reconstructions by reducing mean
816 temporal sampling resolution (samples/yr; see **Fig. 89**), and because ~~specific~~ parts of the record are
817 undersampled. The effect on accuracy depends strongly on the timing of changes in growth rate or the
818 occurrence of hiatuses. Cases 2-6 simulate specific growth rate effects and can be used to test these
819 differences. The **smoothing** method is especially sensitive to changes in growth rate that take place in
820 specific seasons, such as hiatuses in winter (case 2) or summer (case 3) and growth peaks in summer
821 (case 5) or spring (case 6). The other reconstruction approaches are less affected by this bias, because
822 they generally do not mix samples from different seasons ~~and therefore produce less smoothing~~. The $\delta^{18}\text{O}$
823 method is especially well suited to deal with changes in growth rate because it does not require combining
824 different aliquots for accurate SST reconstructions. The **binning** and **optimization** approaches are slightly
825 less ~~accurate-reliable~~ in cases where growth rate decreases linearly or seasonally along the entire record
826 (cases 4-6; **Fig. 52**). ~~This likely occurs because these two methods consider all samples in the records at~~
827 ~~once, instead of only a subset at any one time (as in the smoothing method), and they are therefore more~~
828 sensitive to changes in temporal sampling resolution along the record. It is worth noting that **optimization**
829 is especially sensitive to sharp changes in growth rate in summer (e.g. cases 11, 14, 16 and 17) because
830 those conditions force the **optimization** routine to use larger sample sizes or include samples outside the
831 warmest month for summer temperature estimates. A potential solution to this problem could be to allow
832 sample sizes of summer and winter groups to vary independently in the **optimization** routine (see 2.1).
833 This would allow sample size in the undersampled season (in this case: summer) to become larger than
834 that at the other end of the $\delta^{18}\text{O}_c$ spectrum, reducing uncertainty on the more densely sampled season and
835 therefore improving the entire seasonality reconstruction.

Formatted: Font: (Default) Arial, 10 pt

Formatted: Font: Not Bold

836 A worst-case scenario ~~of reconstructions hampered by growth rate variability and hiatuses~~ is represented
837 by case 18, where the ~~entire~~ cold half of the year is not recorded. Such cases result in strong biases in
838 reconstructions of mean annual and seasonal ranges in SST and $\delta^{18}\text{O}_w$, $\delta^{48}\text{O}_{\text{sw}}$, regardless of which method
839 is used. In such extreme cases the record simply contains insufficient information to reconstruct variability
840 in growth rate, SST and $\delta^{18}\text{O}_w$, $\delta^{48}\text{O}_{\text{sw}}$, and it seems that no statistical method would enable this missing
841 information to be recovered. ~~In such cases, the only way to eliminate bias~~ solution for in these
842 reconstructions would be to establish reliable age models, independent of $\delta^{18}\text{O}$ or Δ_{47} data, which show
843 that a large part of the seasonal cycle is missing.

Formatted: Font: (Default) Arial, 10 pt

844 All methods used in this study rely on a conversion of SST and $\delta^{18}\text{O}_w$ reconstructions to the time domain
845 to define monthly time bins. This conversion breaks down in fossil examples when the seasonal cycle
846 cannot be extracted from the archive, which happens when half of the seasonal cycle or more is obscured
847 by growth hiatuses, as exemplified in case 18.

Formatted: Font: (Default) Arial, 10 pt

848 While hiatuses encompassing half of the seasonal cycle are uncommon, changes in growth rate are
849 common in accretionary carbonate archives because conditions for (biotic or abiotic) carbonate
850 mineralization often vary over time. This variability is either driven by biological constraints, such as
851 senescence (e.g. Schöne, 2008; Hendriks et al., 2012), the reproductive cycle (Gaspar et al., 1999) or
852 stress (Surge et al., 2001; Compton et al., 2007) or by variations in the environment that promote or inhibit
853 carbonate production, such as seasonal variations in temperature (Crossland, 1984; Bahr et al., 2017) or
854 precipitation (Dayem et al., 2010; Van Rampelbergh et al., 2014). In general, such conditions occur more
855 frequently in mid- to high-latitude environments than in low-latitudes, and in more coastal environments
856 rather than in open marine settings, because these environments contain stronger variations in the factors
857 that influence growth rates (e.g. temperature, precipitation or freshwater influx; e.g. Surge et al., 2001;
858 Ullmann et al., 2010). This difference was simulated in the cases representing natural variability (case 14-
859 18 and 30-33), with a accuracy in the coastal high-latitude settings (cases 16, 18 and 29) are indeed more
860 strongly affected by changes in growth rate. Because in such highly variable environments growth rate
861 variability often co-occurs with variability in $\delta^{18}\text{O}_w$, $\delta^{48}\text{O}_{\text{sw}}$, using $\delta^{18}\text{O}_c$ -based reconstructions is not advised,
862 unless $\delta^{18}\text{O}_w$, $\delta^{48}\text{O}_{\text{sw}}$ variability can be constrained or neglected (which is rare in these environments).

Formatted: Font: (Default) Arial, 10 pt

Formatted: Font: (Default) Arial, 10 pt

863 ~~An additional complications include is that that the lack of constraint on~~ growth rate variability ~~cannot~~
864 ~~always be resolved~~ because of uncertainties in the record's age model (see 4.1.3) ~~and the effect of growth~~
865 ~~rate variability on the sampling resolution. The effect of growth rate on sample size~~ time-averaging within
866 ~~samples was not specifically tested in this study, but~~ study but introduces uncertainty in practice when
867 ~~archives with variable growth rate are sampled at a constant sampling resolution in the depth domain. In~~
868 ~~this case, parts of the archive with a lower growth rate yield more time-averaged samples, potentially~~
869 ~~dampening one extreme of the seasonal cycle (e.g. Goodwin et al., 2003). Therefore, r~~ reconstructions in
870 ~~these~~ highly dynamic environments ~~may not allow all~~ it is challenging to isolate all variables that introduce
871 bias ~~to be isolated~~, and irregular variability in growth rate and $\delta^{18}\text{O}_w$ $\delta^{18}\text{O}_{sw}$ will invariably introduce
872 uncertainty in SST reconstructions, even when applying the best Δ_{47} -based approaches (e.g. **binning** and
873 **optimization**). In such examples, the results of natural variability cases (14-18 and 30-33) and of the real
874 oyster data (**Fig. 56**) ~~may~~ serve as benchmarks for the degree of uncertainty that may remain unexplained
875 in these records.

876

Formatted: Font: (Default) Arial, 10 pt

877 **5.4.2.3 Variability in $\delta^{18}\text{O}_w\delta^{18}\text{O}_{sw}$**

878 ~~Large increases in uncertainty on reconstructions are caused by variations in $\delta^{18}\text{O}_w\delta^{18}\text{O}_{sw}$ (see Fig. 6 and~~
879 ~~7).~~ As discussed in 4.1.1, these ~~variations in $\delta^{18}\text{O}_w$ variations~~ have a large effect on the accuracy of $\delta^{18}\text{O}_c$ -
880 based reconstructions, and their occurrence constitutes the main advantage of applying the Δ_{47}
881 thermometer (Eiler, 2011). However, results of cases 7-11 in Fig. 7-8 and Table 4-2 show that ~~$\delta^{18}\text{O}_w\delta^{18}\text{O}_{sw}$~~
882 variations can also bias Δ_{47} -based reconstructions, especially those of seasonal ranges and using the
883 **smoothing** approach. **Smoothing** reconstructions are biased by these ~~$\delta^{18}\text{O}_w\delta^{18}\text{O}_{sw}$~~ shifts in much the
884 same way as they are affected by shifts in growth rate (see 4.24.2). The **optimization** approach, ~~especially~~
885 ~~when used for reconstructions of $\delta^{18}\text{O}_{sw}$ seasonality,~~ is sensitive to seasonal changes in ~~$\delta^{18}\text{O}_w\delta^{18}\text{O}_{sw}$~~ in
886 antiphase with SST seasonality and by increases in ~~$\delta^{18}\text{O}_w\delta^{18}\text{O}_{sw}$~~ in summer (e.g. due to excess
887 evaporation; ~~e.g. case 11~~), ~~especially when used for reconstructions of $\delta^{18}\text{O}_w$ seasonality~~. This effect arises
888 because the **optimization** approach orders data based on $\delta^{18}\text{O}_c$ and Δ_{47} seasonality to isolate the
889 ~~$\delta^{18}\text{O}_w\delta^{18}\text{O}_{sw}$ -SST relationship. Both antiphase $\delta^{18}\text{O}_w\delta^{18}\text{O}_{sw}$ seasonality and summer evaporation dampen~~
890 the seasonal $\delta^{18}\text{O}_c$ cycle and therefore influences the reconstruction of the ~~$\delta^{18}\text{O}_w\delta^{18}\text{O}_{sw}$ -SST relationship~~.
891 A good example of this is seen in the real oyster data (Fig. 56), where ~~$\delta^{18}\text{O}_w\delta^{18}\text{O}_{sw}$~~ and SST vary in phase
892 and ~~$\delta^{18}\text{O}_w\delta^{18}\text{O}_{sw}$~~ dampens the SST seasonality. The **binning** approach is more robust against ~~$\delta^{18}\text{O}_w\delta^{18}\text{O}_{sw}$~~
893 variability that dampens the seasonal cycle and is therefore a better choice for absolute SST
894 reconstructions in environments where summer evaporation or other ~~$\delta^{18}\text{O}_w\delta^{18}\text{O}_{sw}$~~ variability in phase with
895 SST seasonality is expected to occur, if the age model is reliable enough to allow monthly binning of raw
896 data (see 4.1.3). Indeed, reconstructions from the lagoonal environment (case 16) and Red Sea case (case
897 32 which is characterized by strong summer evaporation; e.g. Titschack et al., 2010) show that **binning** is
898 the most reliable choice in these environments.

899 **5.4.2.4 Variability in sampling resolution and record length**

900 Other factors influencing the effectivity of reconstructions are the sampling resolution and the length of the
901 record. Many of the cases discussed in this study represent idealized cases with comparatively high
902 sampling resolutions over comparatively long (12 yr) paleoseasonality records, which yield large sample
903 sizes. By comparison, the typical age of mollusks, which are often used as paleoseasonality archives, is 2-

Formatted: Font: (Default) Arial, 10 pt

904 5 years (Ivany, 2012). Records with the highest sampling resolutions (0.1 and 0.2 mm) contain up to 1200
905 samples. ~~This is not an unfeasible number of samples~~Generating such records is not impossible, but it is
906 highly unlikely to be applied in paleoclimate studies given the limitation of resources (e.g. instrument time)
907 and the desire to analyze multiple records from different specimens, species, localities or ages to gain a
908 better understanding of the variability in paleoseasonality (e.g. Goodwin et al., 2003; Schöne et al., 2006;
909 Petersen et al., 2016). In some cases large datasets are meticulously collected from single carbonate
910 records (e.g. Schöne et al., 2005; Vansteenberge et al., 2016; de Winter et al., 2020a; Shao et al., 2020).
911 However, in such studies, the aim is often to investigate variability at a higher (e.g. daily; de Winter et al.,
912 2020a) resolution or longer timescales (e.g. decadal to millennial; Schöne et al., 2005; Vansteenberge et
913 al., 2016; Shao et al., 2020) in addition to the seasonal cycle, rather than to improve the reliability of
914 reconstructing one type of variability (e.g. seasonality) alone. ~~In this study, extreme (sometimes unnatural,
915 e.g. case 18) cases were chosen deliberately to explore the effect of different conditions and guide
916 researchers in deciding their sampling strategy to optimize their samples and resources in function to their
917 various research goals.~~

918 **Fig. 8-9** shows that increasing temporal sampling resolution (samples/yr) improves both the accuracy and
919 precision of all Δ_{47} -based reconstructions. This occurs because Δ_{47} samples have a large analytical
920 uncertainty (see **54.1.2**) and grouping of data therefore improves reconstructions. ~~Interestingly, The
921 decrease in precision in of $\delta^{18}\text{O}_c$ -based reconstructions precision decreases with increasing sample size
922 while accuracy increases (Fig. 8C9C-D). This~~ is explained by the fact that the analytical uncertainty of $\delta^{18}\text{O}_c$
923 measurements is much smaller than the variability introduced by natural sub-annual variability in SST and
924 ~~$\delta^{18}\text{O}_w$ $\delta^{18}\text{O}_{sw}$~~ unrelated to the seasonal cycle (see **S4**). Therefore, higher sampling resolutions allow $\delta^{18}\text{O}_c$
925 records to better capture this sub-seasonal variability, which introduces more noise on the seasonal cycle
926 (reducing precision) but causes monthly mean SST and ~~$\delta^{18}\text{O}_w$ $\delta^{18}\text{O}_{sw}$~~ to be more accurately reconstructed.
927 Towards higher sampling resolutions, the gap in precision between $\delta^{18}\text{O}_c$ - and Δ_{47} -based reconstructions
928 closes, eventually (in an ideal case) diminishing the advantage of high analytical precision in $\delta^{18}\text{O}_c$
929 measurements (**Fig. 8C9C-D**).

Formatted: Font: (Default) Arial, 10 pt

Formatted: Font: (Default) Arial, 10 pt

930 ~~The rate of increase in precision and accuracy with sampling resolution is not the same for each method,~~
931 ~~and a~~n optimum sample resolution can be defined for each method after which improving sampling
932 resolution does not significantly improve the reliability of the reconstruction (as in de Winter et al., 2017).

933 **Figure 8-9** shows that this optimum ~~is different~~varies depending on which variable (MAT, SST seasonality,
934 mean annual $\delta^{18}\text{O}_w$ $\delta^{18}\text{O}_{sw}$ or $\delta^{18}\text{O}_w$ $\delta^{48}\text{O}_{sw}$ seasonality) is reconstructed. Therefore, **Fig. 8-9** will allow future
935 researchers to determine the sampling resolution that is tailored to their purpose. In general, the
936 improvement after a sample size of 20-30 samples per year is negligible for the **binning** and **optimization**
937 methods if the total number of samples (depending on both sampling resolution and record length) is
938 sufficient for monthly temperature reconstructions. Our data show that 200-250 paired $\delta^{18}\text{O}_c$ and Δ_{47}
939 measurements are in general sufficient for a standard deviation of 2-3°C on monthly SST reconstructions
940 using the **binning** or **optimization** approach (**Fig. 8-10; S5**).

941 Record length only has a minimal influence on the **optimization** method but for very short records (≤ 2
942 years) **binning** becomes very imprecise, especially at low sampling resolutions (**Fig. 4-11**). The reason ~~for~~
943 ~~this~~ is that the sample size within monthly time bins becomes too small in these cases, while the more
944 flexible sample size window of the optimization routine circumvents this problem. The choice between these
945 two approaches should therefore be based on a tradeoff between the length of the record (in time) and the
946 number of samples that can be retrieved from it. As a result, shorter-lived, fast-growing climate archives,
947 such as large or fast-growing (e.g. juvenile) mollusk shells, are best sampled using a high temporal
948 resolution ($\geq 30+$ samples/yr) sampling strategy with the **optimization** approach. Longer lived archives with
949 a lower mineralization rate, such as annually laminated speleothems, corals and gerontic mollusks, are
950 best sampled using long time series at monthly resolution using the **binning** approach.

951 A simplified decision tree that could guide sampling strategies for future paleoseasonality studies is shown
952 in **Figure 4-14**. Note that choices and tradeoffs for these reconstructions may differ depending on the
953 archive and environment in which it formed (see discussion above).

Formatted: Font: (Default) Arial, 10 pt

Formatted: Font: (Default) Arial, 10 pt

Schematic guide to reconstructing SST and $\delta^{18}\text{O}_w$ from accretionary carbonate archives

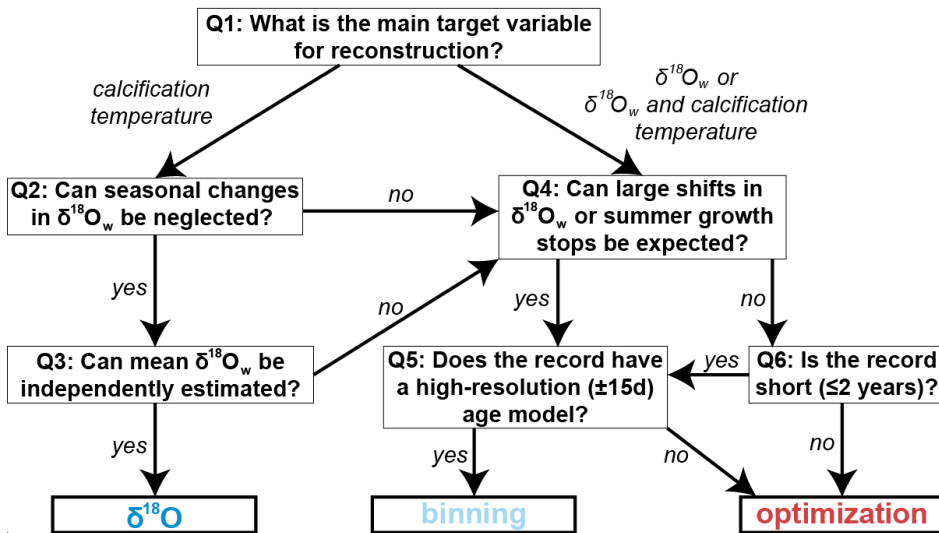


Figure 15: Schematic guide to choosing the right approach for reconstructing annual mean or seasonality in SST and $\delta^{18}\text{O}_w$ from accretionary carbonate archives. Recommendations are based on the results of testing all four approaches on the entire range of cases. Researchers can follow the six steps (questions Q1-6) to decide on the right approach for reconstructing the target variable. Guidelines are based on minimizing both accuracy and precision (see details in S44S9). Note that the **smoothing** approach is never the best choice. The choice between the two remaining Δ_{47} -based approaches (**binning** and **optimization**) relies heavily on the situation and may be driven by a preference for more accurate or more precise results.

54.3 Implications for clumped isotope sample size

The **optimization** technique for grouping Δ_{47} aliquots for accurate SST and $\delta^{18}\text{O}_w$ reconstructions allows us to assess the limitations of the clumped isotope thermometer for temperature reconstructions from high-resolution carbonate archives. The **actual**-optimal sample size given by the approach is different for different cases and depends on the temporal sampling resolution and the characteristics of the record (see S5S4). As expected, in cases more **similar-to-like** the ideal case (case 1), optimal sample sizes are low (~14--24), while sample sizes **quickly** increase in more complicated cases based on simulated natural environments (case 14--18) or cases based on actual SST and SSS data (cases 30-33). More confined SST seasonality (cases 19-21) also requires larger samples to reconstruct (up to 100 samples in some

Formatted: Font: (Default) Arial, 10 pt

Formatted: Font: (Default) Arial, 10 pt

Formatted: Font: (Default) Arial, 10 pt

972 cases). This is not surprising, because variability within samples will increase in ~~more complicated~~ records
973 in which the seasonality is smaller or more obscured by other environmental variability. The optimal sample
974 size between cases and sampling resolutions is not normally distributed but tails towards high sample sizes
975 with some extreme outliers (Shapiro Wilk test $p \ll 0.05$; ~~S12S10~~). The median sample size of all our
976 simulations is 17 aliquots. This number lies between the minimum number of 14 ~100 μg replicates of
977 standards calculated by Fernandez et al. (2017) and the minimum of 20-40 ~100 μg aliquots required for
978 optimal paleoseasonality reconstruction from fossil bivalves by de Winter et al. (2020a2020b). This is to be
979 expected since many of the cases explored in this study represent ideal cases compared with the natural
980 situation. However, in ~~many these virtual~~ cases a measure of random sub-annual variability in SST and
981 $\delta^{18}\text{O}_w$ $\delta^{18}\text{O}_{sw}$ was added (see Fig. 4 and S2), simulating a more realistic environment and resulting in poorer
982 precision than replicates of a carbonate standard (as in Fernandez et al., 2017). Our simulations show that
983 the optimum number of samples to be combined in seasonality studies depends on both the analytical
984 uncertainty of Δ_{47} measurements (as represented by the estimate in Fernandez et al., 2017) and the
985 variability between aliquots pooled within a sample that is attributed to actual variability within the record
986 (as represented by our simulations and the estimate in de Winter et al. 2020a2020b). The optimal sample
987 size is therefore a good measure for the limitations of temperature variability that can be resolved in a
988 record. ~~As such, this number, together with the overview in S1, and~~ can help researchers decide which
989 strategy to apply for combining measurements to obtain the most reliable paleoseasonality estimates, or to
990 decide whether extra sampling is required, even if the chosen approach is not to use the **optimization**
991 routine itself. Note that the optimum sample size is kept equal for summer and winter samples in this study,
992 and that the **optimization** approach can likely achieve better performance by considering unequal sample
993 sizes in opposite seasons (see 4.1.3 and 4.2.2). While this added flexibility comes at a higher computational
994 cost due to the increased number of possible sample size combinations to be considered, future studies
995 should investigate whether this updated **optimization** approach could yield more reliable seasonality
996 reconstructions.

997 **5.4.4 Implications for other sample size problems**

Formatted: Font: (Default) Arial, 10 pt

998 While the discussion above focuses on optimizing approaches for combining samples for clumped
999 isotope analyses in paleoseasonality reconstructions, the problem of combining samples to reduce
1000 uncertainty and isolate variation in datasets is very common (e.g. Zhang et al., 2004; Merz and Thieken,
1001 2005; Tsukakoshi, 2011). Therefore, the approaches outlined and tested in this study have applications
1002 beyond paleoseasonality reconstructions. Examples of other problems that could benefit from applying
1003 similar approaches for reducing the uncertainty of estimates of target variables or while minimizing the
1004 number of analyses required to meet analytical requirements include: (1) reconstructing
1005 paleoenvironmental variability in the terrestrial realm from tooth bioapatite (e.g. Passey and Cerling,
1006 2002; Kohn, 2004; Van Dam and Reichart, 2009; de Winter et al., 2016), (2) quantitative time series
1007 analysis of orbital cycles in stratigraphic records (e.g. Lourens et al., 2010; de Vleeschouwer et al., 2017;
1008 Noorbergen et al., 2017; Westerhold et al., 2020), (3) strontium isotope dating (e.g. McArthur et al., 2012;
1009 de Winter et al., 2020bc), (4) reconstructing sub-seasonal variability from ultra-high-resolution records
1010 (e.g. from fast-growing mollusks and gastropods)-(; e.g. Sano et al., 2012; Warter and Müller, 2017, de
1011 Winter et al., 2020ad; Yan et al., 2020), and (5) reconstructing sea surface and deep-sea temperatures
1012 across short-lived (10–100 kyr) episodes of climate change or climate shifts from deep marine archives
1013 characterized by low sedimentation rates (e.g. Lear et al., 2008; Jenkyns, 2010; Stap et al., 2010;
1014 Lauretano et al., 2018). A more detailed discussion of the implications for other sample size problems is
1015 provided in the **Supplementary Information**.

1016 ~~While the discussion above focuses on optimizing approaches for combining samples for clumped isotope~~
1017 ~~analyses in paleoseasonality reconstructions, the problem of combining samples to lower uncertainty and~~
1018 ~~isolate variation in datasets is very common (e.g. Zhang et al., 2004; Merz and Thieken, 2005; Tsukakoshi,~~
1019 ~~2011). Therefore, the approaches outlined and tested in this study have applications beyond~~
1020 ~~paleoseasonality reconstructions. Below, we briefly highlight four examples of problems that could benefit~~
1021 ~~from applying similar approaches for lowering the uncertainty of estimates of target variables or reducing~~
1022 ~~the number of analyses required to meet analytical requirements.~~

1023 *5.4.1 Tooth bioapatite*

Formatted: Not Highlight

1024 Enamel from vertebrate teeth constitute a useful archive for paleoenvironmental and paleoecological
1025 change in the terrestrial realm, complementing the carbonate records discussed in this work (e.g. Luz and
1026 Kolodny, 1985; Fricke et al., 1996; Balasse, 2002; Van Dam and Reichart, 2009; de Winter et al., 2016).
1027 However, the tooth bioapatite archive suffers from similar limitations of sample size and resolution as
1028 carbonate archives when it comes to reconstructing high-resolution variability (see discussion in Passey
1029 and Gerling, 2002 and Kohn, 2004). Oxygen and carbon isotopes of carbonate and phosphate in tooth
1030 enamel contain valuable information about the animal's life cycle and environment (e.g. Fricke et al., 1996;
1031 Balasse et al., 2002; Van Dam and Reichart, 2009). However, structurally bound carbonate constitutes a
1032 mere 2-5% of tooth enamel (LeGeros et al., 1986), and enamel samples need to be pretreated to remove
1033 labile components, so analyses of $\delta^{18}\text{O}$ in these archives require comparatively large sample sizes (0.5-1
1034 mg; Fricke et al., 1998; Balasse, 2002; Pellegrini and Snoeck, 2016). Phosphate-bound $\delta^{18}\text{O}$ is less
1035 susceptible to diagenesis, but requires a more complicated procedure to analyze, resulting in similar sample
1036 size limitations (Joachimski et al., 2002; Lecuyer et al., 2007). Most applications of isotope profiles from
1037 teeth rely on precise determination of both the phase and amplitude of the seasonal cycle, and therefore
1038 suffer from the same complications as isotope records in carbonate archives (e.g. Balasse et al., 2002;
1039 Straight et al., 2004). The **binning** and **optimization** approaches discussed here could help reduce
1040 uncertainty and provide a basis for better comparison of seasonal profiles in tooth enamel.

1041 *5.4.2 Cyclostratigraphy*

1042 Within the field of cyclostratigraphy, a multitude of stratigraphical approaches have been developed for
1043 signal processing, with the aim to use regular orbital cycles expressed in stratigraphic time series as tools
1044 for dating rock sequences (e.g. Paillard et al., 1996; Meyers, 2014; Sinnesael et al., 2016). However, the
1045 focus on timing has caused many methods for extracting the climatic impact of these orbital cycles from
1046 stratigraphic records (e.g. bandpass filtering; Hilgen, 1991) to remain qualitative. This is unfortunate,
1047 because the magnitude of the effect of this cyclicity on climate and environmental change is of major interest
1048 in paleoclimatology studies (e.g. Berger, 1992; Shackleton, 2000; Zachos et al., 2001; Lourens et al., 2005;
1049 De Vleeschouwer et al., 2017a). The problem of quantitatively extracting the impact of orbital cycles is very
1050 similar to the problem of paleoseasonality reconstructions central to this study, and the same approaches

1051 can therefore be used in the orbital time domain. The time **binning** approach is probably most robust for
1052 this purpose, since cyclostratigraphic records are often longer (record length >> period of the cycle) and
1053 sampling resolutions (samples/cycle) are often lower than in seasonal records (see 5.2.4; e.g. De
1054 Vleeschouwer et al., 2017b). Quantitative analyses of the contribution of orbital cyclicity to rhythmic
1055 changes in paleoclimate can help separate variability in records caused by external forcing from autocyclic
1056 behavior or (positive or negative) feedback of the climate system itself (Lourens et al., 2010; Noorbergen
1057 et al., 2017; Nohl et al., 2018).

1058 *5.4.3 Strontium isotope dating*

1059 Another type of analysis that could benefit from smart combination of measurement results is strontium
1060 isotope dating. The strontium isotope composition ($^{87}\text{Sr}/^{86}\text{Sr}$) of the ocean has evolved over time, and the
1061 isotopic composition of marine carbonates can therefore be used to estimate the age of the sample by
1062 comparing it with a composite strontium isotope curve (Elderfield, 1986; McArthur et al., 2012). In time
1063 intervals where the global marine strontium isotope curve is steep, strontium isotope dating ranks among
1064 the most precise methods for absolute dating in stratigraphy (Wegreich et al., 2012). However, accurate
1065 dating based on the strontium isotope curve requires propagation of errors on the composite curve and the
1066 sample. Doing so results in asymmetric errors due to the non-linear character of the strontium isotope
1067 curve, which require complex error propagation (see Barlow, 2003; 2004; Wan et al., 2019). The state-of-
1068 the-art uncertainty of individual strontium isotope analyses ranges between 240 ppm (1 standard deviation;
1069 Yobregat et al., 2017), which translates to an age uncertainty of 100–200 kyr, (1 standard deviation)
1070 depending strongly on the slope of the global strontium isotope curve at the time interval under study.
1071 Combining multiple strontium isotope analyses from the same stratigraphic unit can reduce the uncertainty
1072 on these composite ages (Korte and Ullmann, 2016; de Winter et al., 2020b), allowing the dating method
1073 to be combined with cyclostratigraphy to produce for orbital scale age models (see 5.4.2). In stratigraphy
1074 studies that use this dating method, the need arises to compromise between the resolution of the age model
1075 and the precision and accuracy of dating, analogous to the tradeoff that occurs when combining Δ_{47}
1076 analyses for paleoseasonality reconstructions outlined in this study. In this case, the **smoothing** approach
1077 with a dynamic moving window discussed in this study is likely the best candidate for combining data to

1078 improve these age models. Such an approach can be seen as a more flexible adaptation of the Δ_{47} -based
1079 approach for SST reconstruction outlined in Rodríguez-Sanz et al. (2017) that provides the flexibility to
1080 adapt the sample window depending on the available data and the slope of the global strontium curve. At
1081 the same time, the shape of the global composite strontium isotope curve itself can be refined by using a
1082 similar protocol on well-dated samples. The approaches discussed in this study are more adaptable to
1083 changes in sampling density over time and can in theory achieve higher precision than the LOWESS fit
1084 approach currently employed for constructing the global composite (McArthur et al., 2012). Similarly,
1085 techniques for compromising between sampling resolution and accuracy and precision can be applied to
1086 improve other dating methods based on matching curves such as radiocarbon dating (Ramsay and Lee,
1087 2013), carbon isotope stratigraphy (Salzman and Thomas, 2012) and dendrochronology (Cook and
1088 Kairiukstis, 2013).

1089 *5.4.4 Sub-seasonal variability*

1090 Ultra-high-resolution records from fast-growing archives (e.g. mollusks) are an emerging phenomenon in
1091 the field of high-resolution paleoclimatology (e.g. Sano et al., 2012; Warter and Müller, 2017; de Winter et
1092 al., 2020a). The emergence of such records allows new information to be obtained about the daily cycle
1093 (Warter et al., 2018; de Winter et al., 2020a) and extreme weather events (Yan et al., 2020) in the past,
1094 potentially bridging the gap between weather and climate reconstructions. The sampling resolution required
1095 to resolve variability at such a fine temporal scale warrants an even more careful consideration of the
1096 tradeoff between sample size, sampling resolution and analytical uncertainty than the paleoseasonality
1097 examples considered here. If quantitative estimates of insolation, temperature and the frequency of extreme
1098 weather events are to be reconstructed from these novel records, a compromise will need to be found
1099 between analytical uncertainty and the temporal resolution of measurements (Sano et al., 2012; de Winter
1100 et al., 2020a; Yan et al., 2020). Applying the temporal (e.g. hourly) binning method (**binning**) discussed
1101 here on long-, (sub-)daily resolved records could yield more accurate and precise records of ultra-high-
1102 resolution variability, given its reliability in extracting accurate cycle amplitude (e.g. seasonality) from long-,
1103 less densely sampled records (see 5.1.3). Fast-growing bivalve and gastropod shells have already been
1104 marked as promising archives for such variability, while other fast-growing archives such as *Acropora* corals

1105 remain to be explored (Bak et al., 2009; Strauss et al., 2014; de Winter et al., 2020c). It must be noted that
1106 models for the timing of carbonate deposition in accretionary carbonate archives at the sub-daily scale are
1107 highly uncertain and that this may complicate the use of the **binning** approach (see 5.1.3), in which case
1108 **optimization** may be more appropriate.

1109 *5.4.5 Event stratigraphy*

1110 Accurate and precise temperature reconstructions of short-lived (10-100 kyr) episodes of climate change
1111 present a problem comparable to resolving seasonality in paleoclimate archives. Examples of such events
1112 include the Mesozoic ocean anoxic events (Hesselbo et al., 2000; Jenkyns, 2010), early Paleogene
1113 hyperthermals (Stap et al., 2010; Lauretano et al., 2015, 2018) and stepwise climate perturbations such as
1114 the Eocene-Oligocene transition (Dupont-Nivet et al., 2007; Lear et al., 2008) studied in deep-sea records.
1115 Currently, reconstructions of temperature variability in the deep-sea during such events are based on
1116 benthic foraminiferal $\delta^{18}\text{O}_v$ (e.g. Erbacher et al., 2001; Lui et al., 2009; Stap et al., 2010; Lauretano et al.,
1117 2015, 2018), but may not be reliable due to assumptions made on $\delta^{18}\text{O}_{sw}$. Deep-sea sedimentary
1118 environments are generally characterized by low sedimentation rates (~1 cm/kyr) as well as low abundance
1119 and small size of microfossils (e.g. foraminifera) which serve as archives of past marine conditions (e.g.
1120 Stap et al., 2010; Jennions et al., 2015). This limits the number of aliquots that can be obtained for Δ_{47} and
1121 other analyses through these climate events. In these studies, a **smoothing** approach would probably
1122 underestimate the 'true' amplitude of temperature or geochemical change. With sufficient record length and
1123 perhaps by combining multiple events, **binning** or **optimization** based on proxy data would be the most
1124 accurate and precise approach to resolve transient temperature change in the deep-sea during the
1125 geological past.

1126

1127 **6.5. Conclusions and recommendations**

1128 The ~~reliability performance~~ of three Δ_{47} -based approaches to reconstruct seasonality from accretionary
1129 carbonate archives was evaluated in comparison with ~~the~~ conventional $\delta^{18}\text{O}_c$ -based reconstructions in a
1130 wide range of case studies. From the results, we conclude that while $\delta^{18}\text{O}_c$ -based reconstructions ($\delta^{18}\text{O}$)
1131 yield superior precision for SST reconstructions, this method runs a high risk of yielding inaccurate results
1132 due to innate assumptions about the value of $\delta^{18}\text{O}_w\delta^{18}\text{O}_{sw}$, which ~~has to~~ must be estimated and assumed
1133 constant year-round. Unless ~~a~~ $\delta^{18}\text{O}_w\delta^{18}\text{O}_{sw}$ can be independently constrained or variability in $\delta^{18}\text{O}_w\delta^{18}\text{O}_{sw}$
1134 can be neglected, Δ_{47} -based reconstructions should be the method of choice for absolute mean annual
1135 temperature and SST seasonality reconstructions. Various techniques for combining Δ_{47} data were
1136 evaluated. Our findings suggest that smoothing Δ_{47} data using a moving average (~~smoothing~~) ~~results in~~
1137 almost all ways cases in a dampening of the seasonal cycle which severely hampers recovery of
1138 seasonality. Applying the **smoothing** approach results in inaccuracies in reconstructions of MAT as well,
1139 especially in cases where part of the seasonal cycle is obscured by variability in growth rate or multi-annual
1140 trends. More reliable seasonality reconstructions are achieved with two approaches for combining Δ_{47} data
1141 using time binning (**binning**) or applying a flexible sample size optimization (**optimization**) approach. Of
1142 these two approaches, **optimization** achieves better precision and can resolve smaller seasonal
1143 temperature differences with confidence. However, **binning** is often more accurate, and outperforms
1144 **optimization** as the most reliable approach. This is especially true in cases with growth stops or
1145 $\delta^{18}\text{O}_w\delta^{18}\text{O}_{sw}$ changes in phase with temperature seasonality (e.g. strong seasonal evaporation or
1146 freshwater influx) and in longer multi-annual time series with a reliable age model. **Optimization** is the
1147 better choice for shorter (<3 years) records, especially if the sampling resolution can be increased, such as
1148 in short, fast growing climate archives.

1149 Despite the ~~distinct~~ focus on the problem of resolving seasonality in carbonate archives, the findings in this
1150 study have applications for other problems in earth science where sample size and sampling resolution put
1151 limits on the ability to resolve specific trends, events, and cycles from time series. ~~Examples include, but~~
1152 ~~are not limited to, resolving sub-annual variability in geochemical records from tooth bioapatite, quantifying~~
1153 ~~the impact of orbital cycles on paleoclimate, refining strontium isotope dating by strategic sample~~

Formatted: Font: (Default) Arial

Formatted: Font: (Default) Arial, 10 pt

1154 combination, resolving daily scale variability and weather patterns in ultra-high-resolution climate records
1155 and quantifying the impact of climate events in the geological record. While the ~~above-mentioned~~above-
1156 mentioned recommendations of the **optimization** and **binning** methods are likely valid for most studies
1157 aiming to quantify the mean and amplitude of a specific cycle or event (equivalent to MAT and SST
1158 seasonality), (dynamic) moving averages (**smoothing**) are expected to yield the best results in studies
1159 quantifying aperiodic trends from longer data series.

1160

1161 **Code availability**

1162 All scripts used to make the calculations described in this study are compiled in the documented R package
1163 "seasonalclumped", which is freely available on the open-source online R-database CRAN (de Winter,
1164 2021a; <https://cran.r-project.org/web/packages/seasonalclumped>). Annotated R scripts used to make
1165 calculations for this study are available in the digital supplement uploaded to the open-source online
1166 repository Zenodo (www.doi.org/10.5281/zenodo.3899926).

1167

1168 **Data availability**

1169 Supplementary data, figures and tables as well as all scripts used to do the calculations and create the
1170 virtual datasets used in this study are deposited in the open-source online repository Zenodo
1171 (www.doi.org/10.5281/zenodo.3899926). Virtual datasets generated within the context of this study are also
1172 made available as datafiles within the R package that contains the scripts used for this study
1173 ("seasonalclumped"; de Winter, 2021a; see <https://cran.r-project.org/web/packages/seasonalclumped>).

1174

1175 **Author contributions**

1176 NJW designed the study, wrote the scripts for all calculations, and created a first draft of the manuscript
1177 text and figures. MZ, TA and NJW worked together from the first draft towards the final manuscript. All

Field Code Changed

Formatted: Font: (Default) Arial, 10 pt

Formatted: Font: (Default) Arial, 10 pt

Field Code Changed

1178 authors contributed to the representation of the data and methods in figures and to the discussion of the
1179 implications of the data in the discussion.

1180

1181 **Competing Interests**

1182 The authors have no potential conflicts of interest to declare with regards to this study.

1183

1184 **Acknowledgements**

1185 The authors would like to thank all members of the Clumped Isotope research group of Utrecht University,
1186 most notably Ilja Kocken and dr. Inigo Müller, for their comments and recommendations on a presentation
1187 of the initial results of this study.

1188

1189 **Financial support**

1190 NJW is funded by the European Commission through a Marie Skłodowska Curie Individual Fellowship
1191 (UNBIAS, grant # 843011) and by the Flemish Research Council (FWO) through a Junior Postdoctoral
1192 Fellowship (12ZB220N).

1193

1194 **References**

1195 [Bahr, K. D., Jokieli, P. L. and Rodgers, K. S.: Seasonal and annual calcification rates of the Hawaiian reef](#)
1196 [coral, *Montipora capitata*, under present and future climate change scenarios, *ICES J Mar Sci*, 74\(4\),](#)
1197 [1083–1091, <https://doi.org/10.1093/icesjms/fsw078>, 2017.](#)

1198 [Bernasconi, S. M., Müller, I. A., Bergmann, K. D., Breitenbach, S. F., Fernandez, A., Hodell, D. A., Jaggi,](#)
1199 [M., Meckler, A. N., Millan, I. and Ziegler, M.: Reducing uncertainties in carbonate clumped isotope](#)
1200 [analysis through consistent carbonate-based standardization, *Geochemistry, Geophysics, Geosystems*,](#)
1201 [19\(9\), 2895–2914, 2018.](#)

1202 [Brand, W. A., Coplen, T. B., Vogl, J., Rosner, M. and Prohaska, T.: Assessment of international reference](#)
1203 [materials for isotope-ratio analysis \(IUPAC Technical Report\), *Pure and Applied Chemistry*, 86\(3\), 425–](#)
1204 [467, <https://doi.org/10.1515/pac-2013-1023>, 2014.](#)

Formatted: Indent: Left: 0", Hanging: 0.13", Space
After: Auto, Line spacing: single

1205 [Briard, J., Pucéat, E., Vennin, E., Daëron, M., Chavagnac, V., Jaillet, R., Merle, D. and de Rafélis, M.: Seawater paleotemperature and paleosalinity evolution in neritic environments of the Mediterranean margin: Insights from isotope analysis of bivalve shells, *Palaeogeography, Palaeoclimatology, Palaeoecology*, 543, 109582, <https://doi.org/10.1016/j.palaeo.2019.109582>, 2020.](#)

1206

1207

1208

1209 [Caldarescu, D. E., Sadatzki, H., Andersson, C., Schäfer, P., Fortunato, H. and Meckler, A. N.: Clumped isotope thermometry in bivalve shells: A tool for reconstructing seasonal upwelling, *Geochimica et Cosmochimica Acta*, 294, 174–191, <https://doi.org/10.1016/j.gca.2020.11.019>, 2021.](#)

1210

1211

1212 [Charles, C. D., Hunter, D. E. and Fairbanks, R. G.: Interaction between the ENSO and the Asian monsoon in a coral record of tropical climate, *Science*, 277\(5328\), 925–928, 1997.](#)

1213

1214 [Comboul, M., Emile-Geay, J., Evans, M. N., Mirnateghi, N., Cobb, K. M. and Thompson, D. M.: A probabilistic model of chronological errors in layer-counted climate proxies: applications to annually banded coral archives, *Climate of the Past*, 10\(2\), 825–841, 2014.](#)

1215

1216

1217 [Compton, T. J., Rijkenberg, M. J. A., Drent, J. and Piersma, T.: Thermal tolerance ranges and climate variability: A comparison between bivalves from differing climates, *Journal of Experimental Marine Biology and Ecology*, 352\(1\), 200–211, <https://doi.org/10.1016/j.jembe.2007.07.010>, 2007.](#)

1218

1219

1220 [Cook, E. R. and Kairiukstis, L. A.: *Methods of dendrochronology: applications in the environmental sciences*, Springer Science & Business Media., 2013.](#)

1221

1222 [Cramer, B. S., Toggweiler, J. R., Wright, J. D., Katz, M. E. and Miller, K. G.: Ocean overturning since the Late Cretaceous: Inferences from a new benthic foraminiferal isotope compilation, *Paleoceanography*, 24\(4\), <https://doi.org/10.1029/2008PA001683>, 2009.](#)

1223

1224

1225 [Crossland, C.: Seasonal variations in the rates of calcification and productivity in the coral *Acropora formosa* on a high-latitude reef, *Marine Ecology Progress Series*, 15, 135–140, <https://doi.org/10.3354/meps015135>, 1984.](#)

1226

1227

1228 [van Dam, J. A. and Reichert, G. J.: Oxygen and carbon isotope signatures in late Neogene horse teeth from Spain and application as temperature and seasonality proxies, *Palaeogeography, Palaeoclimatology, Palaeoecology*, 274\(1–2\), 64–81, <https://doi.org/10.1016/j.palaeo.2008.12.022>, 2009.](#)

1229

1230

1231

1232 [Dattalo, P.: *Determining Sample Size: Balancing Power, Precision, and Practicality*, Oxford University Press, USA., 2008.](#)

1233

1234 [Dayem, K. E., Molnar, P., Battisti, D. S. and Roe, G. H.: Lessons learned from oxygen isotopes in modern precipitation applied to interpretation of speleothem records of paleoclimate from eastern Asia, *Earth and Planetary Science Letters*, 295\(1–2\), 219–230, 2010.](#)

1235

1236

1237 [De Ridder, F., de Brauwere, A., Pintelon, R., Schoukens, J., Dehairs, F., Baeyens, W. and Wilkinson, B. H.: Comment on: Paleoclimatic inference from stable isotope profiles of accretionary biogenic hardparts — a quantitative approach to the evaluation of incomplete data, by Wilkinson, B.H., Ivany, L.C., 2002, *Palaeogeogr. Palaeoclimatol. Palaeoecol.* 185, 95–114, *Palaeogeography, Palaeoclimatology, Palaeoecology*, 248\(3–4\), 473–476, <https://doi.org/10.1016/j.palaeo.2006.08.004>, 2007.](#)

1238

1239

1240

1241

1242 [De Vleeschouwer, D., Vahlenkamp, M., Crucifix, M. and Pälike, H.: Alternating Southern and Northern Hemisphere climate response to astronomical forcing during the past 35 my, *Geology*, 45\(4\), 375–378, 2017.](#)

1243

1244

- 1245 [de Winter, N. J., Snoeck, C. and Claeys, P.: Seasonal Cyclicity in Trace Elements and Stable Isotopes of](#)
1246 [Modern Horse Enamel, *PLoS one*, 11\(11\), e0166678, 2016.](#)
- 1247 [de Winter, N., Sinnesael, M., Makarona, C., Vansteenberge, S. and Claeys, P.: Trace element analyses of](#)
1248 [carbonates using portable and micro-X-ray fluorescence: Performance and optimization of measurement](#)
1249 [parameters and strategies., *Journal of Analytical Atomic Spectrometry*, 32\(6\), 1211–1223,](#)
1250 <https://doi.org/10.1039/C6JA00361C>, 2017.
- 1251 [de Winter, N. J., Vellekoop, J., Vorrsselmans, R., Golreihan, A., Soete, J., Petersen, S. V., Meyer, K. W.,](#)
1252 [Casadio, S., Speijer, R. P. and Claeys, P.: An assessment of latest Cretaceous *Pycnodonte vesicularis*](#)
1253 [\(Lamarck, 1806\) shells as records for palaeoseasonality: a multi-proxy investigation, *Climate of the Past*,](#)
1254 [14\(6\), 725–749, 2018.](#)
- 1255 [de Winter, N. J., Müller, I. A., Kocken, I. J., Thibault, N., Ullmann, C. V., Farnsworth, A., Lunt, D. J., Claeys,](#)
1256 [P. and Ziegler, M.: First absolute seasonal temperature estimates for greenhouse climate from clumped](#)
1257 [isotopes in bivalve shells, *Nature Communications*, in review, <https://doi.org/10.21203/rs.3.rs-39203/v1>,](#)
1258 [2020a.](#)
- 1259 [de Winter, N. J., Ullmann, C. V., Sørensen, A. M., Thibault, N., Goderis, S., Van Malderen, S. J. M., Snoeck,](#)
1260 [C., Goolaerts, S., Vanhaecke, F. and Claeys, P.: Shell chemistry of the boreal Campanian bivalve](#)
1261 [<i>Rastellum diluvianum</i> \(Linnaeus, 1767\) reveals temperature seasonality, growth rates](#)
1262 [and life cycle of an extinct Cretaceous oyster, *Biogeosciences*, 17\(11\), 2897–2922,](#)
1263 <https://doi.org/10.5194/bg-17-2897-2020>, 2020b.
- 1264 [de Winter, N. J., Goderis, S., Malderen, S. J. M. V., Sinnesael, M., Vansteenberge, S., Snoeck, C., Belza,](#)
1265 [J., Vanhaecke, F. and Claeys, P.: Subdaily-Scale Chemical Variability in a *Torreites Sanchezi* Rudist](#)
1266 [Shell: Implications for Rudist Paleobiology and the Cretaceous Day-Night Cycle, *Paleoceanography and*](#)
1267 [Paleoclimatology](#), 35(2), e2019PA003723, <https://doi.org/10.1029/2019PA003723>, 2020c.
- 1268 [de Winter, N. J., Vellekoop, J., Clark, A. J., Stassen, P., Speijer, R. P. and Claeys, P.: The giant marine](#)
1269 [gastropod *Campanile giganteum* \(Lamarck, 1804\) as a high-resolution archive of seasonality in the](#)
1270 [Eocene greenhouse world, *Geochemistry, Geophysics, Geosystems*, 21\(n/a\), e2019GC008794,](#)
1271 <https://doi.org/10.1029/2019GC008794>, 2020d.
- 1272 [de Winter, N. J.: seasonalclumped: Toolbox for Clumped Isotope Seasonality Reconstructions.](#)
1273 <https://CRAN.R-project.org/package=seasonalclumped>, last access: 4 February 2021, 2021 a.
- 1274 [de Winter, N. J.: ShellChron 0.2.8: A new tool for constructing chronologies in accretionary carbonate](#)
1275 [archives from stable oxygen isotope profiles, *Geoscientific Model Development Discussions*, 1–37,](#)
1276 <https://doi.org/10.5194/gmd-2020-401>, 2021b.
- 1277 [Denton, G. H., Alley, R. B., Comer, G. C. and Broecker, W. S.: The role of seasonality in abrupt climate](#)
1278 [change, *Quaternary Science Reviews*, 24\(10\), 1159–1182,](#)
1279 <https://doi.org/10.1016/j.quascirev.2004.12.002>, 2005.
- 1280 [Fairbanks, R. G., Evans, M. N., Rubenstone, J. L., Mortlock, R. A., Broad, K., Moore, M. D. and Charles,](#)
1281 [C. D.: Evaluating climate indices and their geochemical proxies measured in corals, *Coral Reefs*, 16\(1\),](#)
1282 [S93–S100, <https://doi.org/10.1007/s003380050245>, 1997.](#)
- 1283 [Fernandez, A., Müller, I. A., Rodríguez-Sanz, L., van Dijk, J., Looser, N. and Bernasconi, S. M.: A](#)
1284 [reassessment of the precision of carbonate clumped isotope measurements: implications for calibrations](#)
1285 [and paleoclimate reconstructions, *Geochemistry, Geophysics, Geosystems*, 18\(12\), 4375–4386, 2017.](#)

Formatted: Indent: Left: 0", Hanging: 0.13", Space
After: Auto, Line spacing: single

1286 [Gaspar, M. B., Ferreira, R. and Monteiro, C. C.: Growth and reproductive cycle of *Donax trunculus* L., \(Mollusca: Bivalvia\) off Faro, southern Portugal, Fisheries Research, 41\(3\), 309–316, https://doi.org/10.1016/S0165-7836\(99\)00017-X, 1999.](#)

1287

1288

1289 [Goodwin, D. H., Schöne, B. R. and Dettman, D. L.: Resolution and fidelity of oxygen isotopes as paleotemperature proxies in bivalve mollusk shells: models and observations, Palaios, 18\(2\), 110–125, 2003.](#)

1290

1291

1292 [Goodwin, D. H., Paul, P. and Wissink, C. L.: MoGroFunGen: A numerical model for reconstructing intra-annual growth rates of bivalve molluscs, Palaeogeography, Palaeoclimatology, Palaeoecology, 276\(1\), 47–55, https://doi.org/10.1016/j.palaeo.2009.02.026, 2009.](#)

1293

1294

1295 [Harwood, A. J. P., Dennis, P. F., Marca, A. D., Pilling, G. M. and Millner, R. S.: The oxygen isotope composition of water masses within the North Sea, Estuarine, Coastal and Shelf Science, 78\(2\), 353–359, https://doi.org/10.1016/j.ecss.2007.12.010, 2008.](#)

1296

1297

1298 [Hendriks, I. E., Basso, L., Deudero, S., Cabanellas-Reboredo, M. and Álvarez, E.: Relative growth rates of the noble pen shell *Pinna nobilis* throughout ontogeny around the Balearic Islands \(Western Mediterranean, Spain\), Journal of Shellfish Research, 31\(3\), 749–756, 2012.](#)

1299

1300

1301 [Henkes, G. A., Passey, B. H., Grossman, E. L., Shenton, B. J., Yancey, T. E. and Pérez-Huerta, A.: Temperature evolution and the oxygen isotope composition of Phanerozoic oceans from carbonate clumped isotope thermometry, Earth and Planetary Science Letters, 490, 40–50, https://doi.org/10.1016/j.epsl.2018.02.001, 2018.](#)

1302

1303

1304

1305 [Hurrell, J. W.: Decadal trends in the North Atlantic Oscillation: regional temperatures and precipitation, Science, 269\(5224\), 676–679, 1995.](#)

1306

1307 [Huybers, P. and Curry, W.: Links between annual, Milankovitch and continuum temperature variability, Nature, 441\(7091\), 329, 2006.](#)

1308

1309 [Huyghe, D., Lartaud, F., Emmanuel, L., Merle, D. and Renard, M.: Palaeogene climate evolution in the Paris Basin from oxygen stable isotope \(\$\delta^{18}\text{O}\$ \) compositions of marine molluscs, Journal of the Geological Society, 172\(5\), 576–587, 2015.](#)

1310

1311

1312 [Huyghe, D., de Rafélis, M., Ropert, M., Mouchi, V., Emmanuel, L., Renard, M. and Lartaud, F.: New insights into oyster high-resolution hinge growth patterns, Marine biology, 166\(4\), 48, 2019.](#)

1313

1314 [IPCC: IPCC, 2013: Climate Change 2013: The Physical Science Basis. Contribution of Working Group I to the Fifth Assessment Report of the Intergovernmental Panel on Climate Change, 1535 pp, Cambridge Univ. Press, Cambridge, UK, and New York., 2013.](#)

1315

1316

1317 [Ivany, L. C.: Reconstructing paleoseasonality from accretionary skeletal carbonates—challenges and opportunities, The Paleontological Society Papers, 18, 133–166, 2012.](#)

1318

1319 [Jenkyns, H. C.: Geochemistry of oceanic anoxic events, Geochemistry, Geophysics, Geosystems, 11\(3\), https://doi.org/10.1029/2009GC002788, 2010.](#)

1320

1321 [Jones, A. M., Jacumin, P. and Young, E. D.: High-resolution \$\delta^{18}\text{O}\$ analysis of tooth enamel phosphate by isotope ratio monitoring gas chromatography mass spectrometry and ultraviolet laser fluorination, , 8, 1999.](#)

1322

1323

1324 [Judd, E. J., Wilkinson, B. H. and Ivany, L. C.: The life and time of clams: Derivation of intra-annual growth](#)
1325 [rates from high-resolution oxygen isotope profiles, *Palaeogeography, Palaeoclimatology, Palaeoecology*,](#)
1326 [490, 70–83, 2018.](#)

1327 [Keating-Bitonti, C. R., Ivany, L. C., Affek, H. P., Douglas, P. and Samson, S. D.: Warm, not super-hot,](#)
1328 [temperatures in the early Eocene subtropics, *Geology*, 39\(8\), 771–774,](#)
1329 <https://doi.org/10.1130/G32054.1>, 2011.

1330 [Kele, S., Breitenbach, S. F., Capezzuoli, E., Meckler, A. N., Ziegler, M., Millan, I. M., Kluge, T., Deák, J.,](#)
1331 [Hanselmann, K. and John, C. M.: Temperature dependence of oxygen- and clumped isotope fractionation](#)
1332 [in carbonates: a study of travertines and tufas in the 6–95 C temperature range, *Geochimica et*](#)
1333 [Cosmochimica Acta](#), 168, 172–192, 2015.

1334 [Kim, S.-T. and O’Neil, J. R.: Equilibrium and nonequilibrium oxygen isotope effects in synthetic carbonates,](#)
1335 [Geochimica et Cosmochimica Acta](#), 61(16), 3461–3475, [https://doi.org/10.1016/S0016-7037\(97\)00169-](https://doi.org/10.1016/S0016-7037(97)00169-5)
1336 [5](https://doi.org/10.1016/S0016-7037(97)00169-5), 1997.

1337 [Kocken, I. J., Müller, I. A. and Ziegler, M.: Optimizing the Use of Carbonate Standards to Minimize](#)
1338 [Uncertainties in Clumped Isotope Data, *Geochemistry, Geophysics, Geosystems*, 20\(11\), 5565–5577,](#)
1339 <https://doi.org/10.1029/2019GC008545>, 2019.

1340 [Kohn, M. J.: Comment: tooth enamel mineralization in ungulates: implications for recovering a primary](#)
1341 [isotopic time-series, by BH Passey and TE Cerling \(2002\), *Geochimica et Cosmochimica Acta*, 68\(2\),](#)
1342 [403–405, 2004.](#)

1343 [Lauretano, V., Zachos, J. C. and Lourens, L. J.: Orbitally Paced Carbon and Deep-Sea Temperature](#)
1344 [Changes at the Peak of the Early Eocene Climatic Optimum, *Paleoceanography and Paleoclimatology*,](#)
1345 [33\(10\), 1050–1065, <https://doi.org/10.1029/2018PA003422>, 2018.](#)

1346 [Lear, C. H., Bailey, T. R., Pearson, P. N., Coxall, H. K. and Rosenthal, Y.: Cooling and ice growth across](#)
1347 [the Eocene-Oligocene transition, *Geology*, 36\(3\), 251–254, 2008.](#)

1348 [LeGrande, A. N. and Schmidt, G. A.: Global gridded data set of the oxygen isotopic composition in](#)
1349 [seawater, *Geophysical research letters*, 33\(12\), 2006.](#)

1350 [Lisiecki, L. E. and Raymo, M. E.: A Pliocene-Pleistocene stack of 57 globally distributed benthic \$\delta^{18}\text{O}\$](#)
1351 [records, *Paleoceanography*, 20\(1\), <https://doi.org/10.1029/2004PA001071>, 2005.](#)

1352 [Lourens, L. J., Sluijs, A., Kroon, D., Zachos, J. C., Thomas, E., Röhl, U., Bowles, J. and Raffi, I.:](#)
1353 [Astronomical pacing of late Palaeocene to early Eocene global warming events, *Nature*, 435\(7045\),](#)
1354 [1083–1087, <https://doi.org/10.1038/nature03814>, 2005.](#)

1355 [Lourens, L. J., Becker, J., Bintanja, R., Hilgen, F. J., Tuenter, E., Van de Wal, R. S. and Ziegler, M.: Linear](#)
1356 [and non-linear response of late Neogene glacial cycles to obliquity forcing and implications for the](#)
1357 [Milankovitch theory, *Quaternary Science Reviews*, 29\(1–2\), 352–365, 2010.](#)

1358 [McArthur, J. M., Howarth, R. J. and Shields, G. A.: Strontium isotope stratigraphy, *The geologic time scale*,](#)
1359 [1, 127–144, 2012.](#)

1360 [Meckler, A. N., Ziegler, M., Millán, M. I., Breitenbach, S. F. and Bernasconi, S. M.: Long-term performance](#)
1361 [of the Kiel carbonate device with a new correction scheme for clumped isotope measurements, *Rapid*](#)
1362 [Communications in Mass Spectrometry](#), 28(15), 1705–1715, 2014.

- 1363 [Merz, B. and Thieken, A. H.: Separating natural and epistemic uncertainty in flood frequency analysis, *Journal of Hydrology*, 309\(1–4\), 114–132, 2005.](#)
- 1364
- 1365 [Meyers, S. R.: Astrochron: An R package for astrochronology, <http://cran.r-project.org/package=astrochron>.](#)
- 1366 [http://scholar.google.com/scholar?cluster=14876361610707754388&hl=en&oi=scholar](#), last access: 30
- 1367 [May 2017, 2014.](#)
- 1368
- 1369 [Meyers, S. R.: Cyclostratigraphy and the problem of astrochronologic testing, *Earth-Science Reviews*, 190,](#)
- 1370 [190–223, <https://doi.org/10.1016/j.earscirev.2018.11.015>, 2019.](#)
- 1371 [Miyaii, T., Tanabe, K., Matsushima, Y., Sato, S., Yokoyama, Y. and Matsuzaki, H.: Response of daily and](#)
- 1372 [annual shell growth patterns of the intertidal bivalve *Phacosoma japonicum* to Holocene coastal climate](#)
- 1373 [change in Japan, *Palaeogeography, Palaeoclimatology, Palaeoecology*, 286\(3\), 107–120,](#)
- 1374 [https://doi.org/10.1016/j.palaeo.2009.11.032, 2010.](#)
- 1375 [Mook, W. G.: Stable carbon and oxygen isotopes of natural waters in the Netherlands, *Isotope hydrology*,](#)
- 1376 [1970, 163–190, 1970.](#)
- 1377 [Morgan, V. and van Ommen, T. D.: Seasonality in late-Holocene climate from ice-core records, *The*](#)
- 1378 [Holocene, 7\(3\), 351–354, <https://doi.org/10.1177/095968369700700312>, 1997.](#)
- 1379 [Mosley-Thompson, E., Thompson, L. G., Dai, J., Davis, M. and Lin, P. N.: Climate of the last 500 years:](#)
- 1380 [High resolution ice core records, *Quaternary Science Reviews*, 12\(6\), 419–430,](#)
- 1381 [https://doi.org/10.1016/S0277-3791\(05\)80006-X, 1993.](#)
- 1382 [Müller, I. A., Fernandez, A., Radke, J., van Dijk, J., Bowen, D., Schwieters, J. and Bernasconi, S. M.:](#)
- 1383 [Carbonate clumped isotope analyses with the long-integration dual-inlet \(LIDI\) workflow: scratching at](#)
- 1384 [the lower sample weight boundaries: LIDI as key for more precise analyses on much less carbonate](#)
- 1385 [material, *Rapid Communications in Mass Spectrometry*, 31\(12\), 1057–1066,](#)
- 1386 [https://doi.org/10.1002/rcm.7878, 2017.](#)
- 1387 [Noorbergen, L. J., Abels, H. A., Hilgen, F. J., Robson, B. E., Jong, E. de, Dekkers, M. J., Krijgsman, W.,](#)
- 1388 [Smit, J., Collinson, M. E. and Kuiper, K. F.: Conceptual models for short-eccentricity-scale climate control](#)
- 1389 [on peat formation in a lower Palaeocene fluvial system, north-eastern Montana \(USA\), *Sedimentology*,](#)
- 1390 [65\(3\), 775–808, <https://doi.org/10.1111/sed.12405>, 2018.](#)
- 1391 [O'Donnell, M. S. and Ignizio, D. A.: Bioclimatic predictors for supporting ecological applications in the](#)
- 1392 [conterminous United States, *US Geological Survey Data Series*, 691\(10\), 2012.](#)
- 1393 [Passey, B. H. and Cerling, T. E.: Tooth enamel mineralization in ungulates: implications for recovering a](#)
- 1394 [primary isotopic time-series, *Geochimica et Cosmochimica Acta*, 66\(18\), 3225–3234, 2002.](#)
- 1395 [Petersen, S. V., Tabor, C. R., Lohmann, K. C., Poulsen, C. J., Meyer, K. W., Carpenter, S. J., Erickson, J.](#)
- 1396 [M., Matsunaga, K. K., Smith, S. Y. and Sheldon, N. D.: Temperature and salinity of the Late Cretaceous](#)
- 1397 [western interior seaway, *Geology*, 44\(11\), 903–906, 2016.](#)
- 1398 [Philander, S. G. H.: El Nino southern oscillation phenomena, *Nature*, 302\(5906\), 295–301, 1983.](#)
- 1399 [R Core Team: R: A language and environment for statistical computing. R Foundation for Statistical](#)
- 1400 [Computing, Vienna, Austria. <http://www.R-project.org/>, 2013.](#)

Formatted: Indent: Left: 0", Hanging: 0.13", Space After: Auto, Line spacing: single

1401 [Rodríguez-Sanz, L., Bernasconi, S. M., Marino, G., Heslop, D., Müller, I. A., Fernandez, A., Grant, K. M.,](#)
1402 [and Rohling, E. J.: Penultimate deglacial warming across the Mediterranean Sea revealed by clumped](#)
1403 [isotopes in foraminifera, Scientific Reports, 7\(1\), 1–11, <https://doi.org/10.1038/s41598-017-16528-6>,](#)
1404 [2017.](#)

1405 [Rohling, E. J.: Oxygen isotope composition of seawater, The Encyclopedia of Quaternary Science,](#)
1406 [Amsterdam: Elsevier, 2, 915–922, 2013.](#)

1407 [Sano, Y., Kobayashi, S., Shirai, K., Takahata, N., Matsumoto, K., Watanabe, T., Sowa, K. and Iwai, K.:](#)
1408 [Past daily light cycle recorded in the strontium/calcium ratios of giant clam shells, Nature](#)
1409 [Communications, 3, 761, 2012.](#)

1410 [Sato, S.: Temporal change of life-history traits in fossil bivalves: an example of *Phacosoma japonicum* from](#)
1411 [the Pleistocene of Japan, Palaeogeography, Palaeoclimatology, Palaeoecology, 154\(4\), 313–323,](#)
1412 [https://doi.org/10.1016/S0031-0182\(99\)00106-6](https://doi.org/10.1016/S0031-0182(99)00106-6), 1999.

1413 [Schmitt, J., Schneider, R., Elsig, J., Leuenberger, D., Lourantou, A., Chappellaz, J., Kohler, P., Joos, F.,](#)
1414 [Stocker, T. F., Leuenberger, M. and Fischer, H.: Carbon Isotope Constraints on the Deglacial CO₂ Rise](#)
1415 [from Ice Cores, Science, 336\(6082\), 711–714, <https://doi.org/10.1126/science.1217161>, 2012.](#)

1416 [Scholz, D. and Hoffmann, D. L.: StalAge—An algorithm designed for construction of speleothem age models,](#)
1417 [Quaternary Geochronology, 6\(3–4\), 369–382, 2011.](#)

1418 [Schöne, B. R.: The curse of physiology—challenges and opportunities in the interpretation of geochemical](#)
1419 [data from mollusk shells, Geo-Marine Letters, 28\(5–6\), 269–285, 2008.](#)

1420 [Schöne, B. R., Fiebig, J., Pfeiffer, M., Gleß, R., Hickson, J., Johnson, A. L., Dreyer, W. and Oschmann, W.:](#)
1421 [Climate records from a bivalved *Methuselah* \(*Arctica islandica*, Mollusca; Iceland\), Palaeogeography,](#)
1422 [Palaeoclimatology, Palaeoecology, 228\(1–2\), 130–148, 2005.](#)

1423 [Schöne, B. R., Rodland, D. L., Fiebig, J., Oschmann, W., Goodwin, D., Flessa, K. W. and Dettman, D.:](#)
1424 [Reliability of multitaxon, multiproxy reconstructions of environmental conditions from accretionary](#)
1425 [biogenic skeletons, The Journal of geology, 114\(3\), 267–285, 2006.](#)

1426 [Scourse, J., Richardson, C., Forsythe, G., Harris, I., Heinemeier, J., Fraser, N., Briffa, K. and Jones, P.:](#)
1427 [First cross-matched floating chronology from the marine fossil record: data from growth lines of the long-](#)
1428 [lived bivalve mollusc *Arctica islandica*, The Holocene, 16\(7\), 967–974,](#)
1429 <https://doi.org/10.1177/0959683606h987rp>, 2006.

1430 [Sha, L., Mahata, S., Duan, P., Luz, B., Zhang, P., Baker, J., Zong, B., Ning, Y., Brahim, Y. A., Zhang, H.,](#)
1431 [Edwards, R. L. and Cheng, H.: A novel application of triple oxygen isotope ratios of speleothems,](#)
1432 [Geochimica et Cosmochimica Acta, 270, 360–378, <https://doi.org/10.1016/j.gca.2019.12.003>, 2020.](#)

1433 [Shao, D., Mei, Y., Yang, Z., Wang, Y., Yang, W., Gao, Y., Yang, L. and Sun, L.: Holocene ENSO variability](#)
1434 [in the South China Sea recorded by high-resolution oxygen isotope records from the shells of *Tridacna*](#)
1435 [spp., Scientific Reports, 10\(1\), 3921, <https://doi.org/10.1038/s41598-020-61013-2>, 2020.](#)

1436 [Sinnesael, M., De Vleeschouwer, D., Zeeden, C., Batenburg, S. J., Da Silva, A.-C., de Winter, N. J.,](#)
1437 [Dinarès-Turell, J., Drury, A. J., Gambacorta, G. and Hilgen, F. J.: The Cyclostratigraphy Intercomparison](#)
1438 [Project \(CIP\): consistency, merits and pitfalls, Earth-Science Reviews, 102965, 2019.](#)

1439 [Stap, L., Lourens, L. J., Thomas, E., Sluijs, A., Bohaty, S. and Zachos, J. C.: High-resolution deep-sea](#)
1440 [carbon and oxygen isotope records of Eocene Thermal Maximum 2 and H2, *Geology*, 38\(7\), 607–610,](#)
1441 [2010.](#)

1442 [Steffensen, J. P., Andersen, K. K., Bigler, M., Clausen, H. B., Dahl-Jensen, D., Fischer, H., Goto-Azuma,](#)
1443 [K., Hansson, M., Johnsen, S. J. and Jouzel, J.: High-resolution Greenland ice core data show abrupt](#)
1444 [climate change happens in few years, *Science*, 321\(5889\), 680–684, 2008.](#)

1445 [Steuber, T., Rauch, M., Masse, J.-P., Graaf, J. and Malkoč, M.: Low-latitude seasonality of Cretaceous](#)
1446 [temperatures in warm and cold episodes, *Nature*, 437\(7063\), 1341–1344,](#)
1447 [https://doi.org/10.1038/nature04096, 2005.](#)

1448 [Surge, D., Lohmann, K. C. and Dettman, D. L.: Controls on isotopic chemistry of the American oyster,](#)
1449 [Crassostrea virginica: implications for growth patterns, *Palaeogeography, Palaeoclimatology,*](#)
1450 [Palaeoecology, 172\(3\), 283–296, 2001.](#)

1451 [Titschack, J., Zuschin, M., Spötl, C. and Baal, C.: The giant oyster Hyotissa hyotis from the northern Red](#)
1452 [Sea as a decadal-scale archive for seasonal environmental fluctuations in coral reef habitats, *Coral*](#)
1453 [Reefs, 29\(4\), 1061–1075, 2010.](#)

1454 [Treble, P., Shelley, J. M. G. and Chappell, J.: Comparison of high resolution sub-annual records of trace](#)
1455 [elements in a modern \(1911–1992\) speleothem with instrumental climate data from southwest Australia,](#)
1456 [Earth and Planetary Science Letters, 216\(1\), 141–153, https://doi.org/10.1016/S0012-821X\(03\)00504-1,](#)
1457 [2003.](#)

1458 [Tsukakoshi, Y.: Sampling variability and uncertainty in total diet studies, *Analyst*, 136\(3\), 533–539,](#)
1459 [https://doi.org/10.1039/C0AN00397B, 2011.](#)

1460 [Tudhope, A. W.: Variability in the El Niño-Southern Oscillation Through a Glacial-Interglacial Cycle,](#)
1461 [Science, 291\(5508\), 1511–1517, https://doi.org/10.1126/science.1057969, 2001.](#)

1462 [Ullmann, C. V., Wiechert, U. and Korte, C.: Oxygen isotope fluctuations in a modern North Sea oyster](#)
1463 [\(Crassostrea gigas\) compared with annual variations in seawater temperature: Implications for](#)
1464 [palaeoclimate studies, *Chemical Geology*, 277\(1\), 160–166, 2010.](#)

1465 [Van Rampelbergh, M., Verheyden, S., Allan, M., Quinif, Y., Keppens, E. and Claeys, P.: Seasonal variations](#)
1466 [recorded in cave monitoring results and a 10 year monthly resolved speleothem δ18O and δ13C record](#)
1467 [from the Han-sur-Lesse cave, Belgium, *Climate of the Past Discussions*, 10, 1821–1856, 2014.](#)

1468 [Vansteenberghe, S., Verheyden, S., Cheng, H., Edwards, R. L., Keppens, E. and Claeys, P.: Paleoclimate](#)
1469 [in continental northwestern Europe during the Eemian and early Weichselian \(125–97 ka\): insights from](#)
1470 [a Belgian speleothem, *Clim. Past*, 12\(7\), 1445–1458, https://doi.org/10.5194/cp-12-1445-2016, 2016.](#)

1471 [Vansteenberghe, S., Winter, N. de, Sinnesael, M., Verheyden, S., Goderis, S., Malderen, S. J. M. V.,](#)
1472 [Vanhaecke, F. and Claeys, P.: Reconstructing seasonality through stable isotope and trace element](#)
1473 [analysis of the Proserpine stalagmite, Han-sur-Lesse Cave, Belgium: indications for climate-driven](#)
1474 [changes during the last 400 years, *Climate of the Past Discussions*, 1–32, https://doi.org/10.5194/cp-](#)
1475 [2019-78, 2019.](#)

1476 [Veizer, J. and Prokoph, A.: Temperatures and oxygen isotopic composition of Phanerozoic oceans, *Earth-*](#)
1477 [Science Reviews, 146, 92–104, https://doi.org/10.1016/j.earscirev.2015.03.008, 2015.](#)

1478 [Vleeschouwer, D. D., Vahlenkamp, M., Crucifix, M. and Pälike, H.: Alternating Southern and Northern](#)
1479 [Hemisphere climate response to astronomical forcing during the past 35 m.y., *Geology*, 45\(4\), 375–378,](#)
1480 <https://doi.org/10.1130/G38663.1>, 2017.

1481 [Warter, V. and Müller, W.: Daily growth and tidal rhythms in Miocene and modern giant clams revealed via](#)
1482 [ultra-high resolution LA-ICPMS analysis—A novel methodological approach towards improved](#)
1483 [sclerochemistry, *Palaeogeography, Palaeoclimatology, Palaeoecology*, 465, 362–375, 2017.](#)

1484 [Westerhold, T., Marwan, N., Drury, A. J., Liebrand, D., Agnini, C., Anagnostou, E., Barnet, J. S., Bohaty,](#)
1485 [S. M., De Vleeschouwer, D. and Florindo, F.: An astronomically dated record of Earth's climate and its](#)
1486 [predictability over the last 66 million years, *Science*, 369\(6509\), 1383–1387, 2020.](#)

1487 [Wilkinson, B. H. and Ivany, L. C.: Paleoclimatic inference from stable isotope profiles of accretionary](#)
1488 [biogenic hardparts – a quantitative approach to the evaluation of incomplete data, *Palaeogeography,*](#)
1489 [*Palaeoclimatology, Palaeoecology*, 185\(1\), 95–114, \[https://doi.org/10.1016/S0031-0182\\(02\\)00279-1\]\(https://doi.org/10.1016/S0031-0182\(02\)00279-1\),](#)
1490 [2002.](#)

1491 [Yan, H., Liu, C., An, Z., Yang, W., Yang, Y., Huang, P., Qiu, S., Zhou, P., Zhao, N. and Fei, H.: Extreme](#)
1492 [weather events recorded by daily to hourly resolution biogeochemical proxies of marine giant clam shells,](#)
1493 [*Proceedings of the National Academy of Sciences*, 2020. \[Bahr K. D., Jekiel P. L. and Rodgers K. S.\]\(#\)](#)
1494 [\(2017\) Seasonal and annual calcification rates of the Hawaiian reef coral, *Montipora capitata*, under](#)
1495 [present and future climate change scenarios. *ICES J Mar Sci* **74**, 1083–1091.](#)

1496 [Bak R., P., Nieuwland G. and Meesters E. H. \(2009\) Coral growth rates revisited after 31 years: what is](#)
1497 [causing lower extension rates in *Acropora palmata*? *Bulletin of Marine Science* **84**, 287–294.](#)

1498 [Balasse M. \(2002\) Reconstructing dietary and environmental history from enamel isotopic analysis: time](#)
1499 [resolution of intra-tooth sequential sampling. *International Journal of Osteoarchaeology* **12**, 155–165.](#)

1500 [Balasse M., Ambrose S. H., Smith A. B. and Price T. D. \(2002\) The Seasonal Mobility Model for Prehistoric](#)
1501 [Herders in the South-western Cape of South Africa Assessed by Isotopic Analysis of Sheep Tooth](#)
1502 [Enamel. *Journal of Archaeological Science* **29**, 917–932.](#)

1503 [Barlow R. \(2004\) Asymmetric errors. *arXiv preprint physics/0401042*.](#)

1504 [Barlow R. \(2003\) Asymmetric systematic errors. *arXiv preprint physics/0306138*.](#)

1505 [Berger A. L. \(1992\) Astronomical theory of paleoclimates and the last glacial-interglacial cycle. *Quaternary*](#)
1506 [*Science Reviews* **11**, 571–584.](#)

1507 [Bernasconi S. M., Müller I. A., Bergmann K. D., Breitenbach S. F., Fernandez A., Hodell D. A., Jaggi M.,](#)
1508 [Meckler A. N., Millan I. and Ziegler M. \(2018\) Reducing uncertainties in carbonate-clumped isotope](#)
1509 [analysis through consistent carbonate-based standardization. *Geochemistry, Geophysics, Geosystems*](#)
1510 [**19**, 2895–2914.](#)

1511 [Bowen, G.J. \(2020\) \[WaterIsotopes.org\]\(http://waterisotopes.org\). Available at: <http://wateriso.utah.edu/waterisotopes> Accessed](#)
1512 [August 4, 2020.](#)

1513 [Brand W. A., Coplen T. B., Vogl J., Rosner M. and Prohaska T. \(2014\) Assessment of international](#)
1514 [reference materials for isotope-ratio analysis \(IUPAC Technical Report\). *Pure and Applied Chemistry* **86**,](#)
1515 [425–467.](#)

1516 Briard J., Pucéat E., Vennin E., Daëron M., Chavagnac V., Jaillet R., Merle D. and de Rafélis M. (2020)
 1517 Seawater paleotemperature and paleosalinity evolution in neritic environments of the Mediterranean
 1518 margin: Insights from isotope analysis of bivalve shells. *Palaeogeography, Palaeoclimatology,
 1519 Palaeoecology* **543**, 100582.

1520 Charles C. D., Hunter D. E. and Fairbanks R. G. (1997) Interaction between the ENSO and the Asian
 1521 monsoon in a coral record of tropical climate. *Science* **277**, 925–928.

1522 Comboul M., Emile-Geay J., Evans M. N., Mirnateghi N., Cobb K. M. and Thompson D. M. (2014) A
 1523 probabilistic model of chronological errors in layer-counted climate proxies: applications to annually
 1524 banded coral archives. *Climate of the Past* **10**, 825–841.

1525 Compton T. J., Rijkenberg M. J. A., Drent J. and Piersma T. (2007) Thermal tolerance ranges and climate
 1526 variability: A comparison between bivalves from differing climates. *Journal of Experimental Marine
 1527 Biology and Ecology* **352**, 200–211.

1528 Cook E. R. and Kairiukstis L. A. (2013) *Methods of dendrochronology: applications in the environmental
 1529 sciences.*, Springer Science & Business Media.

1530 Cramer B. S., Toggweiler J. R., Wright J. D., Katz M. E. and Miller K. G. (2009) Ocean overturning since
 1531 the Late Cretaceous: Inferences from a new benthic foraminiferal isotope compilation. *Paleoceanography*
 1532 **24**. Available at: <http://agupubs.onlinelibrary.wiley.com/doi/abs/10.1029/2008PA001683> [Accessed
 1533 March 31, 2020].

1534 Crossland C. (1984) Seasonal variations in the rates of calcification and productivity in the coral *Acropora*
 1535 *formosa* on a high-latitude reef. *Marine Ecology Progress Series* **15**, 135–140.

1536 van Dam J. A. and Reichert G. J. (2009) Oxygen and carbon isotope signatures in late Neogene horse
 1537 teeth from Spain and application as temperature and seasonality proxies. *Palaeogeography,
 1538 Palaeoclimatology, Palaeoecology* **274**, 64–81.

1539 Dattalo P. (2008) *Determining Sample Size: Balancing Power, Precision, and Practicality.*, Oxford
 1540 University Press, USA.

1541 Dayem K. E., Molnar P., Battisti D. S. and Roe G. H. (2010) Lessons learned from oxygen isotopes in
 1542 modern precipitation applied to interpretation of speleothem records of paleoclimate from eastern Asia.
 1543 *Earth and Planetary Science Letters* **295**, 219–230.

1544 De Ridder F., de Brauwere A., Pintelon R., Schoukens J., Dehairs F., Baeyens W. and Wilkinson B. H.
 1545 (2007) Comment on: Paleoclimatic inference from stable isotope profiles of accretionary biogenic
 1546 hardparts—a quantitative approach to the evaluation of incomplete data, by Wilkinson, B.H., Ivany, L.C.,
 1547 2002. *Palaeogeogr. Palaeoclimatol. Palaeoecol.* **185**, 95–114. *Palaeogeography, Palaeoclimatology,
 1548 Palaeoecology* **248**, 473–476.

1549 De Vleeschouwer D., Da Silva A. C., Sinnesael M., Chen D., Day J. E., Whalen M. T., Guo Z. and Claeys
 1550 P. (2017a) Timing and pacing of the Late Devonian mass extinction event regulated by eccentricity and
 1551 obliquity. *Nature Communications* **8**, 1–11.

1552 De Vleeschouwer D., Vahlenkamp M., Crucifix M. and Pälike H. (2017b) Alternating Southern and Northern
 1553 Hemisphere climate response to astronomical forcing during the past 35 my. *Geology* **45**, 375–378.

1554 de Winter N., Sinnesael M., Makarona C., Vansteenberge S. and Claeys P. (2017) Trace element analyses
 1555 of carbonates using portable and micro-X-ray fluorescence: Performance and optimization of

1556 measurement parameters and strategies. *Journal of Analytical Atomic Spectrometry* **32**, 1211–1223.
 1557 Winter N. J., Goderis S., Malderen S. J. M. V., Sinnesael M., Vansteenberge S., Snoeck C., Belza J.,
 1558 Vanhaecke F. and Claeys P. (2020a) Subdaily-Scale Chemical Variability in a *Torreites Sanchezi* Rudist
 1559 Shell: Implications for Rudist Paleobiology and the Cretaceous Day–Night Cycle. *Paleoceanography and*
 1560 *Paleoclimatology* **35**, e2019PA003723.

1561 de Winter N. J., Snoeck C. and Claeys P. (2016) Seasonal Cyclicity in Trace Elements and Stable Isotopes
 1562 of Modern Horse Enamel. *PLoS one* **11**, e0166678.

1563 de Winter N. J., Ullmann C. V., Sørensen A. M., Thibault N., Goderis S., Van Malderen S. J. M., Snoeck
 1564 C., Goolaerts S., Vanhaecke F. and Claeys P. (2020b) Shell chemistry of the boreal Campanian bivalve
 1565 *Rastollum diluvianum* (Linnaeus, 1767) reveals temperature seasonality, growth rates and life cycle of
 1566 an extinct Cretaceous oyster. *Biogeosciences* **17**, 2897–2922.

1567 de Winter N. J., Vellekoop J., Clark A. J., Stassen P., Speijer R. P. and Claeys P. (2020c) The giant marine
 1568 gastropod *Campanile giganteum* (Lamarck, 1804) as a high-resolution archive of seasonality in the
 1569 Eocene greenhouse world. *Geochemistry, Geophysics, Geosystems* **n/a**, e2019GC008794.

1570 de Winter N. J., Vellekoop J., Vorrsselmans R., Golreihani A., Soete J., Petersen S. V., Meyer K. W., Casadio
 1571 S., Speijer R. P. and Claeys P. (2019) An assessment of latest Cretaceous *Pyenodonte vesicularis*
 1572 (Lamarck, 1806) shells as records for palaeoseasonality: a multi-proxy investigation. *Climate of the Past*
 1573 **14**, 725–749.

1574 Denton G. H., Alley R. B., Comer G. C. and Broecker W. S. (2005) The role of seasonality in abrupt climate
 1575 change. *Quaternary Science Reviews* **24**, 1159–1182.

1576 Dupont Nivet G., Krijgsman W., Langereis C. G., Abels H. A., Dai S. and Fang X. (2007) Tibetan plateau
 1577 aridification linked to global cooling at the Eocene–Oligocene transition. *Nature* **445**, 635–638.

1578 Elderfield H. (1986) Strontium isotope stratigraphy. *Palaeogeography, palaeoclimatology, palaeoecology*
 1579 **57**, 71–90.

1580 Erbacher J., Huber B. T., Norris R. D. and Markey M. (2001) Increased thermohaline stratification as a
 1581 possible cause for an ocean anoxic event in the Cretaceous period. *Nature* **409**, 325–327.

1582 Fairbanks R. G., Evans M. N., Rubenstone J. L., Mortlock R. A., Broad K., Moore M. D. and Charles C. D.
 1583 (1997) Evaluating climate indices and their geochemical proxies measured in corals. *Coral Reefs* **16**,
 1584 S93–S100.

1585 Fernandez A., Müller I. A., Rodríguez-Sanz L., van Dijk J., Looser N. and Bernasconi S. M. (2017) A
 1586 reassessment of the precision of carbonate clumped isotope measurements: implications for calibrations
 1587 and paleoclimate reconstructions. *Geochemistry, Geophysics, Geosystems* **18**, 4375–4386.

1588 Fricke H. C. and D'Neil J. R. (1996) Inter- and intra-tooth variation in the oxygen isotope composition of
 1589 mammalian tooth enamel phosphate: implications for. *Palaeogeography, Palaeoclimatology,*
 1590 *Palaeoecology* **126**, 91–99.

1591 Gaspar M. B., Ferreira R. and Monteiro C. C. (1999) Growth and reproductive cycle of *Donax trunculus* L.,
 1592 (Mollusca: Bivalvia) off Faro, southern Portugal. *Fisheries Research* **41**, 309–316.

1593 Goodwin D. H., Paul P. and Wissink C. L. (2009) MoGroFunGen: A numerical model for reconstructing
 1594 intra-annual growth rates of bivalve molluscs. *Palaeogeography, Palaeoclimatology, Palaeoecology* **276**,
 1595 47–55.

- 1596 Goodwin D. H., Schöne B. R. and Dettman D. L. (2003) Resolution and fidelity of oxygen isotopes as
1597 paleotemperature proxies in bivalve mollusk shells: models and observations. *Palaios* **18**, 110–125.
- 1598 Harwood A. J. P., Dennis P. F., Marca A. D., Pilling G. M. and Millner R. S. (2008) The oxygen isotope
1599 composition of water masses within the North Sea. *Estuarine, Coastal and Shelf Science* **78**, 353–359.
- 1600 Hendriks I. E., Basso L., Deudero S., Cabanellas-Reboredo M. and Álvarez E. (2012) Relative growth rates
1601 of the noble pen shell *Pinna nobilis* throughout ontogeny around the Balearic Islands (Western
1602 Mediterranean, Spain). *Journal of Shellfish Research* **31**, 749–756.
- 1603 Henkes, G. A., Passey, B. H., Grossman, E. L., Shenton, B. J., Yancey, T. E. and Pérez-Huerta, A. (2018)
1604 Temperature evolution and the oxygen isotope composition of Phanerozoic oceans from carbonate
1605 clumped isotope thermometry. *Earth and Planetary Science Letters* **490**, 40–50,
1606 doi:10.1016/j.epsl.2018.02.001.
- 1607 Hesselbo S. P., Gröcke D. R., Jenkyns H. C., Bjerrum C. J., Farrimond P., Morgans-Bell H. S. and Green
1608 O. R. (2000) Massive dissociation of gas hydrate during a Jurassic oceanic anoxic event. *Nature* **406**,
1609 392–395.
- 1610 Hilgen F. J. (1991) Astronomical calibration of Gauss to Matuyama sapropels in the Mediterranean and
1611 implication for the Geomagnetic Polarity Time Scale. *Earth and Planetary Science Letters* **104**, 226–244.
- 1612 Hurrell J. W. (1995) Decadal trends in the North Atlantic Oscillation: regional temperatures and precipitation.
1613 *Science* **269**, 676–679.
- 1614 Huybers P. and Curry W. (2006) Links between annual, Milankovitch and continuum temperature variability.
1615 *Nature* **441**, 329.
- 1616 Huyghe D., Lartaud F., Emmanuel L., Merle D. and Renard M. (2015) Palaeogene climate evolution in the
1617 Paris Basin from oxygen stable isotope ($\delta^{18}\text{O}$) compositions of marine molluscs. *Journal of the
1618 Geological Society* **172**, 576–587.
- 1619 Huyghe D., de Rafélis M., Ropert M., Mouchi V., Emmanuel L., Renard M. and Lartaud F. (2019) New
1620 insights into oyster high-resolution hinge growth patterns. *Marine biology* **166**, 48.
- 1621 IPCC (2013) *IPCC, 2013: Climate Change 2013: The Physical Science Basis. Contribution of Working
1622 Group I to the Fifth Assessment Report of the Intergovernmental Panel on Climate Change, 1535 pp.*,
1623 Cambridge Univ. Press, Cambridge, UK, and New York.
- 1624 Ivany L. C. (2012) Reconstructing paleoseasonality from accretionary skeletal carbonates—challenges and
1625 opportunities. *The Paleontological Society Papers* **18**, 133–166.
- 1626 Jenkyns H. C. (2010) Geochemistry of oceanic anoxic events. *Geochemistry, Geophysics, Geosystems* **11**.
1627 Available at: <http://agupubs.onlinelibrary.wiley.com/doi/abs/10.1029/2009GC002788> [Accessed July 8,
1628 2020].
- 1629 Jennions, S. M., Thomas, E., Schmidt, D. N., Lunt, D., & Ridgwell, A. (2015). Changes in benthic
1630 ecosystems and ocean circulation in the Southeast Atlantic across Eocene Thermal Maximum 2.
1631 *Paleoceanography*, **30**(8), 1059-1077.
- 1632 Jones A. M., Iacumin P. and Young E. D. (1999) High-resolution $\delta^{18}\text{O}$ analysis of tooth enamel phosphate
1633 by isotope ratio monitoring gas chromatography mass spectrometry and ultraviolet laser fluorination., **8**-

- 1634 Judd E. J., Wilkinson B. H. and Ivany L. C. (2018) The life and time of clams: Derivation of intra-annual
 1635 growth rates from high-resolution oxygen isotope profiles. *Palaeogeography, Palaeoclimatology,
 1636 Palaeoecology* **490**, 70–83.
- 1637 Kele S., Breitenbach S. F., Capezzuoli E., Meckler A. N., Ziegler M., Millan I. M., Kluge T., Deák J.,
 1638 Hanselmann K. and John C. M. (2015) Temperature dependence of oxygen and clumped isotope
 1639 fractionation in carbonates: a study of travertines and tufas in the 6–95 C temperature range. *Geochimica
 1640 et Cosmochimica Acta* **168**, 172–192.
- 1641 Kim S.-T. and O'Neil J. R. (1997) Equilibrium and nonequilibrium oxygen isotope effects in synthetic
 1642 carbonates. *Geochimica et Cosmochimica Acta* **61**, 3461–3475.
- 1643 Kocken, I. J., Müller, J. A. and Ziegler, M.: Optimizing the Use of Carbonate Standards to Minimize
 1644 Uncertainties in Clumped Isotope Data, *Geochemistry, Geophysics, Geosystems*, 20(11), 5565–5577,
 1645 doi:10.1029/2019GC008545, 2019.
- 1646 Kohn, M.J., 2004. Comment: tooth enamel mineralization in ungulates: implications for recovering a primary
 1647 isotopic time series, by BH Passey and TE Cerling (2002). *Geochimica et Cosmochimica Acta* **68**, 403–
 1648 405.
- 1649 Korte C. and Ullmann C. V. (2018) Permian strontium isotope stratigraphy. *Geological Society, London,
 1650 Special Publications* **450**, 105–118.
- 1651 Laurentano V., Littler K., Polling M., Zachos J. C. and Lourens L. J. (2015) Frequency, magnitude and
 1652 character of hyperthermal events at the onset of the Early Eocene Climatic Optimum. *Climate of the Past*
 1653 **11**, 1313–1324.
- 1654 Laurentano V., Zachos J. C. and Lourens L. J. (2018) Orbitally Paced Carbon and Deep-Sea Temperature
 1655 Changes at the Peak of the Early Eocene Climatic Optimum. *Paleoceanography and Paleoclimatology*
 1656 **33**, 1050–1065.
- 1657 Lear C. H., Bailey T. R., Pearson P. N., Coxall H. K. and Rosenthal Y. (2008) Cooling and ice growth across
 1658 the Eocene-Oligocene transition. *Geology* **36**, 251–254.
- 1659 LeGrande A. N. and Schmidt G. A. (2006) Global gridded data set of the oxygen isotopic composition in
 1660 seawater. *Geophysical research letters* **33**.
- 1661 Legros R., Balmain N. and Bonel G. (1986) Structure and composition of the mineral phase of periosteal
 1662 bone. *Journal of chemical research. Synopses*, 8–9.
- 1663 Lisiecki L. E. and Raymo M. E. (2005) A Pliocene-Pleistocene stack of 57 globally distributed benthic $\delta^{18}O$
 1664 records. *Paleoceanography* **20**. Available at:
 1665 <http://agupubs.onlinelibrary.wiley.com/doi/abs/10.1029/2004PA001071> [Accessed March 31, 2020].
- 1666 Lourens L. J., Becker J., Bintanja R., Hilgen F. J., Tuenter E., Van de Wal R. S. and Ziegler M. (2010)
 1667 Linear and non-linear response of late Neogene glacial cycles to obliquity forcing and implications for the
 1668 Milankovitch theory. *Quaternary Science Reviews* **29**, 352–365.
- 1669 Lourens L. J., Sluijs A., Kroon D., Zachos J. C., Thomas E., Röhl U., Bowles J. and Raffi I. (2005)
 1670 Astronomical pacing of late Palaeocene to early Eocene global warming events. *Nature* **435**, 1083–1087.
- 1671 Liu Z., Pagani M., Zinniker D., DeConto R., Huber M., Brinkhuis H., Shah S. R., Leckie R. M. and Pearson
 1672 A. (2009) Global cooling during the Eocene-Oligocene climate transition. *Science* **323**, 1187–1190.

- 1673 Luz B. and Kolodny Y. (1985) Oxygen isotope variations in phosphate of biogenic apatites, IV. Mammal
1674 teeth and bones. *Earth and Planetary Science Letters* **75**, 29–36.
- 1675 McArthur J. M., Howarth R. J. and Shields G. A. (2012) Strontium isotope stratigraphy. *The geologic time*
1676 *scale* **1**, 127–144.
- 1677 Meckler A. N., Ziegler M., Millán M. I., Breitenbach S. F. and Bernasconi S. M. (2014) Long-term
1678 performance of the Kiel carbonate device with a new correction scheme for clumped isotope
1679 measurements. *Rapid Communications in Mass Spectrometry* **28**, 1705–1715.
- 1680 Merz B. and Thielen A. H. (2005) Separating natural and epistemic uncertainty in flood frequency analysis.
1681 *Journal of Hydrology* **309**, 114–132.
- 1682 Meyers S. R. (2014) *Astrochron: An R package for astrochronology.*, [http://cran.r-](http://cran.r-project.org/package=astrochron)
1683 [project.org/package=astrochron.](http://cran.r-project.org/package=astrochron) Available at:
1684 <http://scholar.google.com/scholar?cluster=14876361610707754388&hl=en&oi=scholar>. [Accessed May
1685 30, 2017].
- 1686 Meyers S. R. (2019) Cyclostratigraphy and the problem of astrochronologic testing. *Earth-Science Reviews*
1687 **190**, 190–223.
- 1688 Miyaji, T., Tanabe, K., Matsushima, Y., Sato, S., Yokoyama, Y. and Matsuzaki, H.: Response of daily and
1689 annual shell growth patterns of the intertidal bivalve *Phacosoma japonicum* to Holocene coastal climate
1690 change in Japan, *Palaeogeography, Palaeoclimatology, Palaeoecology*, **286**(3), 107–120,
1691 doi:10.1016/j.palaeo.2009.11.032, 2010.
- 1692 Meek W. G. (1970) Stable carbon and oxygen isotopes of natural waters in the Netherlands. *Isotope*
1693 *hydrology* **1970**, 163–190.
- 1694 Morgan V. and van Ommen T. D. (1997) Seasonality in late-Holocene climate from ice-core records. *The*
1695 *Holocene* **7**, 351–354.
- 1696 Mosley-Thompson E., Thompson L. G., Dai J., Davis M. and Lin P. N. (1993) Climate of the last 500 years:
1697 High-resolution ice core records. *Quaternary Science Reviews* **12**, 419–430.
- 1698 Müller I. A., Fernandez A., Radke J., van Dijk J., Bowen D., Schwieters J. and Bernasconi S. M. (2017)
1699 Carbonate clumped isotope analyses with the long-integration dual-inlet (LIDI) workflow: scratching at
1700 the lower sample weight boundaries: LIDI as key for more precise analyses on much less carbonate
1701 material. *Rapid Communications in Mass Spectrometry* **31**, 1057–1066.
- 1702 Nohl T., Jarochovska E. and Munnecke A. (2018) Revealing the genesis of limestone-marl alternations: a
1703 taphonomic approach. *Palaios* **34**, 15–31.
- 1704 Noorbergen L. J., Abels H. A., Hilgen F. J., Robson B. E., Jong E. de, Dekkers M. J., Krijgsman W., Smit
1705 J., Collinson M. E. and Kuiper K. F. (2018) Conceptual models for short-eccentricity-scale climate control
1706 on peat formation in a lower Palaeocene fluvial system, north-eastern Montana (USA). *Sedimentology*
1707 **65**, 775–808.
- 1708 Paillard D., Labeyrie L. D. and Yiou P. (1996) AnalySeries 1.0: a Macintosh software for the analysis of
1709 geophysical time series. *Eos* **77**, 379.
- 1710 Passey B. H. and Cerling T. E. (2002) Tooth enamel mineralization in ungulates: implications for recovering
1711 a primary isotopic time series. *Geochimica et Cosmochimica Acta* **66**, 3225–3234.

- 1712 Pellegrini M. and Snoeck C. (2016) Comparing bioapatite carbonate pre-treatments for isotopic
1713 measurements: Part 2—Impact on carbon and oxygen isotope compositions. *Chemical Geology* **420**, 88–
1714 96.
- 1715 Petersen S. V., Tabor C. R., Lohmann K. C., Poulsen C. J., Meyer K. W., Carpenter S. J., Erickson J. M.,
1716 Matsunaga K. K., Smith S. Y. and Sheldon N. D. (2016) Temperature and salinity of the Late Cretaceous
1717 western interior seaway. *Geology* **44**, 903–906.
- 1718 Philander S. G. H. (1983) El Niño southern oscillation phenomena. *Nature* **302**, 295–301.
- 1719 R Core Team (2013) *R: A language and environment for statistical computing*. R Foundation for Statistical
1720 Computing, Vienna, Austria. Available at: <http://www.R-project.org/>.
- 1721 Ramsey C. B. and Lee S. (2013) Recent and Planned Developments of the Program OxCal. *Radiocarbon*
1722 **55**, 720–730.
- 1723 Rodríguez-Sanz L., Bernasconi S. M., Marino G., Heslop D., Müller I. A., Fernandez A., Grant K. M. and
1724 Rohling E. J. (2017) Penultimate deglacial warming across the Mediterranean Sea revealed by clumped
1725 isotopes in foraminifera. *Scientific Reports* **7**, 1–11.
- 1726 Rohling E. J. (2013) Oxygen isotope composition of seawater. *The Encyclopedia of Quaternary Science*.
1727 Amsterdam: Elsevier **2**, 915–922.
- 1728 Saltzman M. R. and Thomas E. (2012) Carbon isotope stratigraphy. *The geologic time scale* **1**, 207–232.
- 1729 Sano Y., Kobayashi S., Shirai K., Takahata N., Matsumoto K., Watanabe T., Sowa K. and Iwai K. (2012)
1730 Past daily light cycle recorded in the strontium/calcium ratios of giant clam shells. *Nature Communications*
1731 **3**, 761.
- 1732 Sato, S.: Temporal change of life-history traits in fossil bivalves: an example of *Phacosoma japonicum* from
1733 the Pleistocene of Japan, *Palaeogeography, Palaeoclimatology, Palaeoecology*, **154**(4), 313–323,
1734 doi:10.1016/S0031-0182(99)00106-6, 1999.
- 1735 Schmitt J., Schneider R., Elsig J., Leuenberger D., Laurantou A., Chappellaz J., Kohler P., Joos F., Stocker
1736 T. F., Leuenberger M. and Fischer H. (2012) Carbon Isotope Constraints on the Deglacial CO₂ Rise from
1737 Ice Cores. *Science* **336**, 711–714.
- 1738 Scholz D. and Hoffmann D. L. (2011) StalAge—An algorithm designed for construction of speleothem age
1739 models. *Quaternary Geochronology* **6**, 369–382.
- 1740 Schöne B. R. (2008) The curse of physiology—challenges and opportunities in the interpretation of
1741 geochemical data from mollusk shells. *Geo-Marine Letters* **28**, 269–285.
- 1742 Schöne B. R., Fiebig J., Pfeiffer M., Gleß R., Hickson J., Johnson A. L., Dreyer W. and Oschmann W.
1743 (2005) Climate records from a bivalved *Methuselah* (*Arctica islandica*, Mollusca; Iceland).
1744 *Palaeogeography, Palaeoclimatology, Palaeoecology* **228**, 130–148.
- 1745 Schöne B. R., Rodland D. L., Fiebig J., Oschmann W., Goodwin D., Flessa K. W. and Dettman D. (2006)
1746 Reliability of multitaxon, multiproxy reconstructions of environmental conditions from accretionary
1747 biogenic skeletons. *The Journal of geology* **114**, 267–285.
- 1748 Scourse, J., Richardson, C., Forsythe, G., Harris, I., Heinemeier, J., Fraser, N., Briffa, K. and Jones, P.:
1749 First cross-matched floating chronology from the marine fossil record: data from growth lines of the long-

- 1750 lived bivalve mollusc *Arctica islandica*, The Holocene, 16(7), 967–974, doi:10.1177/0959683606h1987rp,
1751 2006.
- 1752 Sha L., Mahata S., Duan P., Luz B., Zhang P., Baker J., Zong B., Ning Y., Brahim Y. A., Zhang H., Edwards
1753 R. L. and Cheng H. (2020) A novel application of triple oxygen isotope ratios of speleothems. *Geochimica
1754 et Cosmochimica Acta* **270**, 360–378.
- 1755 Shackleton N. J. (2000) The 100,000-Year Ice-Age Cycle Identified and Found to Lag Temperature, Carbon
1756 Dioxide, and Orbital Eccentricity. *Science* **289**, 1897–1902.
- 1757 Shao, D., Mei, Y., Yang, Z., Wang, Y., Yang, W., Gao, Y., Yang, L. and Sun, L. (2020) Holocene ENSO
1758 variability in the South China Sea recorded by high-resolution oxygen isotope records from the shells of
1759 *Tridacna* spp., *Scientific Reports* **10** (1), 3921, doi:10.1038/s41598-020-61013-2.
- 1760 Sinnesael M., De Vleeschouwer D., Zeeden C., Batenburg S. J., Da Silva A. C., de Winter N. J., Dinarès-
1761 Turell J., Drury A. J., Gambacorta G. and Hilgen F. J. (2019) The Cyclostratigraphy Intercomparison
1762 Project (CIP): consistency, merits and pitfalls. *Earth-Science Reviews*, 102965.
- 1763 Sinnesael M., Zivanovic M., Vleeschouwer D. D., Claeys P. and Schoukens J. (2016) Astronomical
1764 component estimation (ACE v. 1) by time-variant sinusoidal modeling. *Geoscientific Model Development*,
1765 **9**, 3517–3531, 2016.
- 1766 Stap L., Lourens L. J., Thomas E., Sluijs A., Bohaty S. and Zachos J. C. (2010) High-resolution deep-sea
1767 carbon and oxygen isotope records of Eocene Thermal Maximum 2 and H2. *Geology* **38**, 607–610.
- 1768 Steffensen J. P., Andersen K. K., Bigler M., Clausen H. B., Dahl-Jensen D., Fischer H., Goto-Azuma K.,
1769 Hansson M., Johnsen S. J. and Jouzel J. (2008) High-resolution Greenland ice core data show abrupt
1770 climate change happens in few years. *Science* **321**, 680–684.
- 1771 Steuber T., Rauch M., Masse J.-P., Graaf J. and Malkoč M. (2005) Low-latitude seasonality of Cretaceous
1772 temperatures in warm and cold episodes. *Nature* **437**, 1341–1344.
- 1773 Straight W. H., Barrick R. E. and Eberth D. A. (2004) Reflections of surface water, seasonality and climate
1774 in stable oxygen isotopes from tyrannosaurid tooth enamel. *Palaeogeography, Palaeoclimatology,
1775 Palaeoecology* **206**, 239–256.
- 1776 Strauss J., Oleinik A. and Swart P. (2014) Stable isotope profiles from subtropical marine gastropods of the
1777 family Fasciolaridae: growth histories and relationships to local environmental conditions. *Mar Biol* **161**,
1778 1593–1602.
- 1779 Surge D., Lohmann K. C. and Dettman D. L. (2001) Controls on isotopic chemistry of the American oyster,
1780 *Crassostrea virginica*: implications for growth patterns. *Palaeogeography, Palaeoclimatology,
1781 Palaeoecology* **172**, 283–296.
- 1782 Titschack J., Zuschin M., Spötl C. and Baal C. (2010) The giant oyster *Hytissa hyotis* from the northern
1783 Red Sea as a decadal-scale archive for seasonal environmental fluctuations in coral reef habitats. *Coral
1784 Reefs* **29**, 1061–1075.
- 1785 Treble P., Shelley J. M. G. and Chappell J. (2003) Comparison of high resolution sub-annual records of
1786 trace elements in a modern (1911–1992) speleothem with instrumental climate data from southwest
1787 Australia. *Earth and Planetary Science Letters* **216**, 141–153.
- 1788 Tsukakoshi Y. (2011) Sampling variability and uncertainty in total diet studies. *Analyst* **136**, 533–539.

- 1789 Tudhope A. W. (2001) Variability in the El Niño-Southern Oscillation Through a Glacial-Interglacial Cycle.
1790 *Science* **291**, 1511–1517.
- 1791 Ullmann C. V., Wiechert U. and Korte C. (2010) Oxygen isotope fluctuations in a modern North-Sea oyster
1792 (*Crassostrea gigas*) compared with annual variations in seawater temperature: Implications for
1793 palaeoclimate studies. *Chemical Geology* **277**, 160–166.
- 1794 Van Rempelbergh M., Verheyden S., Allan M., Quinif Y., Keppens E. and Claeys P. (2014) Seasonal
1795 variations recorded in cave monitoring results and a 10-year monthly resolved speleothem $\delta^{18}\text{O}$ and
1796 $\delta^{13}\text{C}$ record from the Han-sur-Lesse cave, Belgium. *Climate of the Past Discussions* **10**, 1821–1856.
- 1797 Vansteenberge S., Verheyden S., Cheng H., Edwards R. L., Keppens E. and Claeys P. (2016) Paleoclimate
1798 in continental northwestern Europe during the Eemian and early Weichselian (125–97 ka): insights from
1799 a Belgian speleothem. *Clim. Past* **12**, 1445–1458.
- 1800 Vansteenberge S., Winter N. de, Sinnesael M., Verheyden S., Goderis S., Malderen S. J. M. V., Vanhaecke
1801 F. and Claeys P. (2019) Reconstructing seasonality through stable isotope and trace element analysis of
1802 the Proserpine stalagmite, Han-sur-Lesse Cave, Belgium: indications for climate-driven changes during
1803 the last 400 years. *Climate of the Past Discussions*, 1–32.
- 1804 Veizer J. and Prokoph A. (2015) Temperatures and oxygen isotopic composition of Phanerozoic oceans.
1805 *Earth-Science Reviews* **146**, 92–104.
- 1806 Vleeschouwer D. D., Vahlenkamp M., Crucifix M. and Pälike H. (2017) Alternating Southern and Northern
1807 Hemisphere climate response to astronomical forcing during the past 35 m.y. *Geology* **45**, 375–378.
- 1808 Wan R., Liu W., McArthur J. M. and Wang Z. (2019) Sr-isotope chronology of carbonate rocks: Quantifying
1809 the uncertainty of inversion. In *Stratigraphy & Timescales* Elsevier, pp. 35–72. Available at:
1810 <https://linkinghub.elsevier.com/retrieve/pii/S2468517819300036> [Accessed June 17, 2020].
- 1811 Warter V. and Müller W. (2017) Daily growth and tidal rhythms in Miocene and modern giant clams revealed
1812 via ultra-high resolution LA-ICPMS analysis—A novel methodological approach towards improved
1813 sclerochemistry. *Palaeogeography, Palaeoclimatology, Palaeoecology* **465**, 362–375.
- 1814 Wilkinson, B.H., Ivany, L.C., 2002. Paleoclimatic inference from stable isotope profiles of accretionary
1815 biogenic hardparts—a quantitative approach to the evaluation of incomplete data. *Palaeogeography,*
1816 *Palaeoclimatology, Palaeoecology* **185**, 95–114. [https://doi.org/10.1016/S0031-0182\(02\)00279-4](https://doi.org/10.1016/S0031-0182(02)00279-4)
- 1817 Yan H., Liu C., An Z., Yang W., Yang Y., Huang P., Qiu S., Zhou P., Zhao N. and Fei H. (2020) Extreme
1818 weather events recorded by daily to hourly resolution biogeochemical proxies of marine giant clam shells.
1819 *Proceedings of the National Academy of Sciences*.
- 1820 Yobregat E., Fitoussi C. and Bourdon B. (2017) A new method for TIMS high precision analysis of Ba and
1821 Sr isotopes for cosmochemical studies. *J. Anal. At. Spectrom.* **32**, 1388–1399.
- 1822 Zachos J., Pagani M., Sloan L., Thomas E. and Billups K. (2001) Trends, rhythms, and aberrations in global
1823 climate 65 Ma to present. *Science* **292**, 686–693.
- 1824 Zhang Limin, Tang Wilson H., Zhang Lulu and Zheng Jianguo (2004) Reducing Uncertainty of Prediction
1825 from Empirical Correlations. *Journal of Geotechnical and Geoenvironmental Engineering* **130**, 526–534.

Formatted: Font: 10 pt